SCIENCE APPLICATIONS, INC.

ACOUSTIC IMPLICATIONS OF MESOSCALE OCEANOGRAPHIC PHENOMENA

SAI
ATLANTA • ANN ARBOR • BOSTON • CHICAGO • CLEVELAND • DENVER • HUNTSVILLE • LA JOLLA
LITTLE ROCK • LOS ANGELES • SAN FRANCISCO • SANTA BARBARA • TUCSON • WASHINGTON

ACOUSTIC IMPLICATIONS OF MESOSCALE OCEANOGRAPHIC PHENOMENA

Report to:

Office of Naval Research
Naval Analysis Program
Attn: James G. Smith, Code 431

31 May 1979

Final Report
Contract N00014-77-C-0696
Task Number NR 274-293

Prepared by:

Lorna S. Blumen
John S. Hanna

SAI-80-926-WA

SCIENCE APPLICATIONS, INC.
8400 Westpark Dr.
McLean, Virginia 22101
(703) 821-4300

Unclassified

SECURITY CLASSIFICATION OF THIS PAGE (When Data Entered)

REPORT DOCUMENTATION PAGE		READ INSTRUCTIONS BEFORE COMPLETING FORM
1. REPORT NUMBER	2. GOVT ACCESSION NO.	3. RECIPIENT'S CATALOG NUMBER
4. TITLE (and Subtitle) (6) Acoustic Implications of Mesoscale Oceanographic Phenomena,		5. TYPE OF REPORT & PERIOD COVERED (9) Final rept's
		6. PERFORMING ORG. REPORT NUMBER
7. AUTHOR(s) L. S. Blumen J. S. Hanna		8. CONTRACT OR GRANT NUMBER(s) (15) N00014-77-C-0696
9. PERFORMING ORGANIZATION NAME AND ADDRESS Science Applications, Inc. 8400 Westpark Drive McLean, Virginia 22102		10. PROGRAM ELEMENT, PROJECT, TASK AREA & WORK UNIT NUMBERS 65152N R0145-TW NR 274-293
11. CONTROLLING OFFICE NAME AND ADDRESS Naval Analysis Program (Code 431) Office of Naval Research Arlington, Virginia 22217		(11) 12. REPORT DATE 31 May 1979 13. NUMBER OF PAGES 112
14. MONITORING AGENCY NAME & ADDRESS (if different from Controlling Office) (12) 114		15. SECURITY CLASS. (of this report) Unclassified 15a. DECLASSIFICATION/DOWNGRADING SCHEDULE

16. DISTRIBUTION STATEMENT (of this Report)

Approved for public release; distribution unlimited

(10) Lorna S. /Blumen John S. /Hanna (14) SAI-81-926-W/A

17. DISTRIBUTION STATEMENT (of the abstract entered in Block 20, if different from Report)

Reproduction in whole or in part is permitted for any purpose of the United States Government

18. SUPPLEMENTARY NOTES

(16) R0145 (17) R0145TW

19. KEY WORDS (Continue on reverse side if necessary and identify by block number)

Eddy Modeling
Underwater Acoustic Propagation
Parabolic Equation (PE) Model

20. ABSTRACT (Continue on reverse side if necessary and identify by block number)

This volume documents an investigation into the effects of mesoscale oceanographic features on underwater acoustic propagation. A recent eddy model is evaluated for its application to acoustic analysis. The effects of range-dependence, source-receiver geometry, and source frequency are examined. Descriptive statistics are used to provide a quantitative measure of the energy redistribution caused by the presence of an eddy.

DD FORM 1 JAN 73 1473 EDITION OF 1 NOV 65 IS OBSOLETE S/N 0102-014-6601

Unclassified

SECURITY CLASSIFICATION OF THIS PAGE (When Data Entered)

402 404

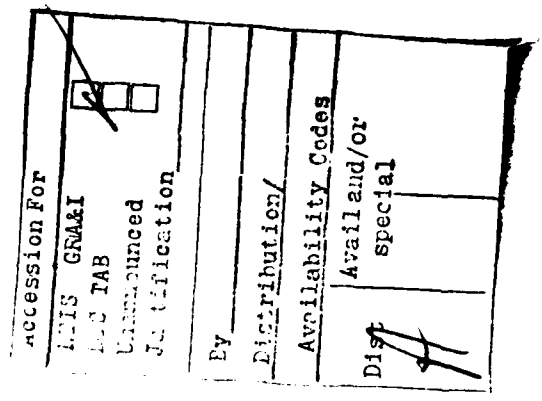

Table of Contents

Tables and Figures

Section 1
INTRODUCTION

For some years there has been a growing interest in the implications of mesoscale oceanographic features for acoustic propagation. One major obstacle to assessing these implications had been the absence of a propagation model capable of treating the range-dependent oceanography. With the application to underwater acoustics of the parabolic approximation to the wave equation (Tappert and Hardin, 1973; Tappert, 1974; Brock, 1978) this obstacle was overcome and several investigators have estimated the acoustic field in the presence of such mesoscale features as eddies. Indeed, the spring 1978 meeting of the Acoustical Society of America devoted an entire session to this subject.

Much of the work to date, however, has left unaddressed several significant questions:

- What is a useful, objective measure of the acoustic importance of eddies?
- For the purpose of acoustic studies, can a parametric oceanographic model of eddies be used?

The first question gets at the matter of how to characterize the importance of eddies to ASW systems. Individual point comparisons of the acoustic field with and without an eddy present can generate arbitrarily large differences which are largely misleading. Averaged propagation may indicate

significant differences where they exist, but may obscure interesting differences in the distribution of energy with range and depth. In the work reported here an attempt is made to define a measure of difference which may come closer to being useful in the ASW systems analyses. The second question is of importance primarily to physical oceanographers. However, a satisfactory analytical eddy model would provide a very useful parameterization for acoustic studies. For this reason a recently-developed eddy model (Henrick, 1978; 1979) is examined here in an attempt to characterize measured eddies from some Pacific data collected by ONR.

In the remainder of this report the eddy model is described and applied to measured data. Following this discussion, some acoustic results are summarized and compared. Two major conclusions with respect to the questions raised above are:

- The objective acoustic comparison developed here shows some promise of usefulness, but requires more evaluation before it can be claimed to fulfill the stated need.

- The eddy model is not sufficiently flexible to allow fitting the measured data with enough accuracy for the acoustic studies. Some suggestions for its extension are offered.

Finally, with regard to ASW implications of eddies, the following conclusion is reached:

- Except for the case in which the source (target) is at the center of an eddy and the receiver is outside it, the presence of the eddy has a negligible influence on the acoustic field. In the one case of interest, average level differences of 10 dB are observed at low frequencies (20 Hz) which diminish at high frequencies (300 Hz).

Section 2
EDDY MODEL DESCRIPTION

2.1. Basic Equations

For horizontal nonaccelerated flow in a frictionless ocean, a balance exists between the Coriolis forces and the pressure gradient. This relationship is expressed in (1). In addition, from the hydrodynamic equations, we may describe the vertical pressure gradient as a function of density and gravitational acceleration (2). Differentiating (1) with respect to z (3), (2) with respect to r (4), equating the two, and rearranging terms, we end up with (5). Typically, $\partial\rho/\partial z$ is much larger than $\partial\rho/\partial r$, but the v/ρ factor in front of the $\partial\rho/\partial z$ term reduces the importance of that term. Consider the following situation, in which g, gravitational acceleration, is approximately 10^3 m sec^{-2}, $\rho \sim 1$ and f, the Coriolis parameter, is approximately 10^{-4} sec^{-1}. This gives us a value for $g/\rho f$ on the order of magnitude of 10^7. For v, current velocity, approximately 100 cm sec^{-1}, and if the vertical gradients are a thousand times larger than the horizontal gradients, i.e., $\partial\rho/\partial z = 10^3\,\partial\rho/\partial r$, $\partial v/\partial z$ is approximately equal to $10^7 - 10^5$. We may then effectively ignore the second term in (5), which then becomes (6).

$$fv = \frac{1}{\rho} \frac{\partial p}{\partial r} \tag{1}$$

where

f = Coriolis Parameter = $2\Omega\sin\phi$

v = Current Velocity

ϕ = Latitude

ρ = Density

p = Pressure

r = Horizontal Range

$$\frac{\partial p}{\partial z} = \rho g \tag{2}$$

$$\frac{\partial^2 p}{\partial r \partial z} = \frac{\partial}{\partial z}(\rho f v) = \rho f \frac{\partial v}{\partial z} + f v \frac{\partial \rho}{\partial z} \tag{3}$$

$$\frac{\partial^2 p}{\partial r \partial z} = \frac{\partial}{\partial r} \rho g = g \frac{\partial \rho}{\partial r} \tag{4}$$

$$\rho f \frac{\partial v}{\partial z} + f v \frac{\partial \rho}{\partial z} = g \frac{\partial \rho}{\partial r}$$

$$\frac{\partial v}{\partial z} = \frac{g}{\rho f} \frac{\partial \rho}{\partial r} - \frac{v}{\rho} \frac{\partial \rho}{\partial z} \qquad (5)$$

$$\frac{\partial v}{\partial z} \sim \frac{g}{\rho f} \frac{\partial \rho}{\partial r} \qquad (6)$$

2.2. Henrick Eddy Model

The eddy model developed by R. F. Henrick at RPI (Henrick, 1978; 1979) is defined under the following assumptions:

(a) The eddy is radially symmetric around a vertical axis: i.e., the eddy is circular.

(b) The eddy experiences slow translation. Thus, translational effects may be ignored, and the eddy may be evaluated for a "snapshot" in time.

(c) The environmental effects of the eddy vanish at a distance r_0 from its center.

(d) Environmental effects vanish at a depth z_0.

(e) Salinity is invariant in this model, fixed at 35 $^{o}/_{oo}$.

The eddy model is governed by the stream function seen in (7). This function, $X(r,z)$, consists of two independent and separable terms, one a function of range, r, and

the other a function of depth, z. The constant, k, indicates eddy rotational direction, with $k \geq 0$ implying a warm eddy circulating in a clockwise manner, and $k < 0$ indicating a cold eddy circulating in a counterclockwise manner. Equation (9) shows the depth-dependent component of the stream function χ. The constant B is empirically estimated through a process which will be discussed in detail later.

$$\chi(r,z) = k\left[J_o\left(\frac{\beta_o r}{r_o}\right) - J_o(\beta_o)\right]\left[F^{(1)}{}_{(z)} - F^{(1)}{}_{(z_o)}\right] \quad (7)$$

where

$$k = \pm r_o \left\{\beta_o m \left|F^{(1)}(0) - F^{(1)}(z_o)\right|\right\}^{-1} \quad (8)$$

β_o = First zero of $J_1 = 3.83$

$m = J_1(x)_{max} = .582$

$\pm$ => Eddy rotational direction

$+$ => Anticyclonic (warm, clockwise)

$-$ => Cyclonic (cold, counterclockwise)

$$F^{(1)}(z) = (1+Bz)^{-\frac{1}{2}}\left\{\cos\left[\tfrac{1}{2}\gamma^{(1)}\ell n(1+Bz)\right] + \frac{1}{\gamma^{(1)}}\sin\left[\tfrac{1}{2}\gamma^{(1)}\ell n(1+Bz)\right]\right\} \quad (9)$$

$$\gamma^{(1)} = \frac{2\pi}{\ell n(1+Bz_o)} \qquad (10)$$

This model uses dimensionless parameters scaled in the following manner. All horizontal ranges are scaled by a characteristic length scale, L. All depths are scaled by the depth of the ocean, D. The characteristic length scale is a function of D and S, where S is a dimensionless scaling constant. This scaling constant is a function of g, gravitational acceleration, c_o, surface sound velocity, and the Coriolis parameter, $2\Omega\sin\phi$. For example, the dimensionless horizontal range used in the eddy model is found by scaling the dimensional range, denoted by the star(*), by the characteristic length scale.

$L = DS$ L = Characteristic Length Scale (m)

D = Ocean Depth (m)

$S = \frac{g}{2c_o\Omega\sin\phi}$ (Dimensionless)

ϕ = latitude

$g = 9.8$ m sec^{-2}

c_o = surface sound velocity (m sec^{-1})

Ω = earth's angular velocity $= 7.29 \times 10^{-5}$ sec^{-1}

$r_o = \frac{r_o^*}{L}$ $r = \frac{r^*}{L}$

$z_o = \frac{z_o^*}{D}$ $z = \frac{z^*}{D}$

This stream function is subject to several constraints which result from the initial assumptions (a) - (d) discussed earlier. The stream function $X(r,z)$ vanishes at a horizontal range r_o from the eddy center. Analogously, it vanishes at a depth z_o. In addition, the r derivative $\partial X/\partial r$ and the z derivative $\partial X/\partial z$ vanish at r_o and z_o, respectively. These constraints result from the vanishing of eddy effects at r_o and z_o. $\partial X/\partial r$ and $\partial X/\partial z$ represent eddy velocity and density effects, which also vanish at r_o and z_o. $\partial X/\partial r$ is actually current velocity (11), and the depth derivative of this function appears in equation (12). The value of $\partial X/\partial z$, seen in equation (13), again shows two independent and separable terms, one a function of range and the other a function of depth. The depth-dependent term contains the constant B. We now have an expression for $\partial v/\partial z$ in terms of $\partial X/\partial z$. Returning to equation (6), we see an alternative expression for $\partial v/\partial z$. Equating the two, integrating with respect to r, and evaluating at the boundary conditions to determine the value of the integration constant, we are left with equation (14), where ρ is density inside the eddy and ρ^* is static density, i.e., density outside the eddy. We now have a means for expressing the perturbation to the density field caused by the presence of an eddy.

$$v = \frac{\partial X}{\partial r} \tag{11}$$

$$\frac{\partial v}{\partial z} = \frac{\partial^2 X}{\partial r \partial z} = \frac{\partial}{\partial r}\frac{\partial X}{\partial z} \tag{12}$$

$$\frac{\partial \chi}{\partial z} = k \left[J_o \left(\frac{\beta_o r}{r_o} \right) - J_o \left(\beta_o \right) \right] \left\{ -B(1+Bz)^{-3/2} \left(\varepsilon + \frac{1}{4\varepsilon} \right) \sin\alpha \right\}$$

where

$$\alpha = \varepsilon \ell n(1+Bz)$$

$$\varepsilon = \tfrac{1}{2}\gamma^{(1)} \qquad (13)$$

$$\frac{\partial \chi}{\partial z} = \frac{g}{\rho_o f} \left[\rho - \rho^* \right] \qquad (14)$$

One means by which this density field may be characterized is the equation of state developed by Mamayev, for salinity constant at 35°/oo. This is seen in equation (15). Substituting this expression into equation (14), we get equation (16), where T is the temperature inside the eddy and T* is static temperature, the temperature outside the eddy. Rearranging this relationship and redimensionalizing $\partial \chi / \partial z$ by $U_o g / f c_o$, where U_o is surface current speed, equation (17) results. Substituting the expression for $\partial \chi / \partial z$ from equation (13), we find equation (18), which expresses the relationship between the unperturbed and perturbed temperature, T. Equation (18) is quadratic in T, and may be solved for T. Sound velocity within the eddy may then be computed using Wilson's equation.

$$\rho_s(z) = \left[1 + 10^{-3}\left\{28.152-.0735T-.00469T^2\right\}\right] + 45 \times 10^{-7}z \quad (15)$$

$$\frac{\partial \chi}{\partial z} = \frac{g}{\rho_o f}\left[10^{-3}\left\{-.0735(T-T^*) -.00469(T^2-T^{*2})\right\}\right] \quad (16)$$

$$.00469(T^2-T^{*2}) + .0735(T-T^*) = \frac{-10^3 U_o \rho_o}{c_o}\frac{\partial \chi}{\partial Z} \quad (17)$$

$$.00469(T^2-T^{*2}) + .0735(T-T^*) = \frac{-10^3 U_o \rho_o}{c_o}\left\{k\left[J_o\left(\frac{\beta_o r}{r_o}\right) - J_o(\beta_o)\right]\right.$$

$$\left.\left\{-B(1+Bz)^{-3/2}(\varepsilon+\frac{1}{4\varepsilon})\sin\alpha\right\}\right\} \quad (18)$$

2.3 Empirical Estimation of Model Parameters

Given a static temperature distribution, i.e., the temperature distribution in the absence of an eddy, static density may be expressed as a function of temperature and pressure (depth), for salinity constant at 35°/oo, using Mamayev's equation of state, seen earlier in equation (15). We may then generate a distribution of static density as a function of depth, $\rho_s(z)$, from the temperature data. Henrick fits this density distribution to an algebraic function for static density shown in equation (19). The Levenberg-Marquardt algorithm, a non-linear least squares regression algorithm, is used to fit this functional

form for static density to the observed density (temperature) values. Estimates of ρ_o, A, and B, which minimize the residuals, are returned. This process may be extended to fit this functional form to temperature and sound velocity observations directly.

$$\rho_s(z) = \rho_o \left\{1 + \Delta\left[z + (A(1-(1+Bz)^{-1}))\right]\right\} \quad (19)$$

where

$$\Delta = \frac{gD}{c_o^2}$$

Section 3
DATA

The data used in this analysis were collected during May, 1976 as a part of ONR's ships-of-opportunity program. Six parallel ships centered at 37°N traversed a 2500 km swath from 155°E to 175°W. The lateral spacing between ships was approximately 45 km. The ships made hourly XBT casts, alternating between T-4 and T-7 XBTs. This resulted in a sampling density of 27 km. The resultant temperature data have given us one of the best quasi-synoptic pictures of mesoscale variability to date. Texas A&M University merged the thermal data with deep ocean climatology, to yield a three-dimensional characterization of this swath, in terms of temperature(T), salinity(S), sound velocity(c), and density (σ_T). A schematic of the track may be seen in Figure 1. Appendix A contains isothermal and isovelocity sections for each of the six ship tracks. It is evident from these temperature and sound velocity sections that a significant amount of mesoscale variability is present in this region of the Pacific.

We have modeled most of the eddies on these tracks using the eddy model developed by Henrick. The eddies have been characterized in terms of their horizontal (r_o) and vertical (z_o) extent of influence, as well as the value of the parameters ρ_o, A, and B. Table 1 summarizes the results. Eddies from two of the tracks have been selected as an illustration of the modeling process. A cold-core eddy, located at 450 km along the track of the Schenectady , the northernmost ship, and a warm-core eddy from the start of the track of the Bristol County, the southernmost ship, will be used for illustrative purposes.

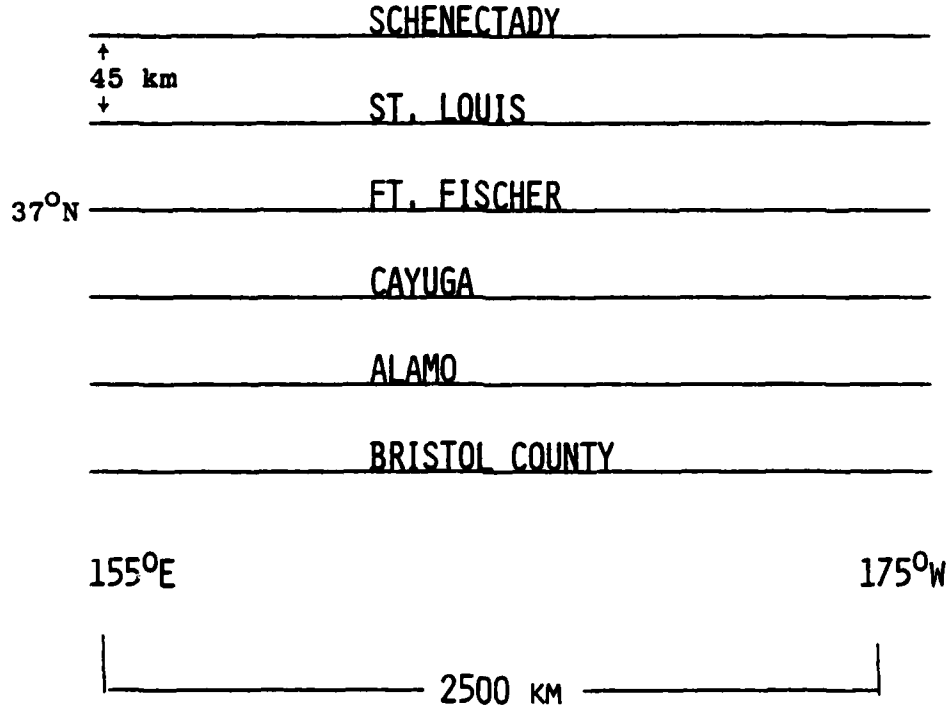

Figure 1. Track Schematic

Track	Range (km)	Data	r_0(km)	z_0(m)	ρ_0	A	B
Schenectady	451.2	Temp	187.5	2000.	1.02596	0.111	17.82
	451.2	SV	187.5	2000.	1.02596	0.110	19.99
St. Louis	512.6	Temp	200.0	2400.	1.02582	0.122	15.41
	512.6	SV	200.0	2400.	1.02581	0.121	17.31
	968.4	Temp	100.0	2100.	1.02597	0.112	14.34
	968.4	SV	100.0	2100.	1.02596	0.112	16.36
	1740.8	Temp	150.0	1600.	1.02572	0.129	13.00
	1740.8	SV	150.0	1600.	-------	-----	-----
	Off track	Temp	57.5	1800.	1.02602	0.108	15.71
	Off track	SV	57.5	1800.	1.02602	0.107	17.83
Ft. Fischer	1746.3	Temp	90.0	2500.	1.02575	0.127	13.05
	1746.3	SV	90.0	2500.	1.02572	0.127	15.06
Cayuga	195.8	Temp	180.0	2500.	1.02526	0.158	13.68
	195.8	SV	180.0	2500.	1.02520	0.159	15.89
	1124.3	Temp	172.5	3000.	1.02595	0.112	17.80
	1124.3	SV	172.5	3000.	-------	-----	-----
Alamo	0.0	Temp	150.0	3000.	1.02522	0.159	17.71
	0.0	SV	150.0	3000.	1.02523	0.158	19.13
Bristol County	0.0	Temp	172.5	2800.	1.02574	0.125	20.46
	0.0	SV	172.5	2800.	1.02579	0.123	21.69

Table 1

Track Mesoscale Features and Corresponding Model Parameters

Section 4
MODEL RESULTS

The cold eddy on the Schenectady track has an effective radius, r_o, of 188 km and extends to a depth of influence, z_o, of 2000 m. The background sound velocity conditions have been modeled using the Henrick model and the resultant values of ρ_o, A, and B may be seen in Table 2. Using these parameters, the background density, temperature, and sound velocity profiles may then be modeled. Figure 2 shows a comparison between the actual density profile and the modeled density profile, determined by the parameters ρ_o, A, and B. The agreement is apparently quite good. Figure 3 shows a similar comparison for the data and modeled temperature profiles. These profiles also agree fairly well, although there are some differences in the upper 600 m. These differences are relatively small, however, with the modeled profile differing from the data on average by only a few tenths of a degree. The modeled sound velocity profile is compared to the data profile in Figure 4. In this instance, there are some fairly significant deviations, once again occurring in the upper 600 m. Note also that while the deep gradients on these profiles are the same, the modeled profile shows an absolute sound velocity at these depths which is consistently greater than the sound velocity seen in the data profile at the same depths.

Additional information may be seen in a comparison of the actual and modeled eddy fields. Figure 5 shows the modeled isothermal structure for this cold-core eddy.

Table 2

Eddy Model Parameters
Selected Cases

Ship Track	Eddy type	Range (km)	r_o(km)	z_o(m)	ρ_o	A	B
Schenectady	cold	451.2	187.5	2000	1.02596	.110	19.99
Bristol County	warm	0.0	172.5	2800	1.02579	.123	21.69

Fig. 2

Background Density Profiles Cold Eddy

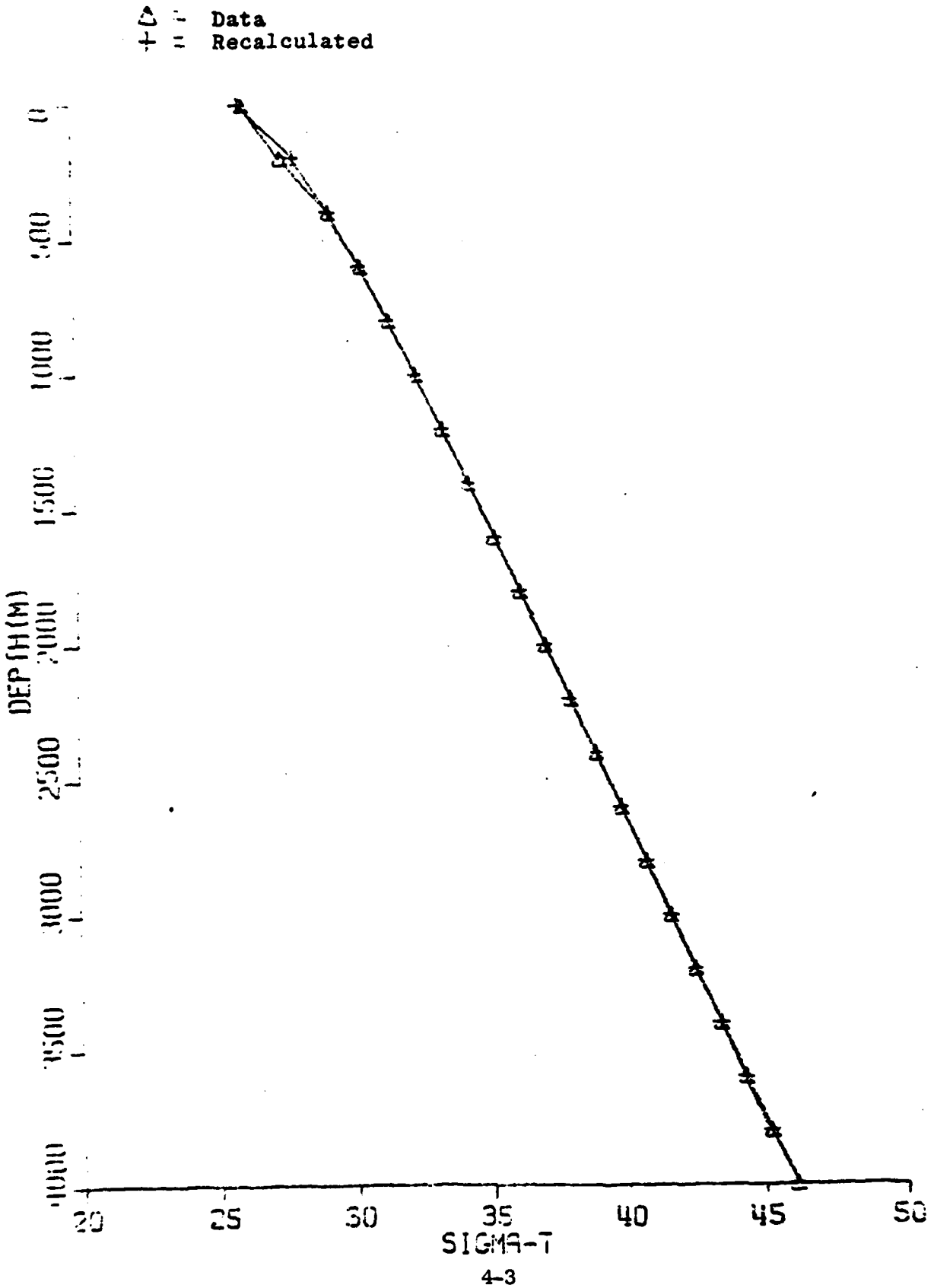

Fig. 3

Background Temperature Profiles Cold Eddy

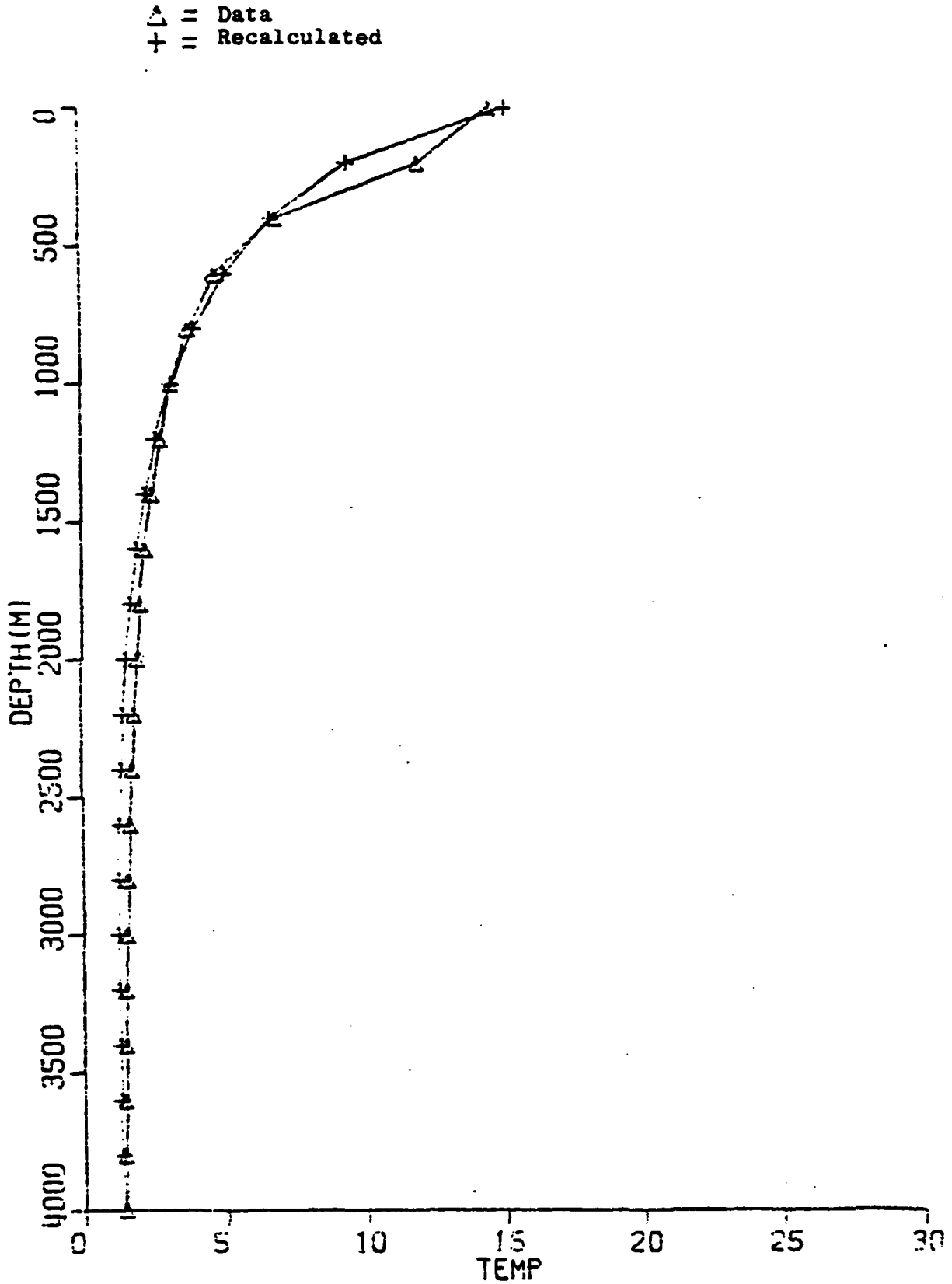

Fig. 4

Background Sound Velocity Profiles Cold Eddy

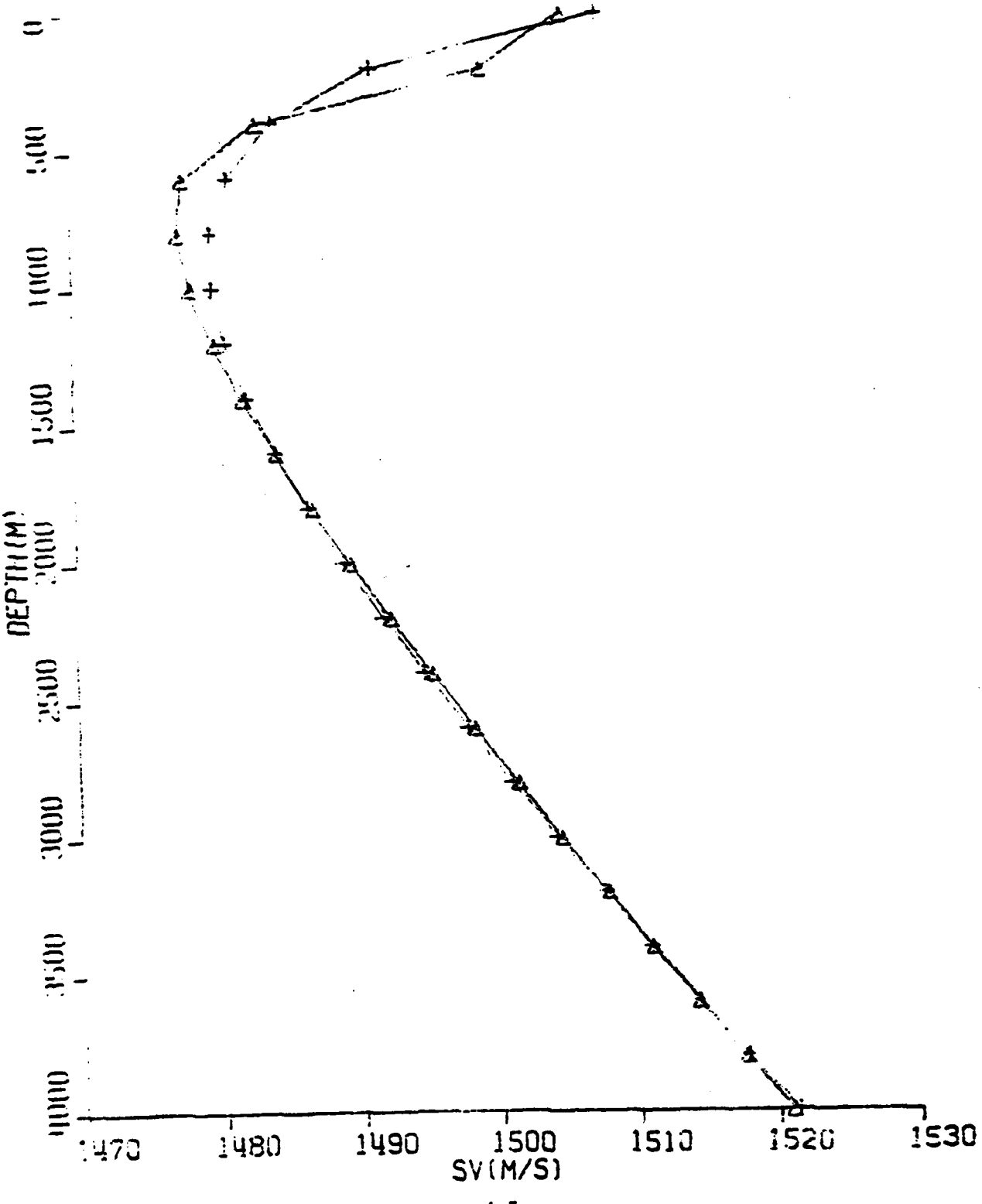

Figure 5 Eddy Model Isotherms for Cold-Core Eddy

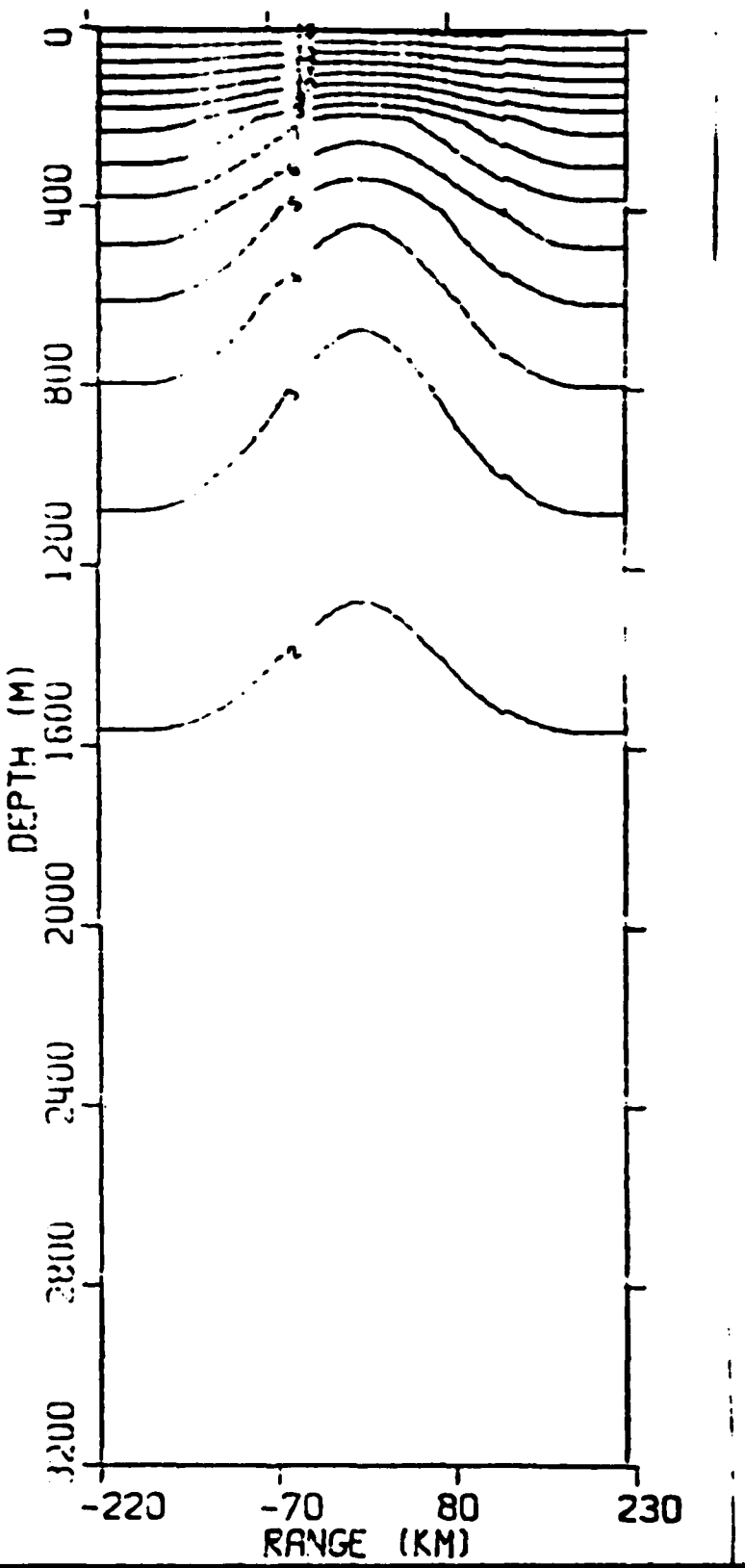

Figure 6 shows a superposition of the model isotherms with the actual isotherms seen along the track. Some significant deviations may be seen. The most significant deviation results from the absence of eddy surface expression in the model, whereas surface expression is clearly present in the data. In addition, the model does not reflect the asymmetry seen within the data. As one of the underlying assumptions for the model is that the eddy is radially symmetric, this represents a fundamental and irrecoverable difference. These differences are perhaps not as large as they appear, as the contouring process itself is quite sensitive to small changes in temperature. Deviations of several tenths of a degree, typically not considered excessive, will result in major displacements of the isotherm depths in regions where the temperature is nearly constant. Figure 7 shows model isovelocity contours for the cold-core eddy. Figure 8 shows the superposition of these model contours with isovelocity contours from the Schenectady track. The same differences between the model and the data which were evident in the isothermal sections are also evident in the isovelocity contours. Once again, we notice the relative lack of surface expression in the model, whereas surface expression is clearly indicated by the data. In addition, the model does not account for the random effects which are characteristic of a particular isotherm.

Turning to the warm-core eddy from the Bristol County track, the effective radius for that eddy is 173 km, slightly smaller than the radius for the cold-core eddy. The depth of influence is slightly greater, extending to 2800 m. Background sound velocity data have been used to estimate the values of the parameters ρ_o, A, and B, which

Figure 6 Eddy Model Isotherms for Cold-Core Eddy

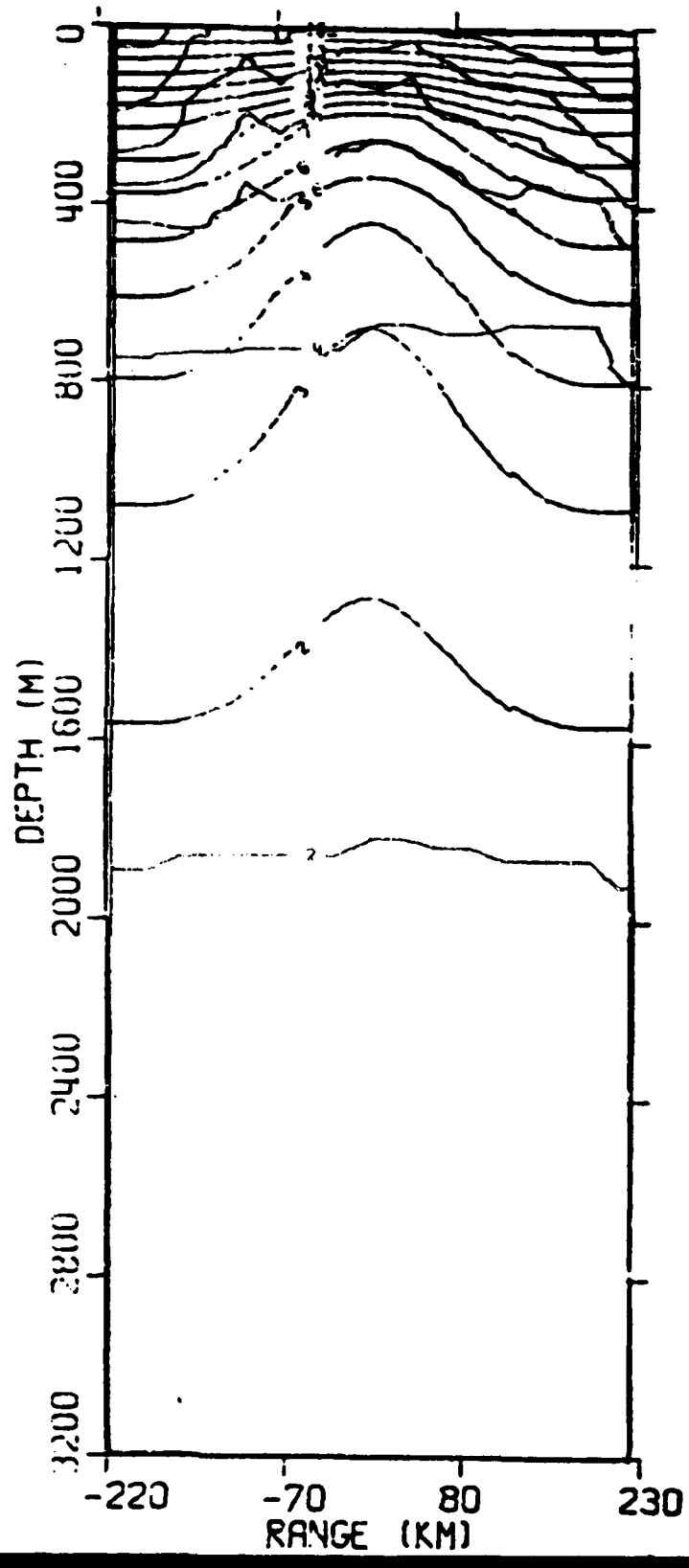

Eddy Model Isovelocity Contours for Cold-Core Eddy

Figure 7

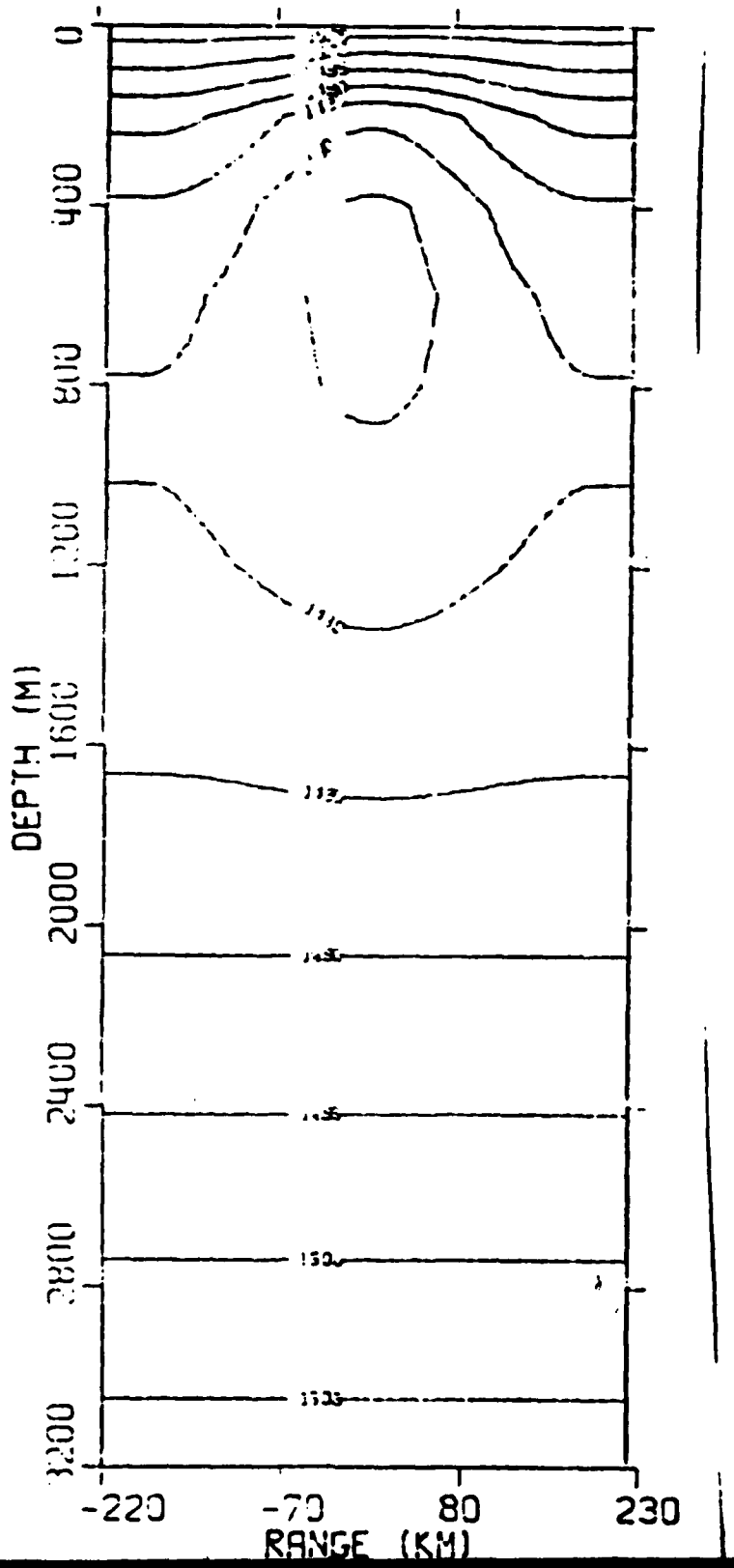

Eddy Model Isovelocity Contours for Cold-Core Eddy

Figure 8

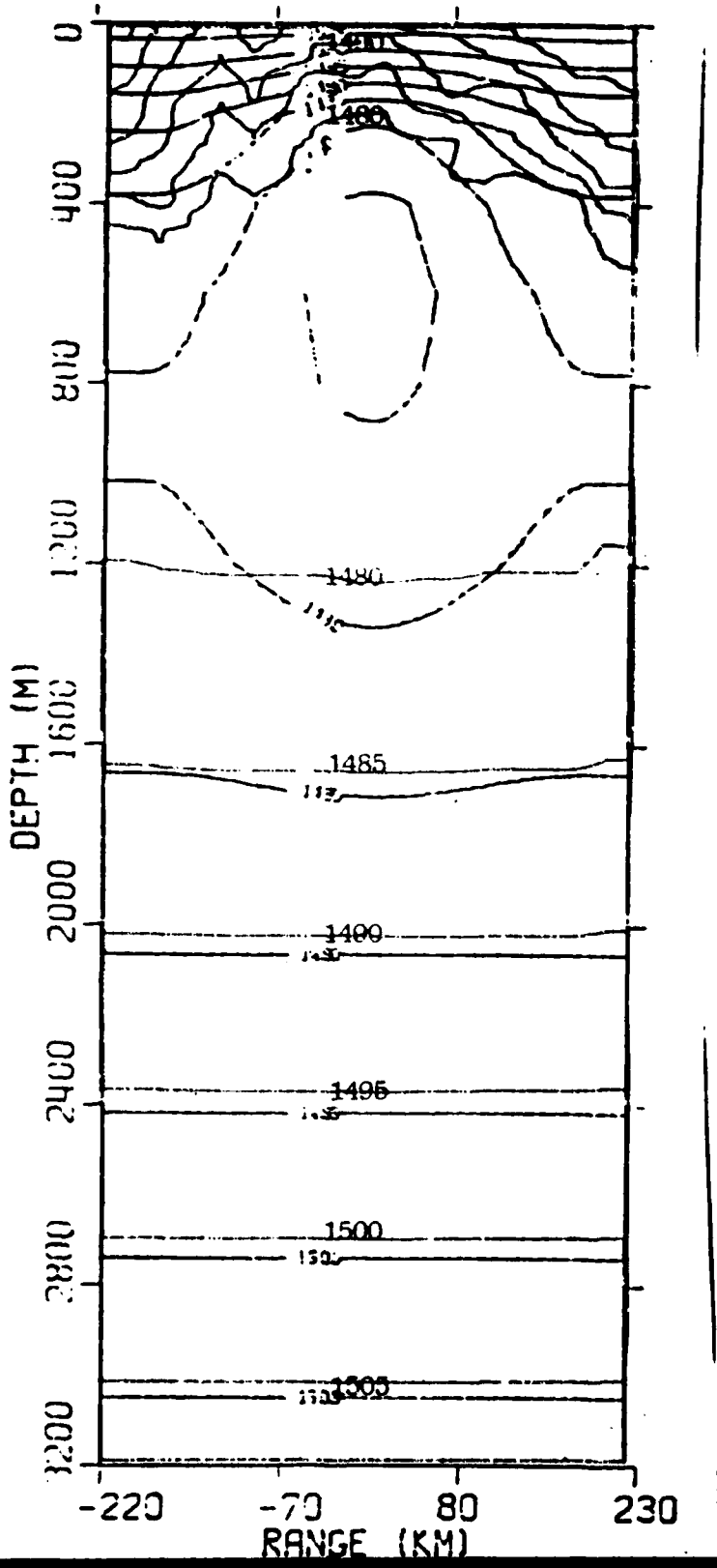

may be seen in Table 2. The background density, temperature, and sound velocity conditions have been modeled. Figure 9 shows a comparison of the density profile generated by the model to the data density profile for this warm-core eddy. As in the cold-core eddy case, the agreement between the density profiles is quite good. Figure 10 shows a similar comparison for the background temperature profiles. Again, the deviations in the temperature profiles are more apparent than those in the density profiles, but the deviations averaged over depth are generally less than several tenths of a degree. The sound velocity comparison seen in Figure 11 does show some major differences. Once again, the area of largest deviation is in the upper 600 meters of the water column. Further, the deep gradient on the the model profile is significantly smaller than that seen in the data profile. This has some serious implications for the acoustical analysis which will be discussed in detail later. Figure 12 shows the eddy model isothermal and isovelocity sections for this warm-core eddy. Figure 13, which is a superposition of these model isotherms and isovelocity sections with the data isothermal and isovelocity sections, again illustrates the lack of surface expression in the model, the inability of the model to account for asymmetry which is present in the data, and also the failure of the model to account for random effects along a given isothermal or isovelocity contour.

Fig. 9

Background Density Profiles Warm Eddy

Δ = Data
\+ = Recalculated

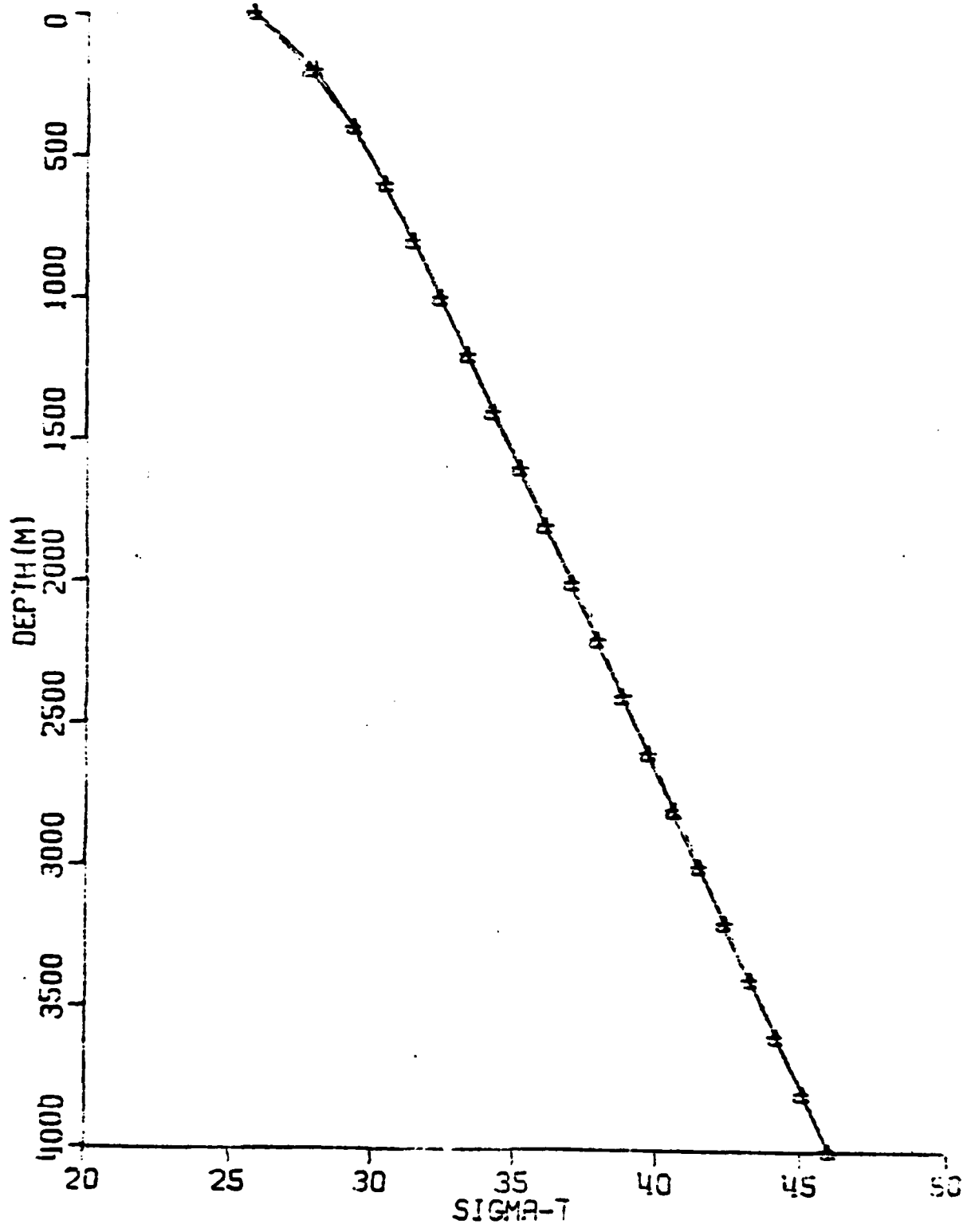

Fig. 10

Background Temperature Profiles Warm Eddy

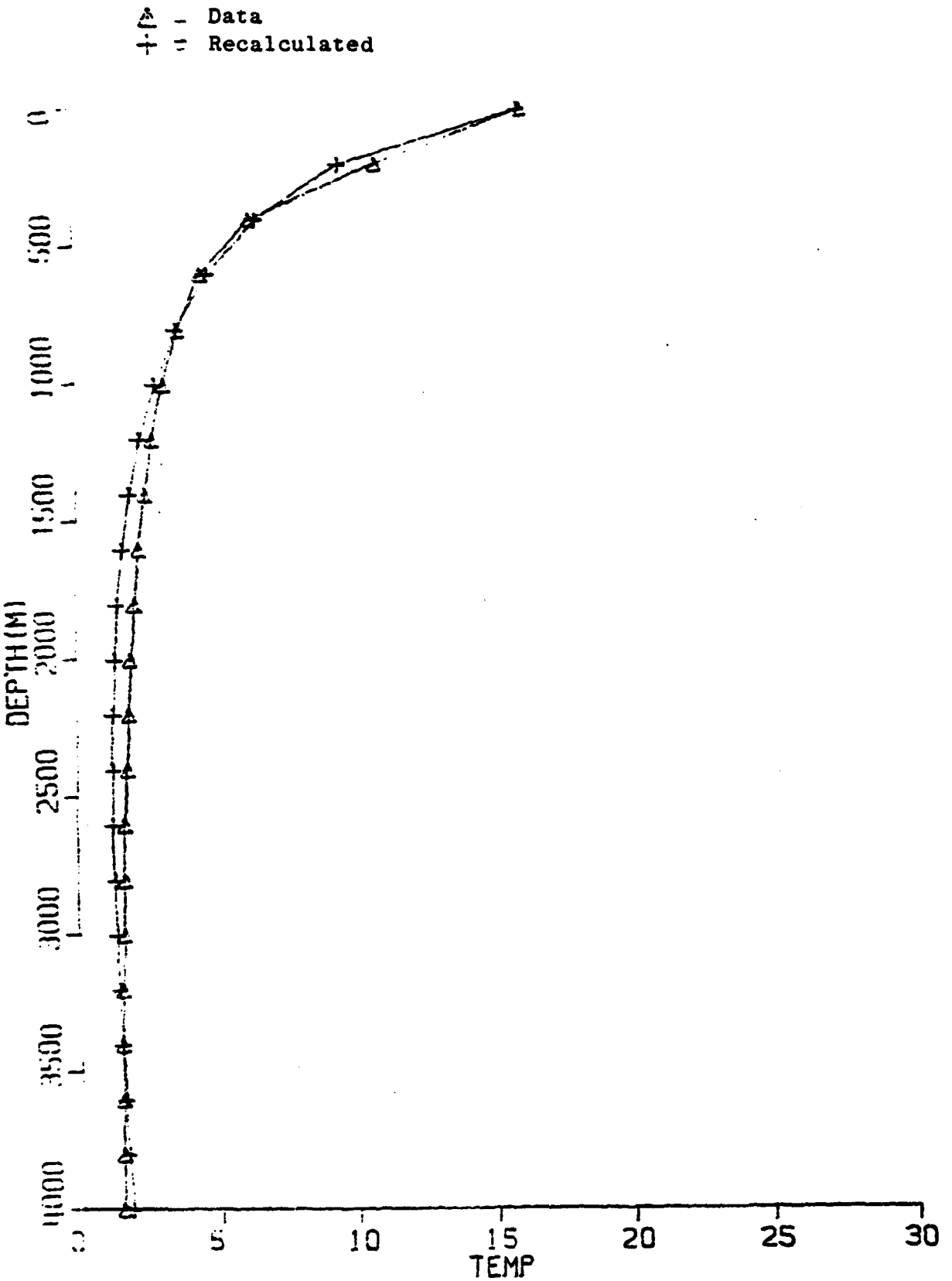

Fig. 11 Background Sound Velocity Profiles Warm Eddy

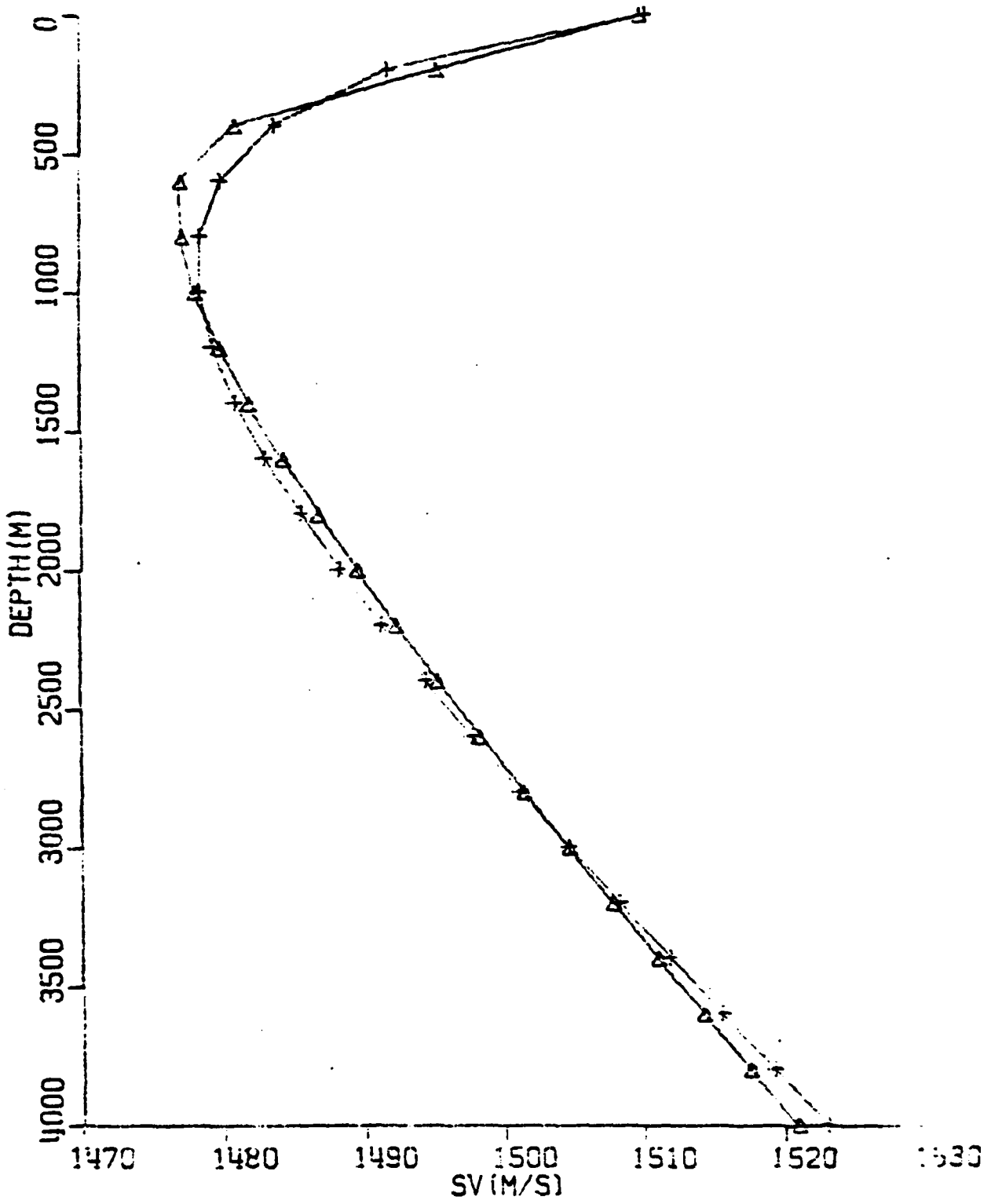

Eddy Model Isothermal and Isovelocity Sections for Warm-Core Eddy

Figure 12

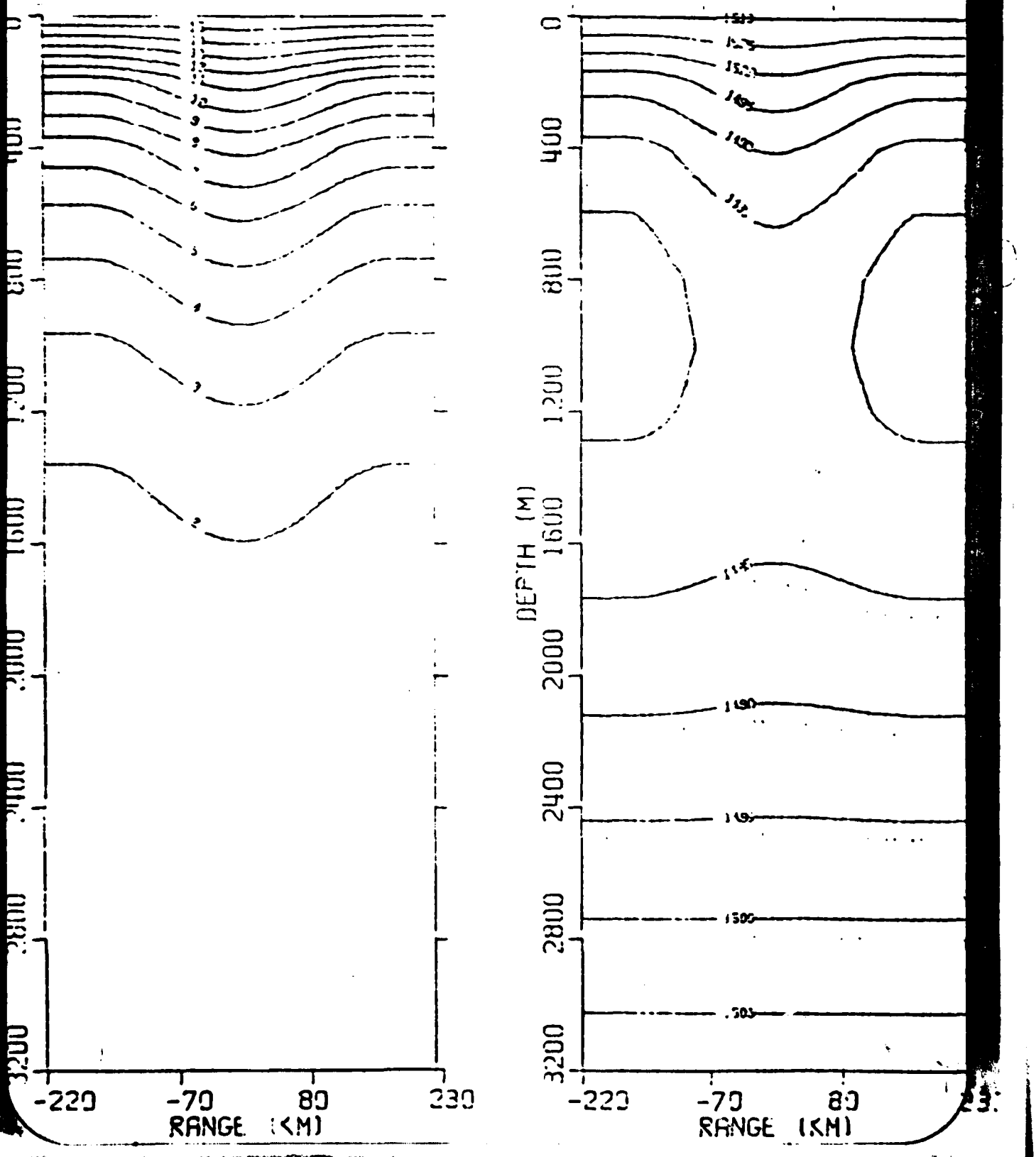

Eddy Model Isothermal and Isovelocity Sections for Warm-Core Eddy

Figure 13

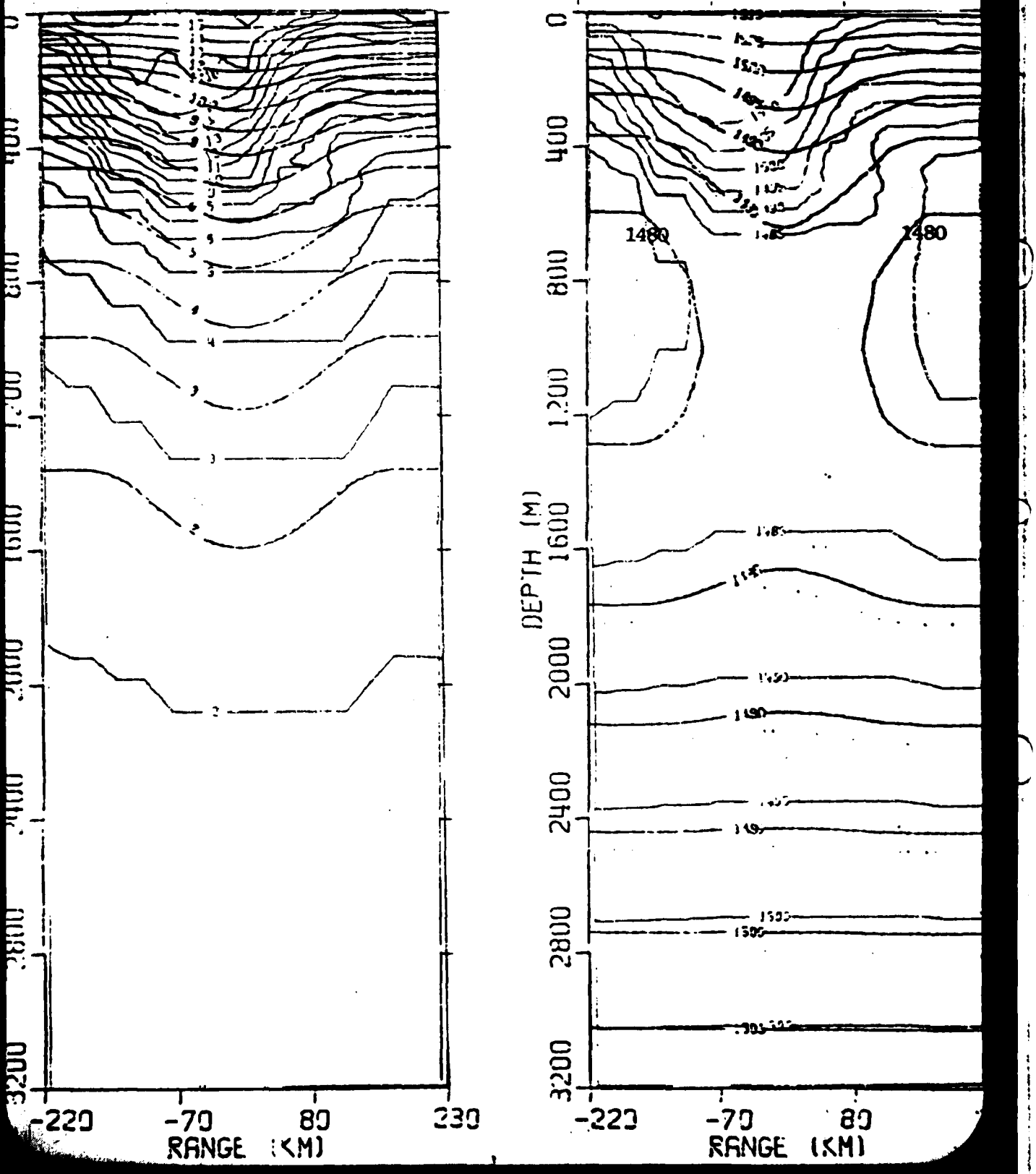

Section 5
EDDY MODEL COMPARATIVE STATISTICS

In order to assess more accurately the differences between the modeled density, temperature, and sound velocity profiles and the corresponding data profiles, direct comparison of the difference in sound velocity at discrete points along the track is quite helpful. That is, for every location in which a temperature or sound velocity observation is available, the observed sound velocity profile may be compared, on a point-by-point basis, to the modeled sound velocity. Such a comparison for the cold eddy is shown in Table 3. The mean sound velocity difference, seen at the bottom of the table, is actually quite small, less than 1.2 m sec^{-1}. Similarly, the mean temperature difference over all depths is small, less than .4°C. This is apparently quite good agreement. Looking in more detail at the differences in sound velocity at selected depths, it may be seen that the largest differences are indeed concentrated in the upper 600 m of the profile. This reinforces the information seen in the graphic display of sound velocity profiles.

Similar statistics for the warm-core eddy may be seen in Table 4, which once again shows a mean sound velocity difference and a mean temperature difference which are quite small. The major differences remain concentrated in the upper 400 to 600 m, with fairly good agreement existing below those depths.

SOUND VELOCITY DIFFERENCE (DATA-MODEL) m sec^{-1}

	RADIAL DISTANCE FROM EDDY CENTER			
Depth(m)	188 km	155 km	77 km	60 km
0	-2.50	-1.07	-12.70	-12.70
200	8.04	7.36	- 1.19	- 4.08
400	-1.07	-0.01	- .49	- 1.00
600	-3.16	-2.70	- .02	.85
800	-2.29	-1.96	.52	.91
1000	-1.52	-1.29	.41	.66
1200	-0.79	- .64	.46	.63
1400	-0.27	- .18	.48	.58
1600	.07	.13	.47	.50
1800	.35	.38	.47	.45
2000	.52	.52	.44	.42
$\mu_{\Delta sv}$	- .24	.05	- 1.01	-1.16
$\mu_{\Delta T}$	.25	.33	- .01	- .05

Table 3
Comparative Statistics Cold Eddy

SOUND VELOCITY DIFFERENCE (DATA-MODEL) m sec^{-1}

	RADIAL DISTANCE FROM EDDY CENTER		
Depth(m)	95 km	65 km	33 km
0	5.18	1.93	1.64
200	15.79	17.00	14.49
400	12.03	12.69	16.47
600	.56	- .99	4.95
800	- .56	-1.79	- .62
1000	.15	- .81	- .10
1200	.76	.03	.51
1400	1.15	.59	.92
1600	1.36	.95	1.15
1800	1.44	1.15	1.29
2000	1.43	1.23	1.33
2200	1.31	1.18	1.25
2400	1.10	1.02	1.11
2600	.79	.76	.83
2800	.49	.49	.56
3000	.07	.07	.12
$\mu_{\Delta sv}$	1.77	1.41	1.91
$\mu_{\Delta T}$	.75	.66	.79

Table 4
Comparative Statistics Warm Eddy

Section 6
EDDY MODEL SUMMARY

The eddy model developed by Henrick has been examined in some detail. This model provides an empirical fit to the static or background density, temperature, and sound velocity profiles for a particular ocean region. These profiles, and thus the region, are characterized in terms of the parameters ρ_o, A, and B. The model then generates the temperature and sound velocity fields within the eddy, giving us an idea of the perturbations to these fields which are caused by the presence of the eddy.

An evaluation of the model reveals that the mean temperature and sound velocity differences are small. Statistically, the modeled profiles are actually a good fit to the data. It has been shown that the largest differences are concentrated in the upper 600 meters. These differences are attributable to the fact that the model does not permit surface expressions. Further, the model fits the background conditions to a smooth, highly regular profile. Thus, any data profiles which are not smooth and regular will differ significantly from the modeled profiles. These differences appear primarily in the upper 600 m, typically the region of the water column experiencing the most variability. This poses somewhat of a problem for the acoustician, as most ASW cases of interest have the source located within that region of the water column. The use of this model for acoustic analysis, therefore, will result in significant differences between the observed and modeled conditions. On the basis of this analysis, it appears as if a model upgrade is in

order before it can be used successfully for ASW prediction. One suggestion for upgrading the capabilities of this model might include the use of cubic splines or other, more flexible, functional forms, which will give better local approximations to these background profiles: also required is an extension to permit eddy surface expressions.

Originally, it was intended that this model be used to fit the data from the six ship tracks and to parameterize the eddies on these tracks in terms of the the constants ρ_o, A, and B. The modeled eddies were then to be used for acoustic analysis. The differences between the modeled and observed sound velocity profiles resulted in significant differences in the acoustic fields generated by these profiles. Preliminary acoustic analysis of the model results showed significant deviations in the manner in which sound propagates under the modeled conditions. For example, the differences in the deep gradient seen in the background sound velocity fit for the warm-core eddy resulted in major changes in the cycle distance of rays propagating under these conditions. It was therefore judged that the model in its present form was unacceptable for acoustic analysis, and that the most accurate assessment of the acoustic properties of these eddies would result from direct use of the measured oceanographic data. The following acoustic analysis therefore is restricted to analysis of these data.

Section 7
ACOUSTIC ANALYSIS

7.1. Introduction

The underlying purpose behind the following acoustic analysis is to assess the acoustic impact of mesoscale fluctuations as a function of varying source-receiver geometry and source frequency. To that end, two tracks have been constructed for use in propagation modeling. The tracks contain the static or background sound velocity profiles at their start. The background profiles are extended for 185 km. Immediately following this range-independent 185 km is a section of track containing an eddy, either the warm- or cold-core eddy from the Schenectady or Bristol County track, respectively. The diameter of both eddies was approximately 370 km. Following the eddy, there is another 185 km of background sound velocity conditions. We therefore have constructed two acoustic tracks, consisting of 185 km of range-independent conditions, followed by 370 km of track containing an eddy (warm or cold), followed by an additional 185 km of range-independent track. For comparative purposes, a totally range-independent track has been constructed, where the background sound velocity profile which exists at 0 km is extended for the length of the track, in this instance 740 km.

To evaluate the impact of varying source-receiver geometry, we have selected four different situations. The first has the source located at 0 km at the start of the totally range-independent track. The second geometry has

the source located at 0 km. along the range-dependent track; i.e., the track containing either the warm or the cold eddy. The third geometry has the source one-half of a convergence zone closer to the eddy, placing it at 30 km along the range-dependent track. Finally, the effect of the source located at the eddy center along the range-dependent track has been considered. The depth of this source was held constant at 30 m throughout this analysis. The receiver depths considered were 95, 450, 700, and 900 m. Three representative frequencies were selected for analysis. Those frequencies were 20, 300, and 1000 Hz. The Parabolic Equation (PE) model has been used to model propagation loss (Tappert and Hardin, 1973; Tappert, 1974; Brock, 1978).

7.2 Cold Eddy 20 Hz.

Transmission loss calculations as a function of horizontal range (in km) for a 20 Hz source located at 30 m as seen by a receiver located at 95 m may be seen in Figure 14. Transmission loss has been calculated for each of the source-receiver geometries discussed previously, viz., a totally range-independent environment, a range-dependent environment with the source located at 0 km, a range-dependent environment with the source located at 30 km, and for a range-dependent environment with the source located at the center of the eddy. For clarity of presentation, the transmission loss curves have been averaged over a horizontal range of one convergence zone, 60 km. Thus, only variations occurring on a scale greater than 60 km are evident in these plots. In general, all four source-receiver geometries considered here experienced similar

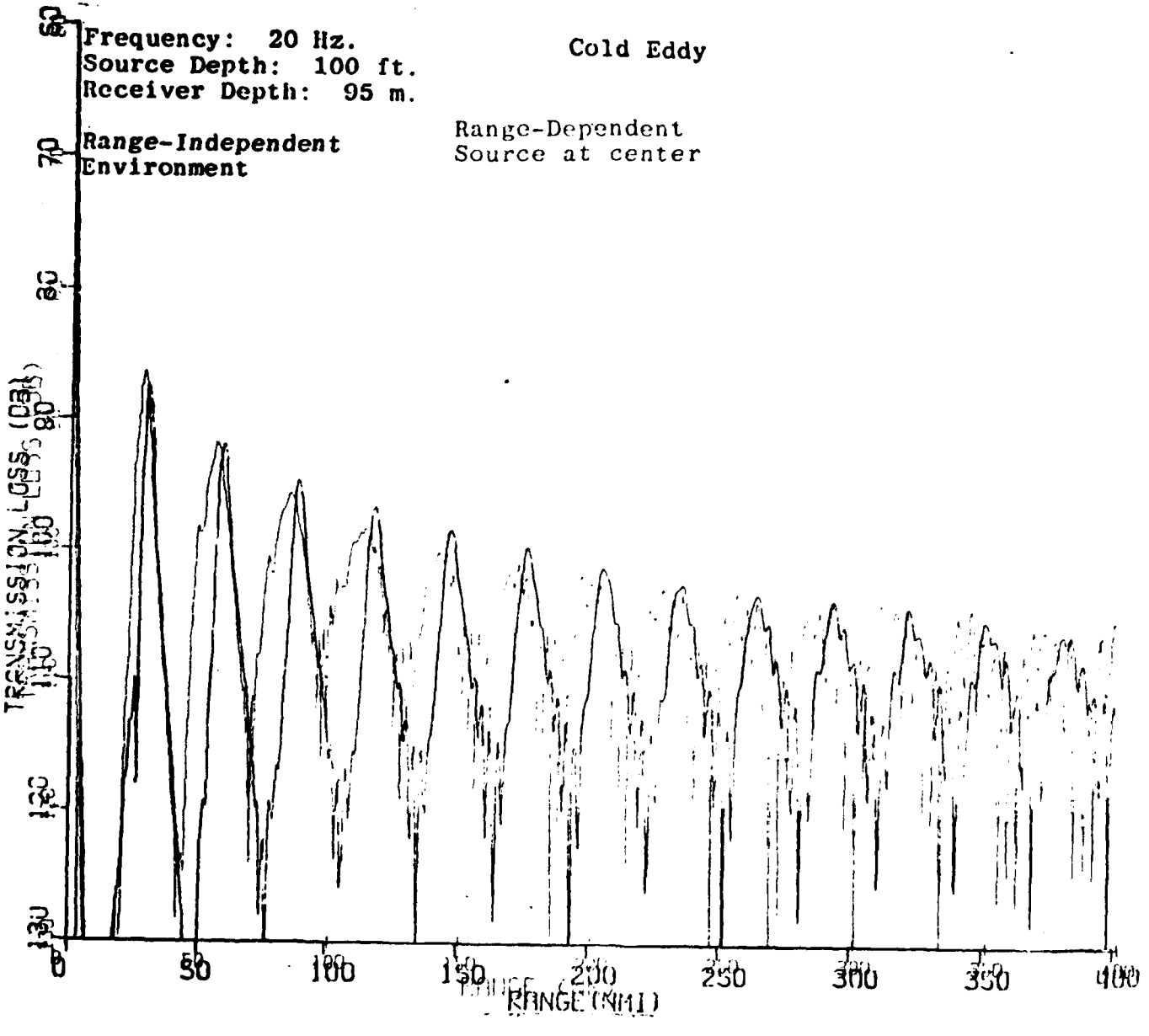
Frequency: 20 Hz.
Source Depth: 100 ft.
Receiver Depth: 95 m.
Range-Independent Environment
Cold Eddy
Range-Dependent
Source at center
TRANSMISSION LOSS (DB)
RANGE (NMI)
0
50
100
150
200
250
300
350
400

Figure 14

levels of transmission loss. The track with the source located at the eddy center experiences 1 - 2 dB less loss than the other source receiver geometries. This is particularly evident in the first 280 km of the track. Also of note is the close correspondence between the range-dependent environment with the source at 0 nm. and the one in which the source is located one half of a convergence zone further into the track, at 30 km.

Unaveraged transmission loss, corresponding to the totally range independent environment and the range dependent environment with the source at the eddy center from Figure 14, may be seen in Figure 15. The convergence zones in the range-independent environment remain narrow, well-defined, and clearly discernable for the length of the track. In contrast, the convergence zones in the range-dependent environment with the source at the eddy center broaden rapidly and show evidence of increasing multipath at the farther ranges. While the peak energy levels in the range-independent case are higher than those in the range-dependent environment, the broader convergence zones in the range-dependent case result in this environment containing more energy, on average, than the range-independent case. This was shown in Figure 14.

Moving the receiver slightly deeper in the water column, to 450 m, produces transmission loss seen in Figure 16. Here we see that the range dependent environment with the source at the eddy center shows clearly less loss than the other environments considered. The totally range independent environment exhibits the highest loss levels, at times as much as 7 dB more than the environment with the

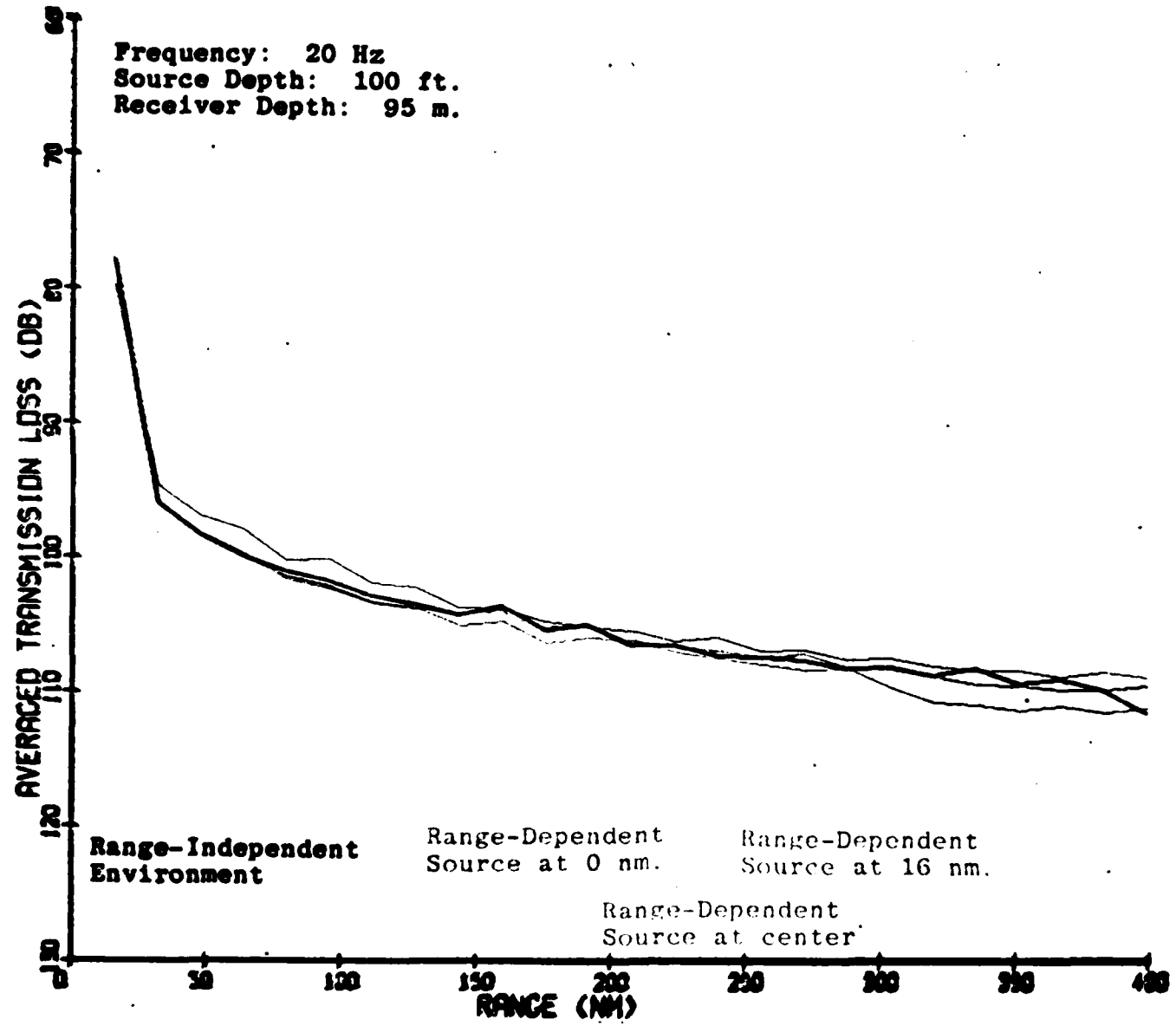
Frequency: 20 Hz
Source Depth: 100 ft.
Receiver Depth: 95 m.
AVERAGED TRANSMISSION LOSS (DB)
70
80
90
100
110
120
130
0
50
100
150
200
250
300
350
400
RANGE (NM)
Range-Independent Environment
Range-Dependent Source at 0 nm.
Range-Dependent Source at 16 nm.
Range-Dependent Source at center

Figure 15

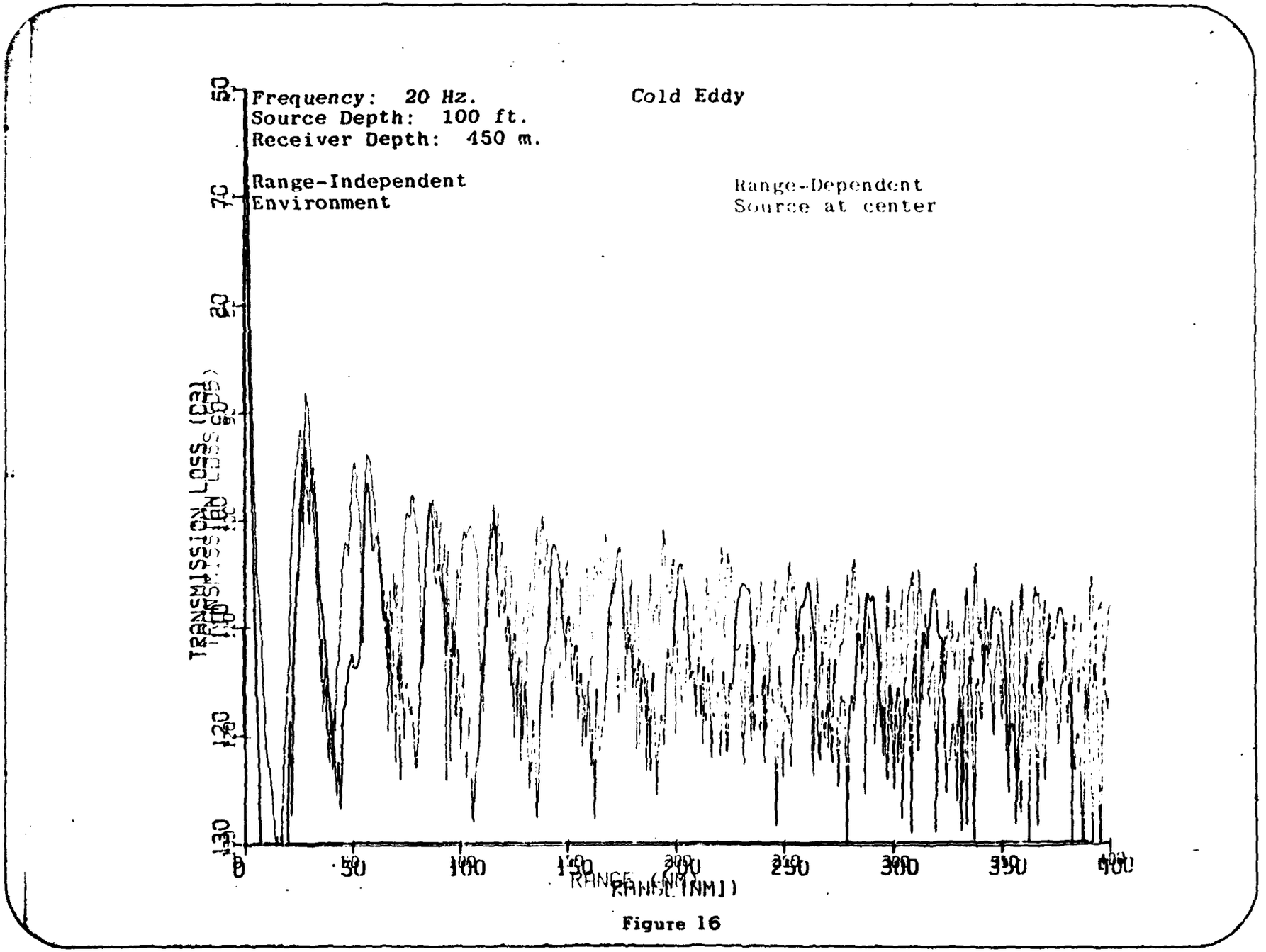
Frequency: 20 Hz.
Source Depth: 100 ft.
Receiver Depth: 450 m.
Range-Independent
Environment
Cold Eddy
Range-Dependent
Source at center
TRANSMISSION LOSS (DB)
50
70
90
110
130
0
50
100
150
200
250
300
350
400
RANGE (NM)

Figure 16

source at the eddy center. This is also evident in Figure 17, which shows unaveraged transmission loss for the two extreme cases, the range-independent environment and the range-dependent environment with the source at the eddy center. Convergence zones in the range dependent case shift and overlap early in the track. Further, there are many additional arrivals seen in the range-dependent track that are absent in the range-independent environment. These conditions result in the overall lower level of propagation loss seen in the range-dependent environment.

Figure 18, which demonstrates the effect of a receiver positioned at 700 m, near the sound channel axis, shows similar findings. Once again, the range-dependent environment with the source at the eddy center clearly exhibits less loss. A receiver located at 900 m (Figure 19) shows the same trends.

7.3 Warm Eddy 20 Hz.

Corresponding transmission loss figures for a warm eddy may be seen in Figures 20 - 23. Figure 20, which shows the effect of a receiver positioned at 95 m in the water column, shows a relationship between source-receiver geometry which is the inverse of that seen in the cold-core eddy. In this instance, the range-dependent environment with the source at the eddy center shows consistently higher levels of loss than do the other environments. The range-independent environment in this instance shows consistently less loss. These differences are even more apparent when considering a receiver located at 450 meters

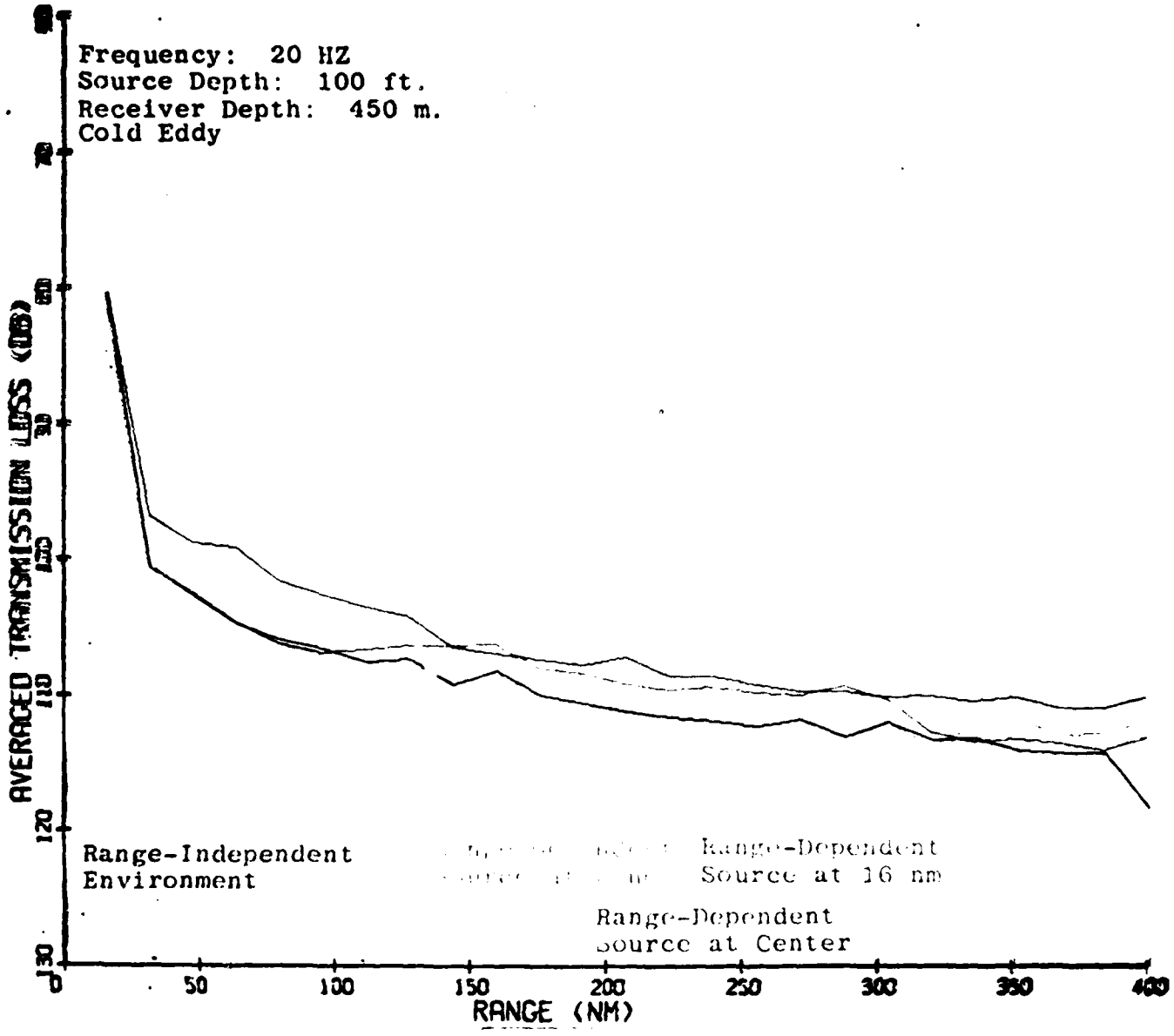
Frequency: 20 HZ
Source Depth: 100 ft.
Receiver Depth: 450 m.
Cold Eddy
AVERAGED TRANSMISSION LOSS (DB)
RANGE (NM)
0
50
100
150
200
250
300
350
400
Range-Independent
Environment
Range-Dependent
Source at 16 nm
Range-Dependent
Source at Center

Figure 17

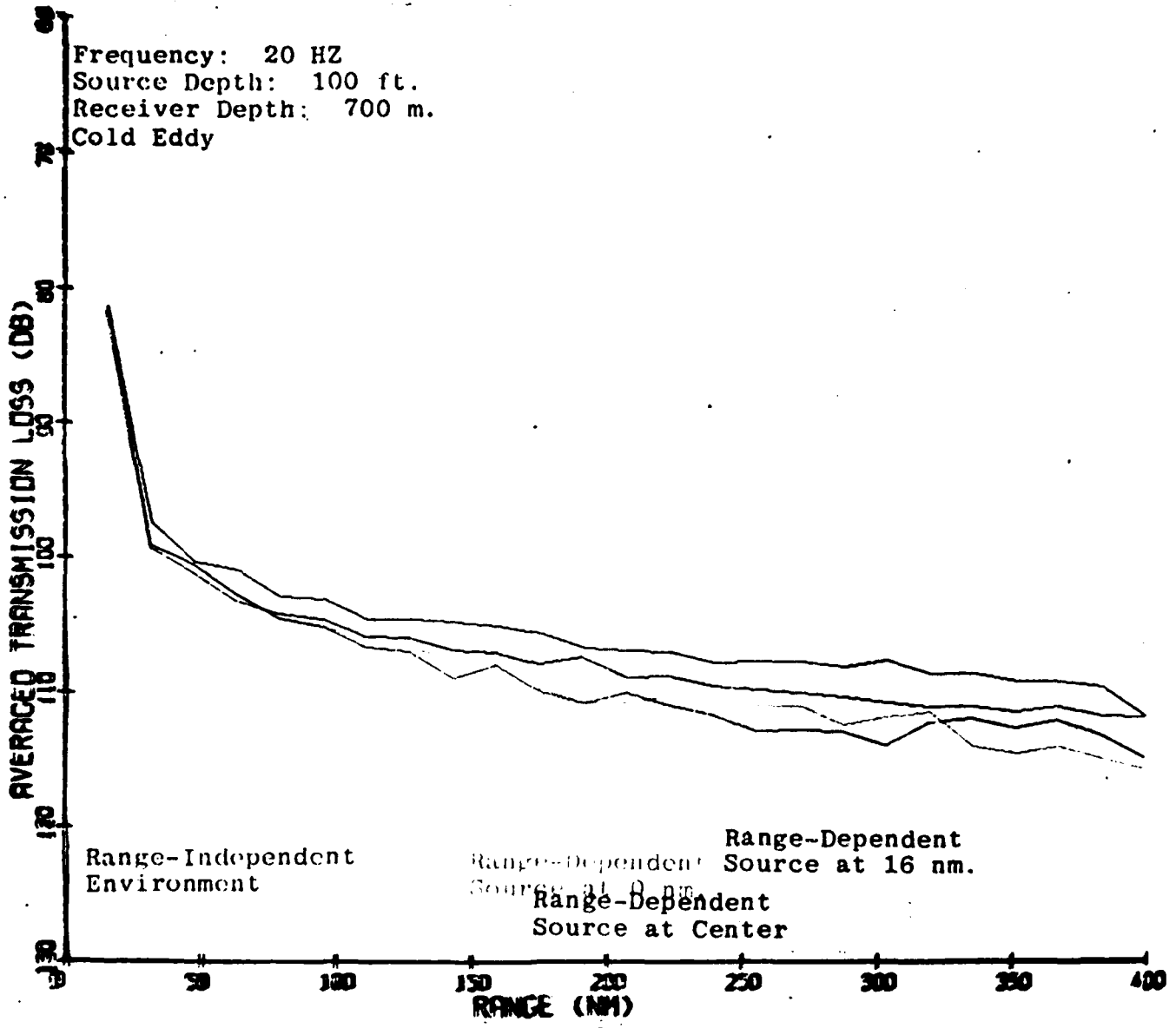
Frequency: 20 HZ
Source Depth: 100 ft.
Receiver Depth: 700 m.
Cold Eddy
AVERAGED TRANSMISSION LOSS (DB)
70
80
90
100
110
120
130
0
50
100
150
200
250
300
350
400
RANGE (NM)
Range-Independent
Environment
Range-Dependent
Source at 16 nm.
Range-Dependent
Source at Center

Figure 18

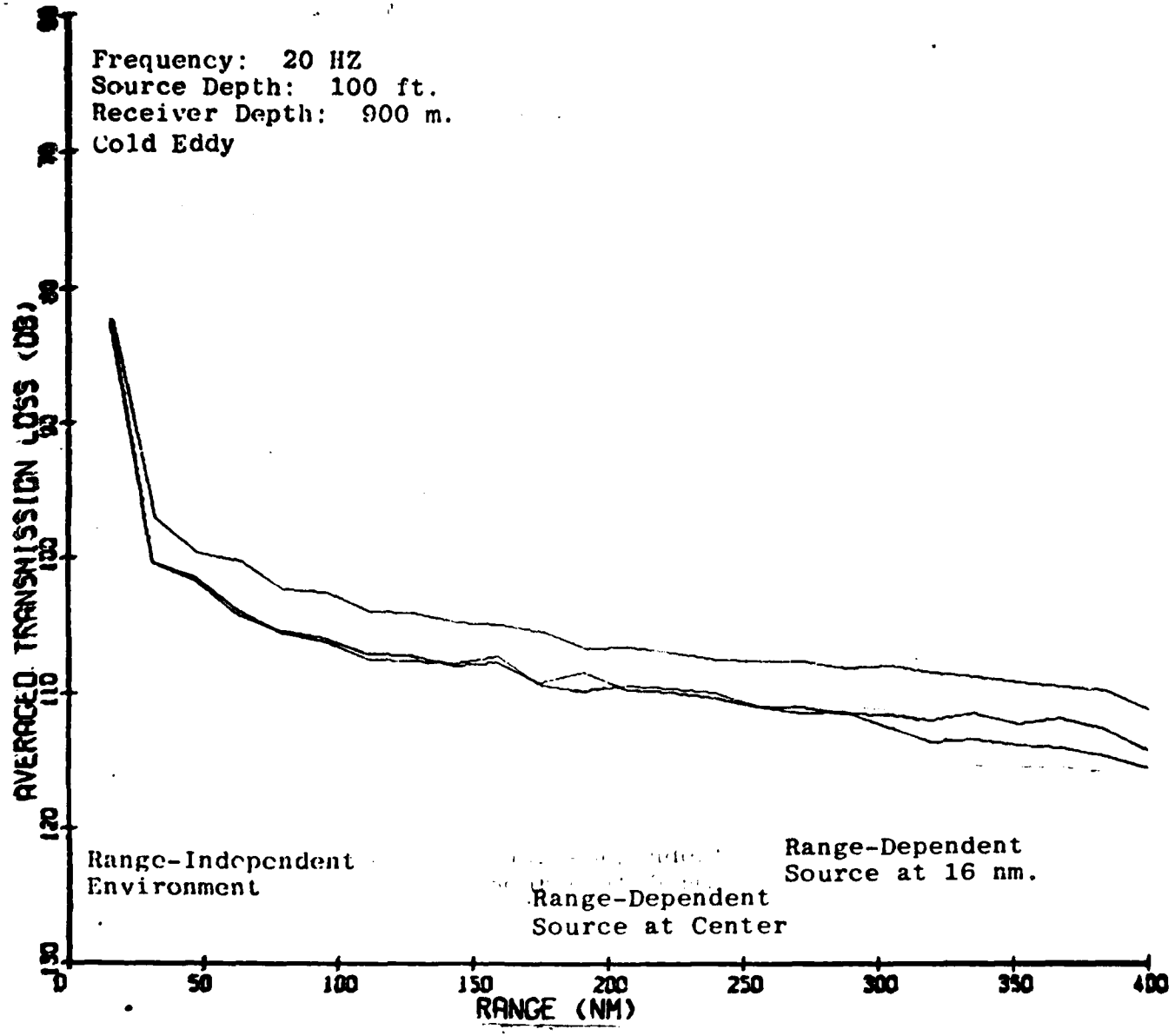
Frequency: 20 HZ
Source Depth: 100 ft.
Receiver Depth: 900 m.
Cold Eddy
AVERAGED TRANSMISSION LOSS (DB)
90
100
110
120
130
0
50
100
150
200
250
300
350
400
RANGE (NM)
Range-Independent
Environment
Range-Dependent
Source at Center
Range-Dependent
Source at 16 nm.

Figure 19

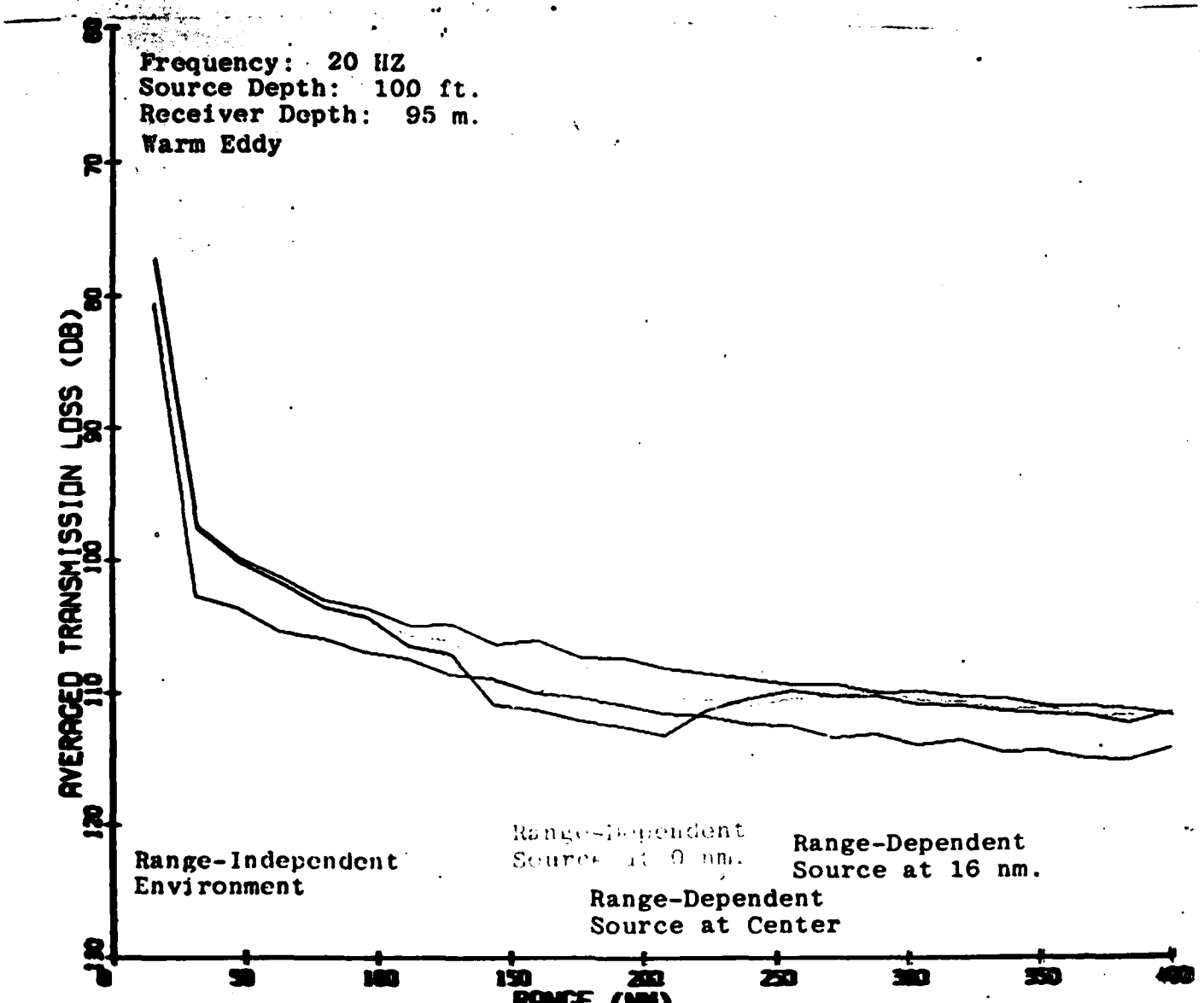
Frequency: 20 HZ
Source Depth: 100 ft.
Receiver Depth: 95 m.
Warm Eddy
AVERAGED TRANSMISSION LOSS (DB)
70
80
90
100
110
120
130
0
50
100
150
200
250
300
350
400
RANGE (NM)
Range-Independent Environment
Range-Dependent Source at Center
Range-Dependent Source at 16 nm.

Figure 20

in the water column (Figure 21). In this instance, the difference in transmission loss between the range-dependent environment with the source at the eddy center relative to the other geometries considered may be as much as 10 dB, with the source at the eddy center experiencing higher levels of loss within the warm eddy. Moving deeper in the water column, a receiver located at 700 m (Figure 22) shows the same general trends, although the differences between the various geometries are not as marked. Figure 23 shows transmission loss through a warm-core eddy for a receiver depth of 900 m. Again, the relative levels of transmission loss are consistent with previous observation. The environment with the source positioned at the eddy center shows as much as 5 dB more loss relative to the other environments.

Comparison of Figures 20 - 23 shows the effect of increasing receiver depth on transmission loss. It is apparent from a comparison of these figures how the distribution of energy changes as a function of receiver depth. The relative levels of transmission loss for each of the four environments considered here remain consistent at each receiver depth. In general, the effect of shifting the source half a convergence zone from 0 to 30 km is negligable. In fact, the transmission loss curves for these two cases often resemble closely that for a range-independent environment. Consequently, for the remainder of this analysis, only the two most extreme cases will be considered, viz., the range-dependent environment with the source located at the eddy center and the totally range-independent track.

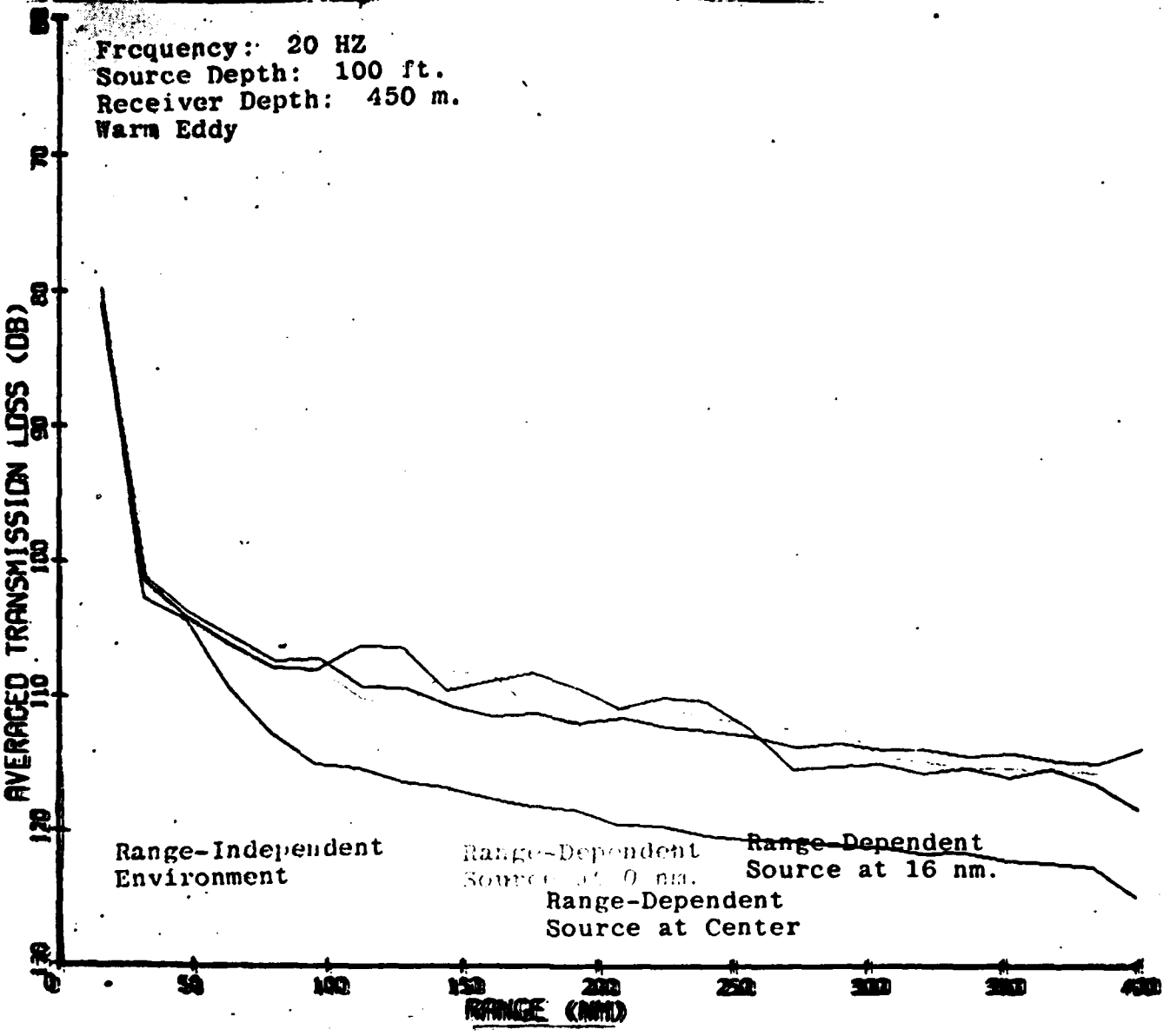
Frcquency: 20 HZ
Source Depth: 100 ft.
Receiver Depth: 450 m.
Warm Eddy
AVERAGED TRANSMISSION LOSS (DB)
70
80
90
100
110
120
130
RANGE (NM)
Range-Independent Environment
Range-Dependent Source at 0 nm.
Range-Dependent Source at Center
Range-Dependent Source at 16 nm.

Figure 21

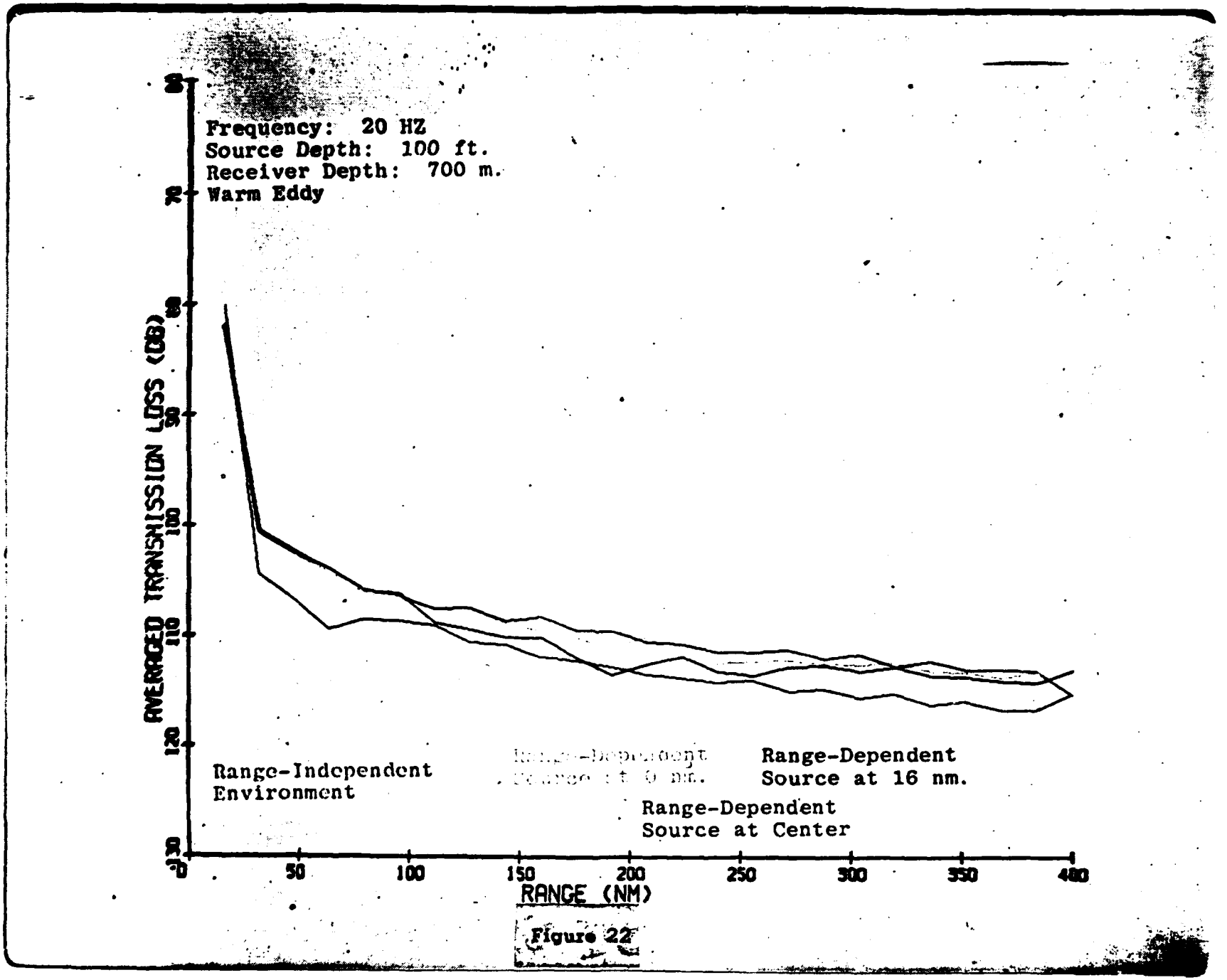
Frequency: 20 HZ
Source Depth: 100 ft.
Receiver Depth: 700 m.
Warm Eddy
AVERAGED TRANSMISSION LOSS (DB)
70
80
90
100
110
120
130
0
50
100
150
200
250
300
350
400
RANGE (NM)
Range-Independent
Environment
Range-Dependent
Source at 16 nm.
Range-Dependent
Source at Center

Figure 22

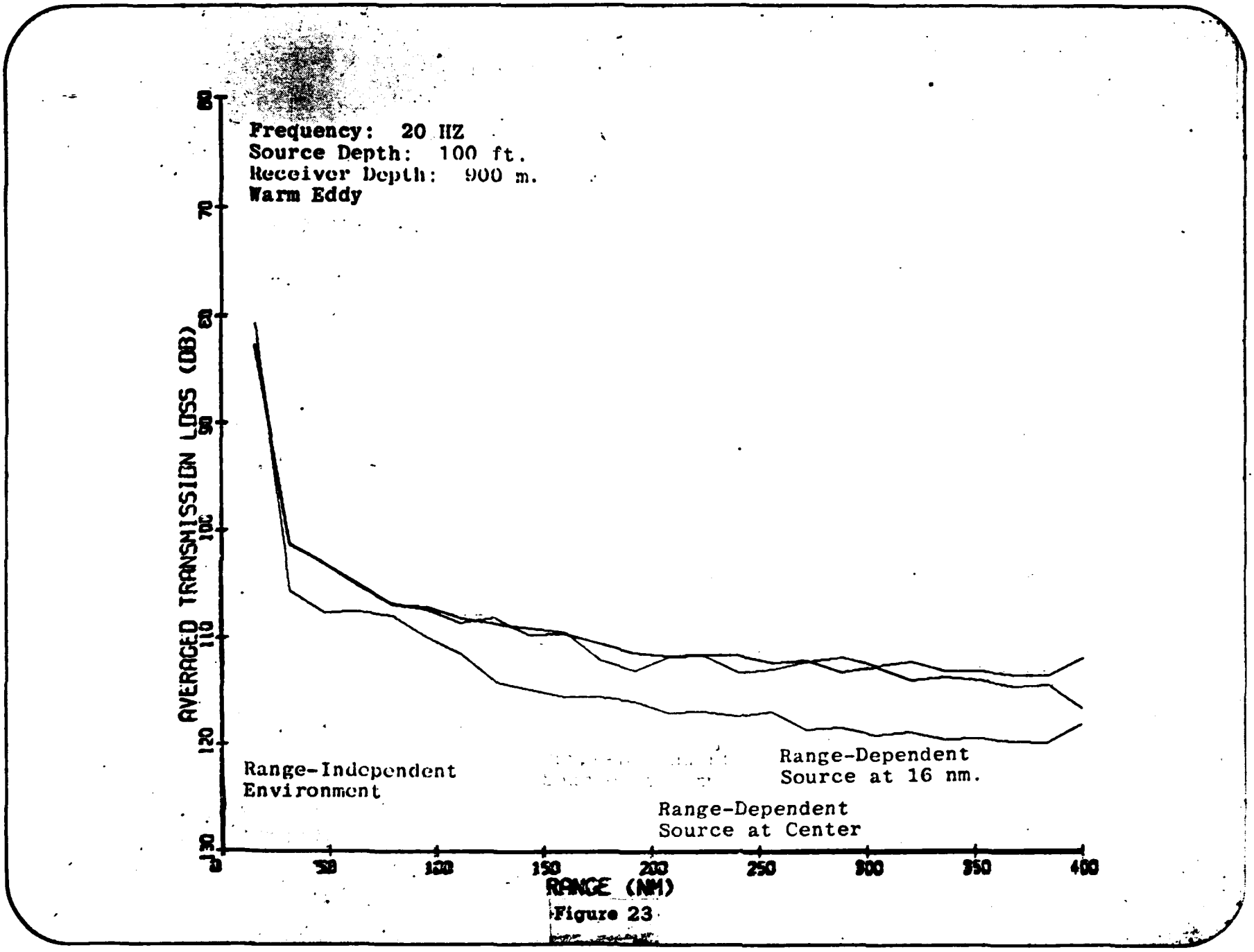
Frequency: 20 HZ
Source Depth: 100 ft.
Receiver Depth: 900 m.
Warm Eddy
AVERAGED TRANSMISSION LOSS (DB)
70
90
110
120
RANGE (NM)
Range-Independent
Environment
Range-Dependent
Source at 16 nm.
Range-Dependent
Source at Center

Figure 23

7.4 Cold Eddy 300 Hz.

An examination of the differences in transmission loss for these same source-receiver geometries at 300 Hz reveals some interesting findings. For the receiver located at 95 m (Figure 24), the range-dependent environment with the source at the eddy center shows 2 - 3 dB more loss than the range-independent environment. This is the reverse of what was seen earlier for the cold eddy case at 20 Hz. This is somewhat of an anomalous observation, as this reversal of the relationship exists only for this case and is seen in no other instance.

Moving to a receiver depth of 450 m, (Figure 25) it may be seen that this relationship has reversed itself, and, once again, the range-dependent environment with the source at the eddy center shows consistently less loss than the range-independent environment. Figures 26 and 27, showing transmission loss for receivers located at 700 and 900 m, respectively, echo these findings. In general, the difference between the two environments is less dramatic at 300 Hz than at 20 Hz.

7.5 Warm Eddy 300 Hz.

Propagation through a warm-core eddy at 300 Hz shows similarly consistent findings. For a receiver located at 95 m (Figure 28), the range-dependent environment with the source at the eddy center generally shows more loss than does the range-independent environment, with the exception of the first 50 nm of the track. This difference

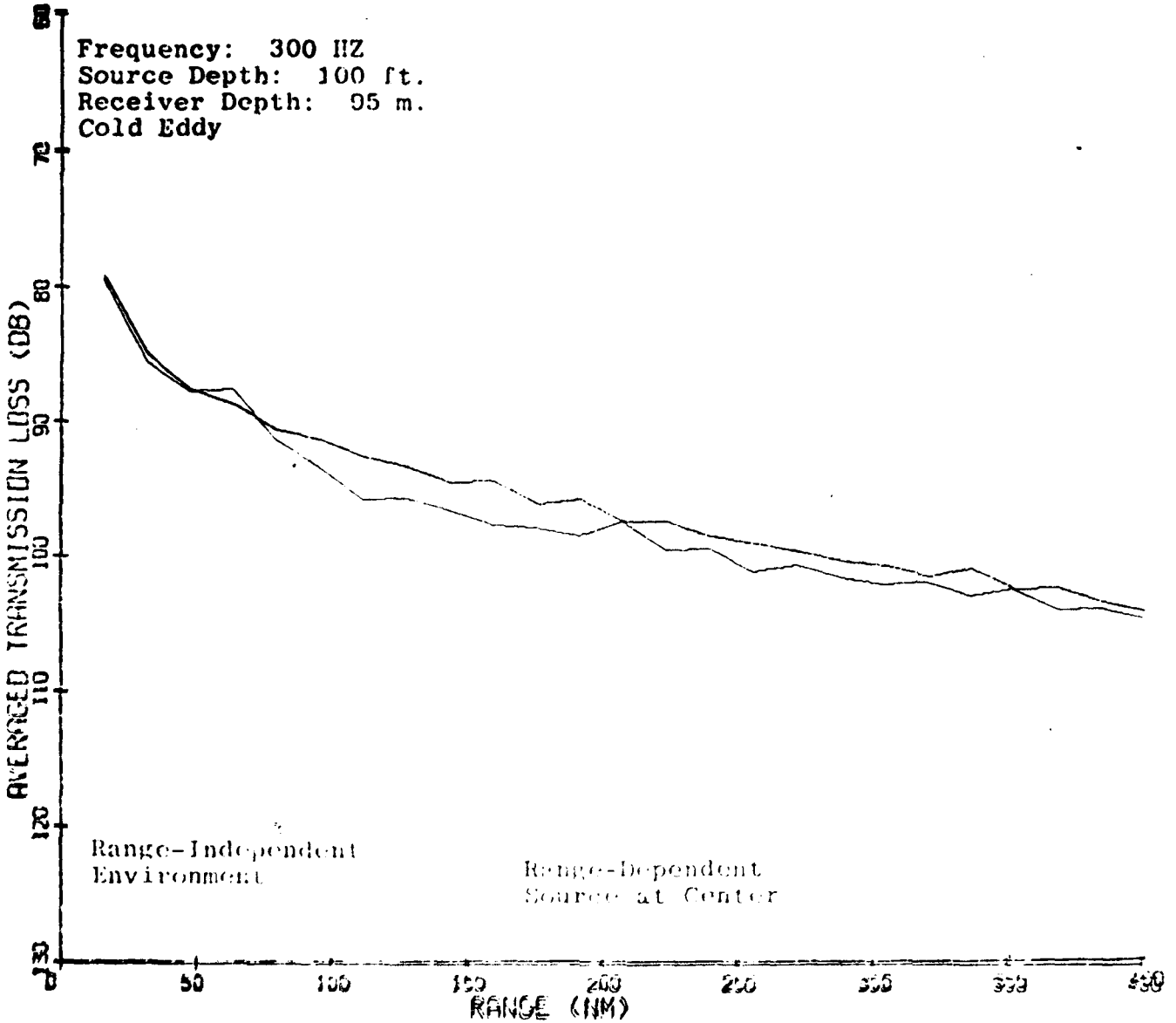
Frequency: 300 HZ
Source Depth: 100 ft.
Receiver Depth: 95 m.
Cold Eddy
AVERAGED TRANSMISSION LOSS (DB)
70
80
90
100
110
120
130
0
50
100
150
200
250
300
350
400
RANGE (NM)
Range-Independent
Environment
Range-Dependent
Source at Center

Figure 24

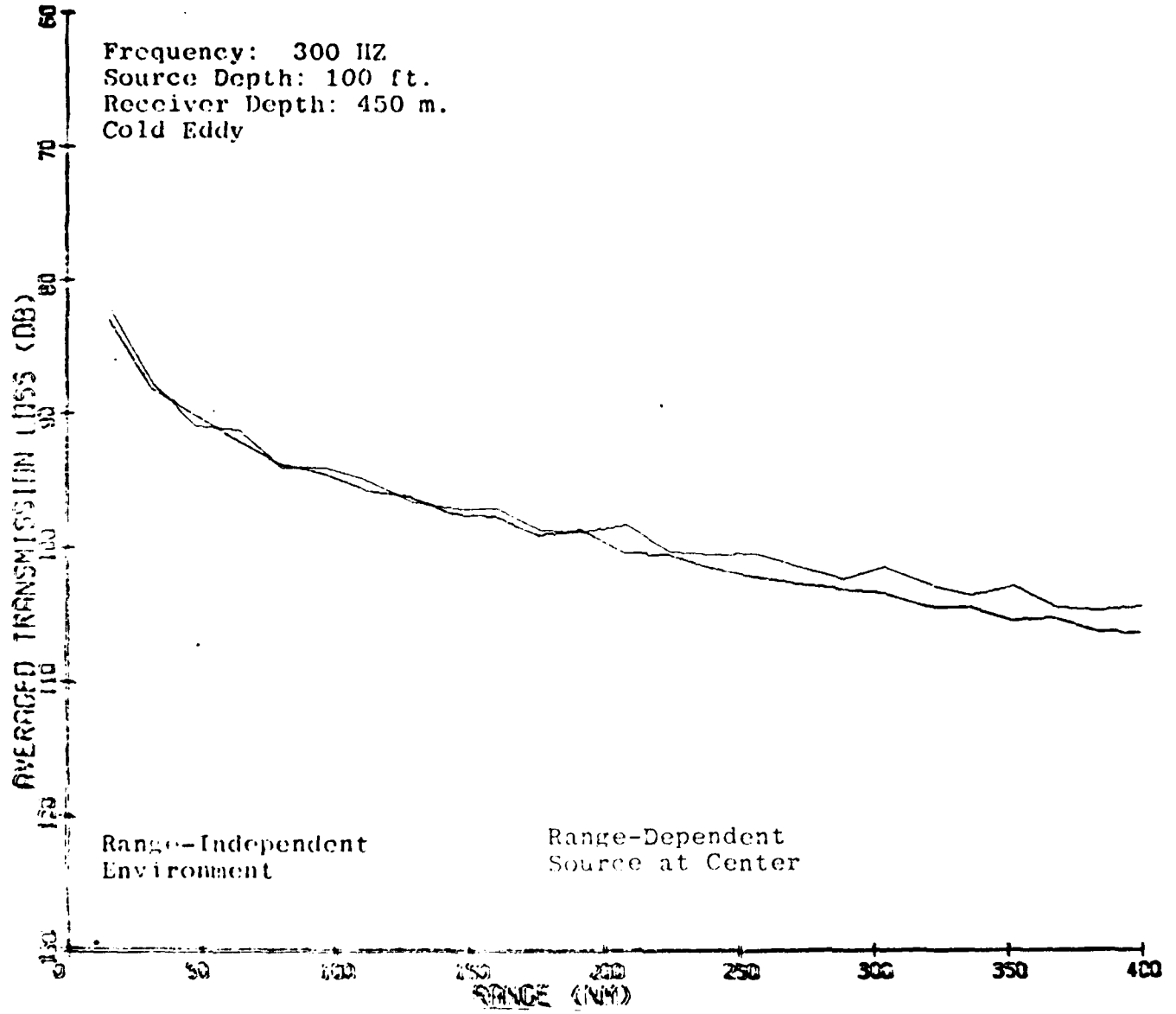
Frequency: 300 HZ
Source Depth: 100 ft.
Receiver Depth: 450 m.
Cold Eddy
AVERAGED TRANSMISSION LOSS (DB)
70
90
110
50
250
300
350
400
Range-Independent
Environment
Range-Dependent
Source at Center

Figure 25

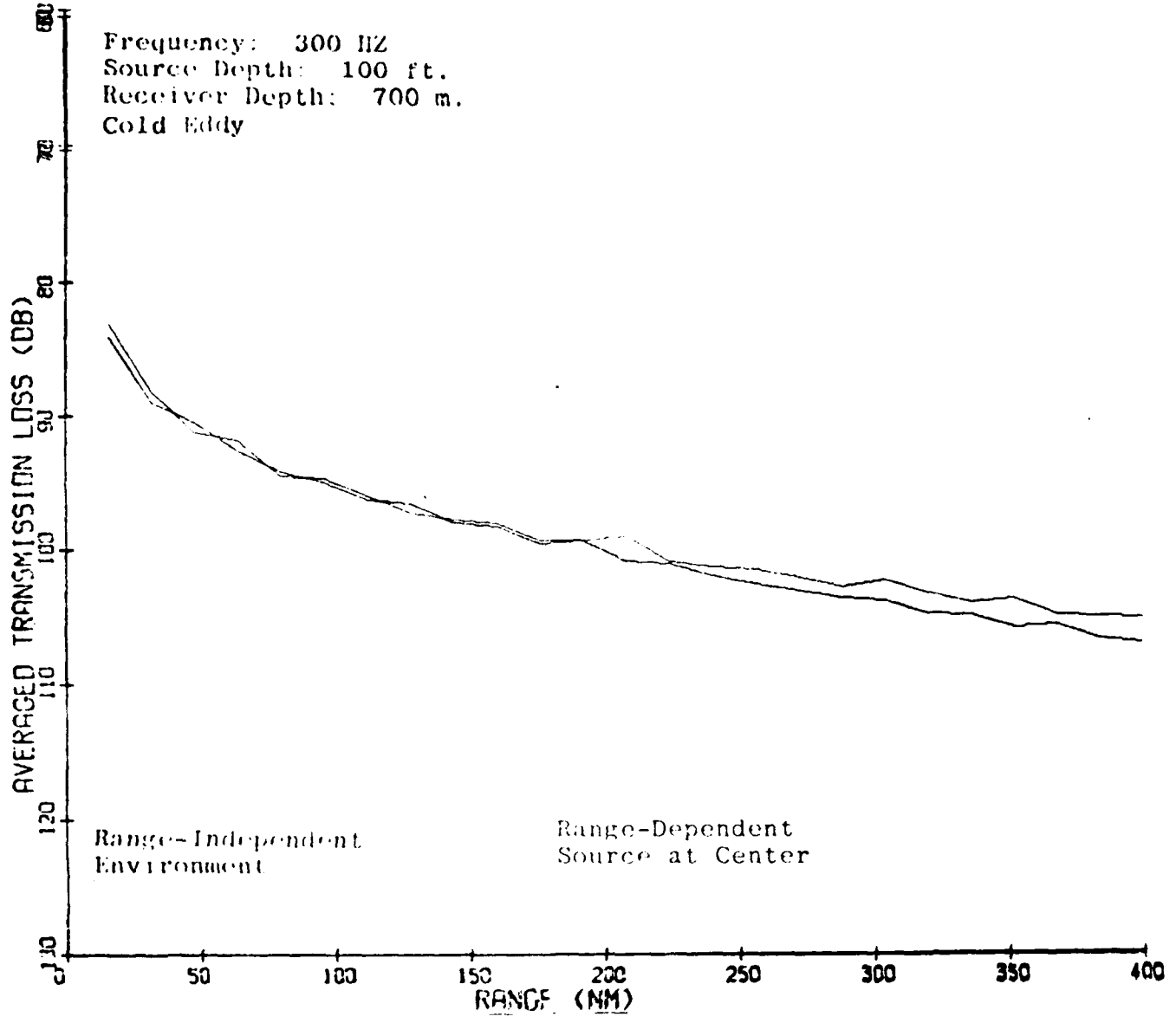
Frequency: 300 HZ
Source Depth: 100 ft.
Receiver Depth: 700 m.
Cold Eddy
AVERAGED TRANSMISSION LOSS (DB)
70
80
90
100
110
120
130
0
50
100
150
200
250
300
350
400
RANGE (NM)
Range-Independent
Environment
Range-Dependent
Source at Center

Figure 26

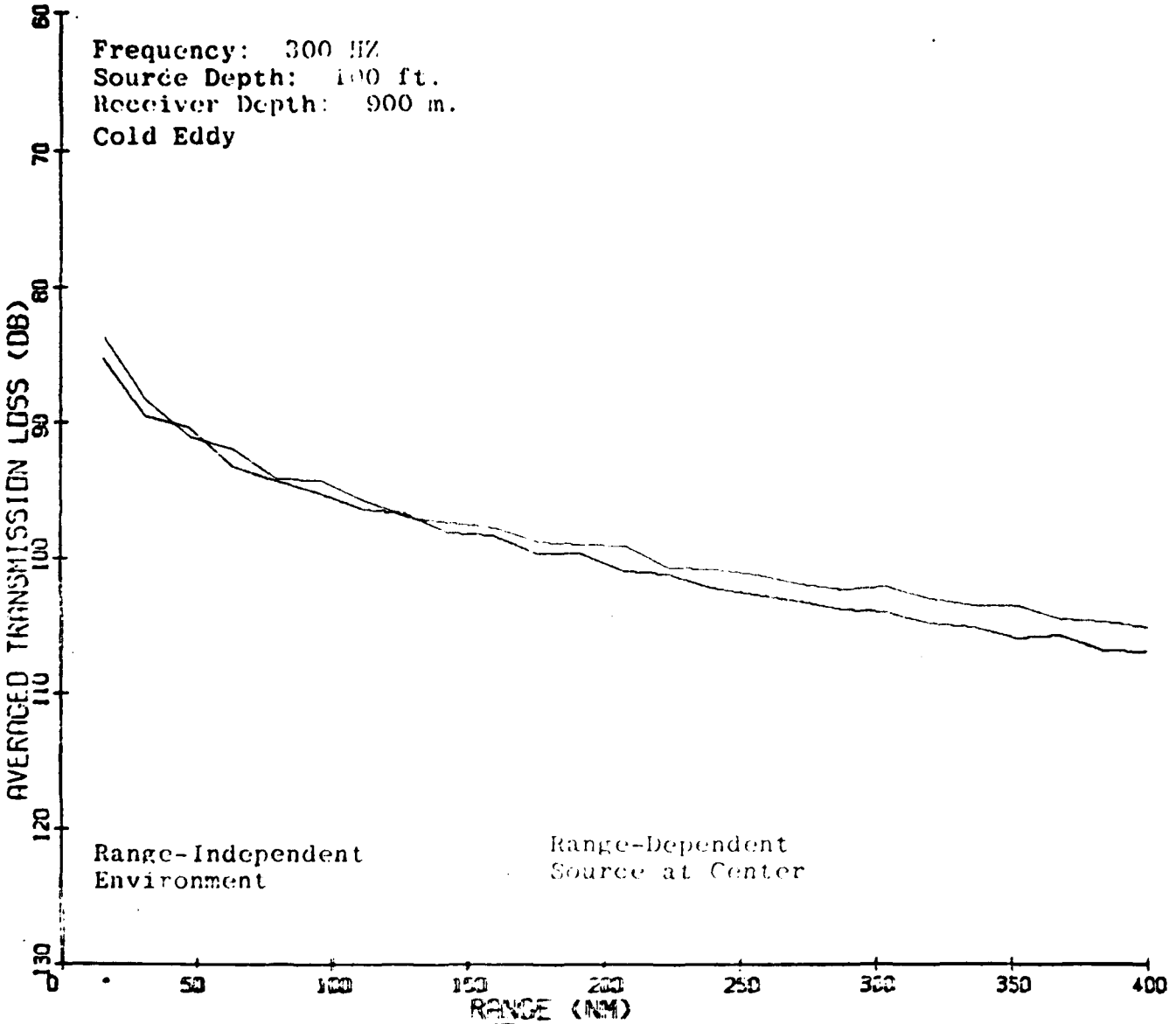
Frequency: 300 HZ
Source Depth: 100 ft.
Receiver Depth: 900 m.
Cold Eddy
AVERAGED TRANSMISSION LOSS (DB)
60
70
80
90
100
110
120
130
0
50
100
150
200
250
300
350
400
RANGE (NM)
Range-Independent
Environment
Range-Dependent
Source at Center

Figure 27

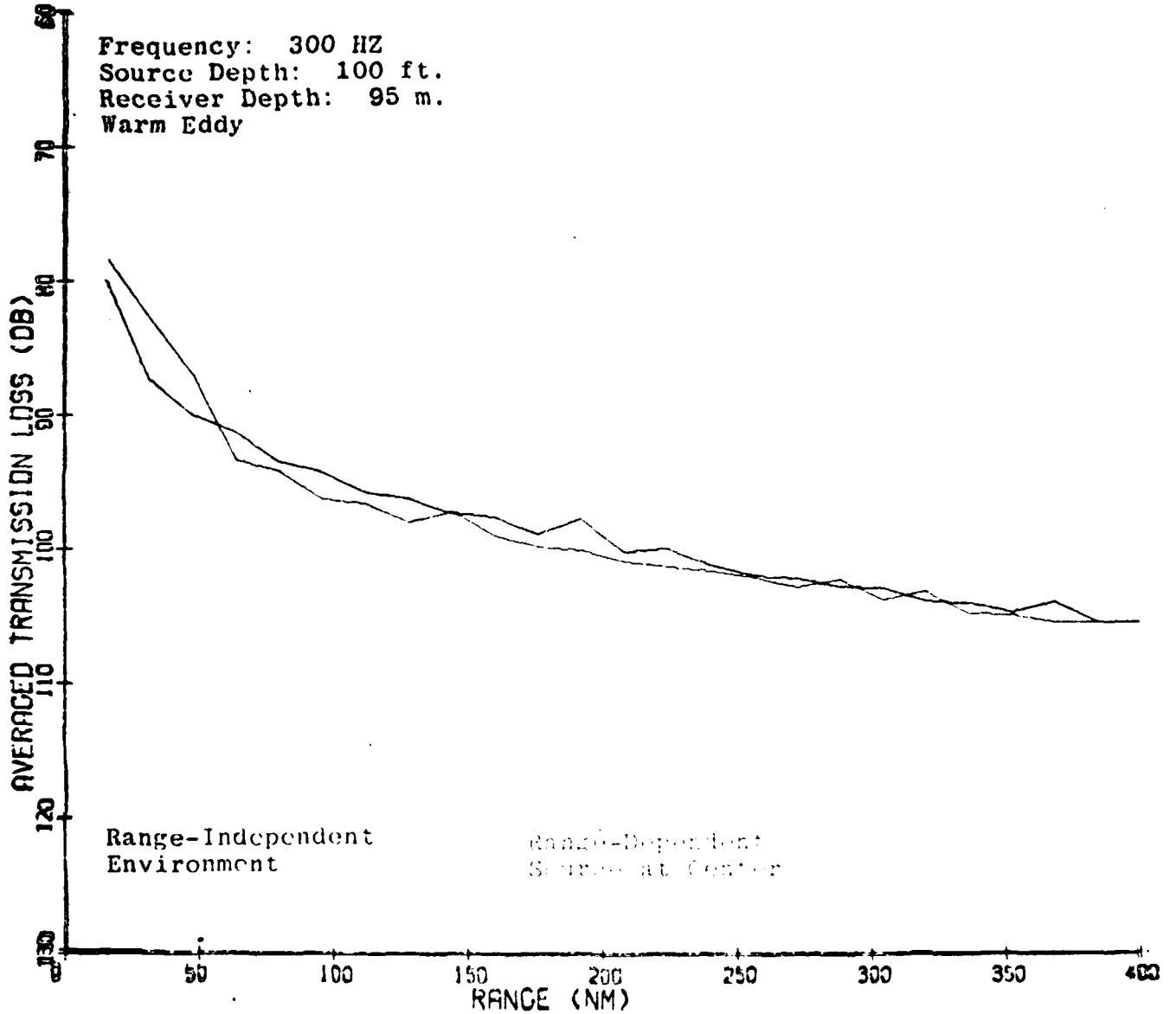
Frequency: 300 HZ
Source Depth: 100 ft.
Receiver Depth: 95 m.
Warm Eddy
AVERAGED TRANSMISSION LOSS (DB)
70
80
90
100
110
120
130
Range-Independent
Environment
0
50
100
150
200
250
300
350
400
RANGE (NM)

Figure 28

is understandable when we look at Figure 29, which shows the unaveraged transmission loss plots for the same environment. Transmission loss for the source at the eddy center shows the presence of a surface duct in the first 90 km of the track. Energy remains trapped in this duct: thus, the observed transmission loss for this range-dependent environment is actually lower than the corresponding range-independent environment. Figure 30, which shows transmission loss for a receiver at 450 m, indicates that transmission loss is consistently higher for the range-dependent environment with the source at the eddy center. It is clear that the surface duct does not extend to this depth, as transmission loss is lower for the source at the eddy center, even in the first 50 nm of the track. Figures 31 and 32, for receiver depths at 700 and 900 m, echo these findings.

7.6 Cold Eddy 1000 Hz.

Figure 33 shows transmission loss at 1 kHz through the cold eddy for a receiver depth of 95 m and the source at the eddy center. In the first 185 km of the track, the range-dependent environment shows less loss than does the range-independent environment. This trend reverses itself past 185 km, with the range-dependent environment showing slightly more loss by the end of the track. The markedly higher level of transmission loss at 1 kHz compared to 300 Hz is due primarily to volume attenuation, which plays a significant role at 1 kHz. Over the length of a 370 km track, volume attenuation, computed by Thorp's Equation, is approximately 25 dB. Volume attenuation plays a smaller role at 300 Hz, amounting to only 5 dB attenuation over a 400 nm track.

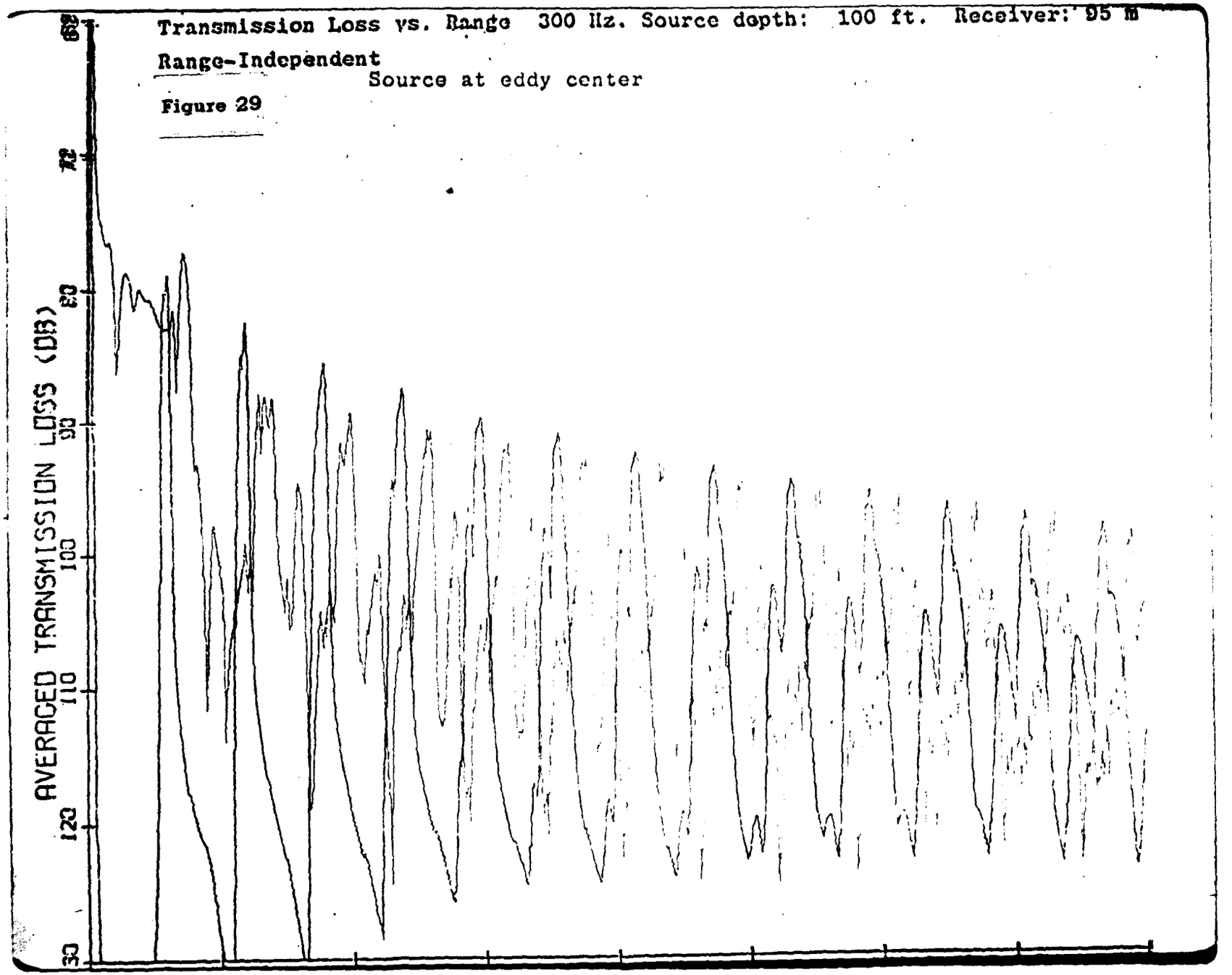
Transmission Loss vs. Range 300 Hz. Source depth: 100 ft. Receiver: 95 m
Range-Independent
Source at eddy center
AVERAGED TRANSMISSION LOSS (DB)
60
70
80
90
100
110
120
130

Figure 29

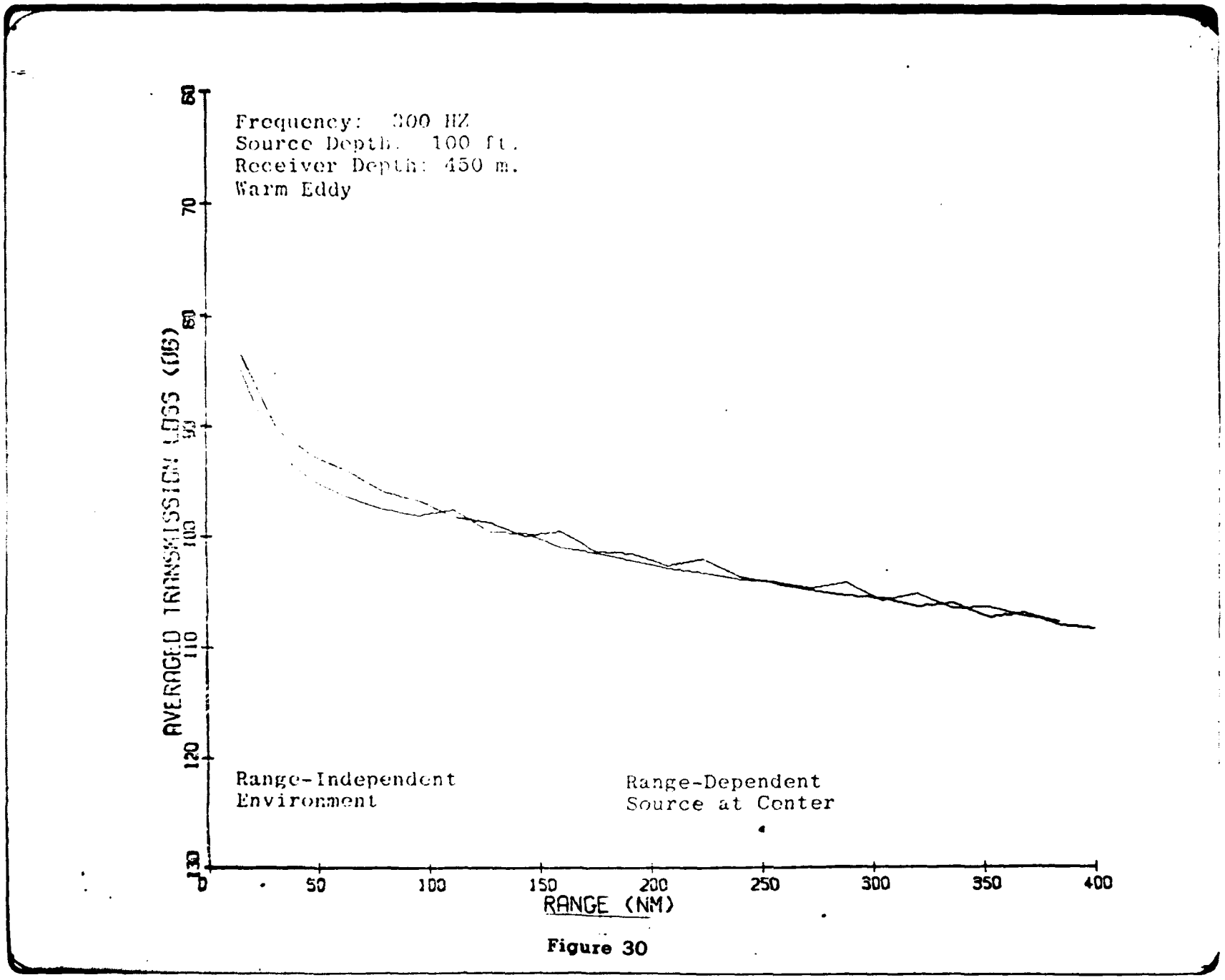
Frequency: 300 HZ
Source Depth: 100 ft.
Receiver Depth: 450 m.
Warm Eddy
AVERAGED TRANSMISSION LOSS (DB)
60
70
80
90
100
110
120
130
Range-Independent
Environment
Range-Dependent
Source at Center
0
50
100
150
200
250
300
350
400
RANGE (NM)

Figure 30

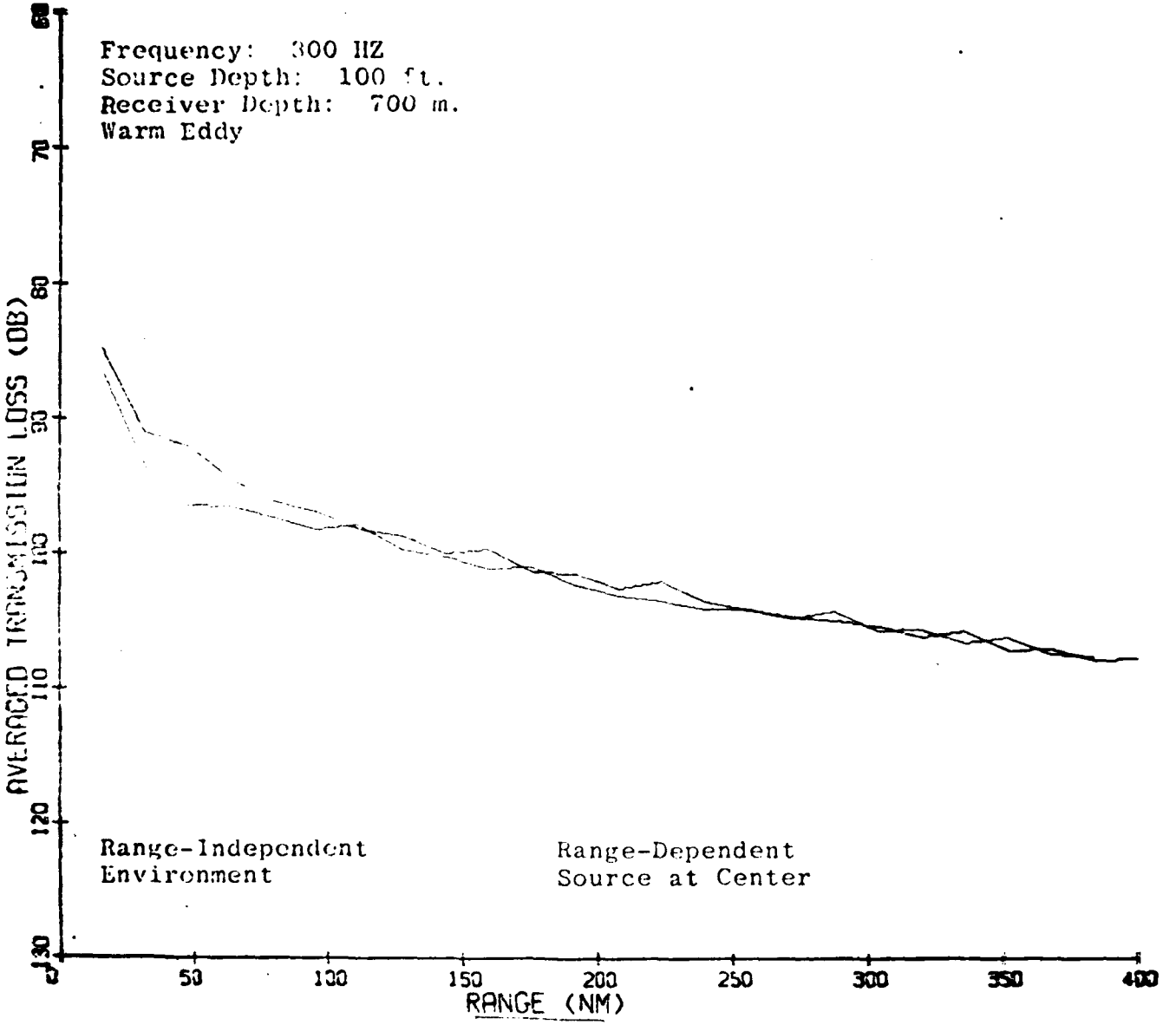
Frequency: 300 HZ
Source Depth: 100 ft.
Receiver Depth: 700 m.
Warm Eddy
AVERAGED TRANSMISSION LOSS (DB)
70
80
90
100
110
120
130
Range-Independent
Environment
Range-Dependent
Source at Center
50
100
150
200
250
300
350
400
RANGE (NM)

Figure 31

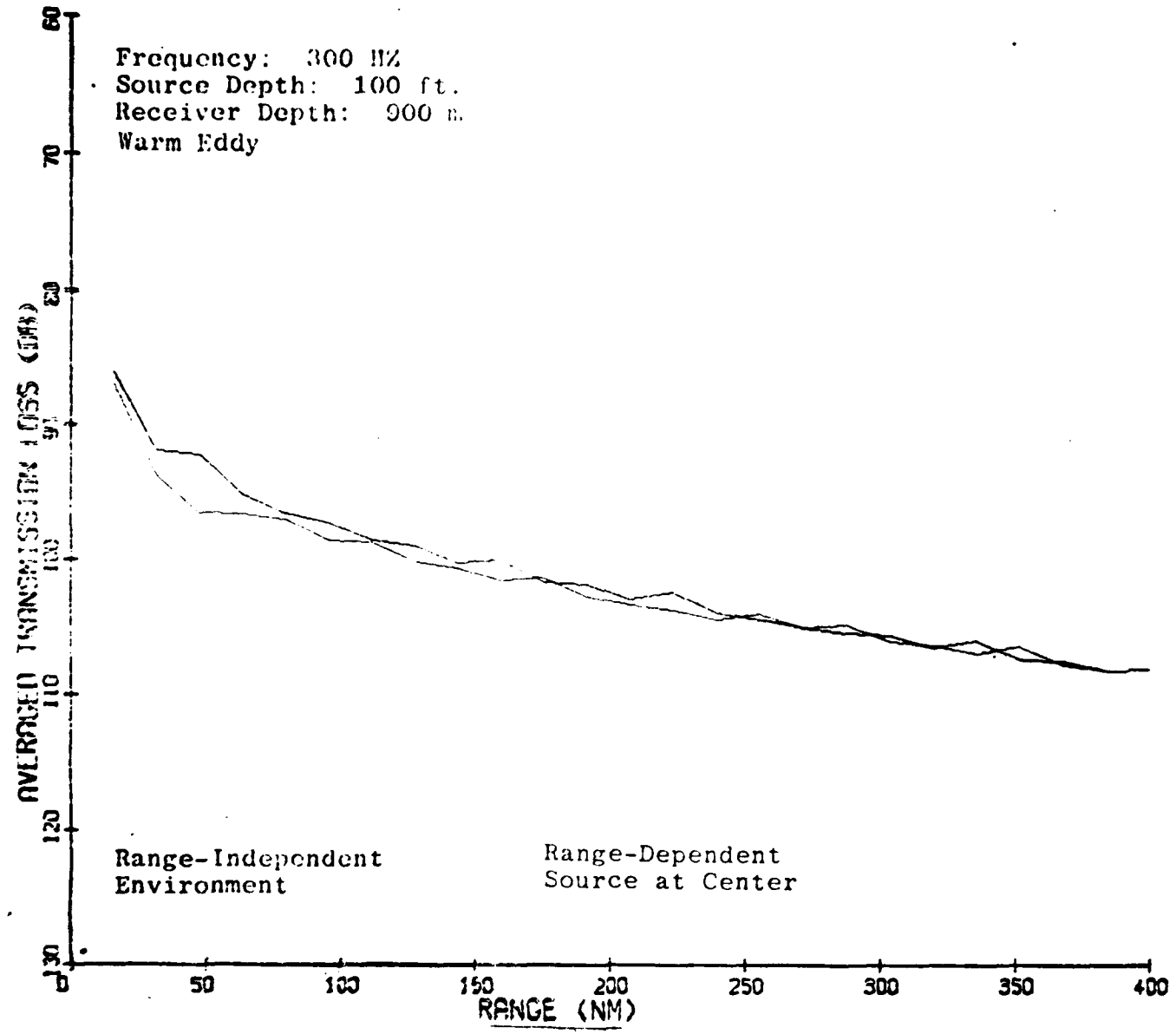
Frequency: 300 HZ
Source Depth: 100 ft.
Receiver Depth: 900 ft.
Warm Eddy
OVERRAGED TRANSMISSION LOSS (DB)
60
70
80
90
100
110
120
130
0
50
100
150
200
250
300
350
400
RANGE (NM)
Range-Independent
Environment
Range-Dependent
Source at Center

Figure 32

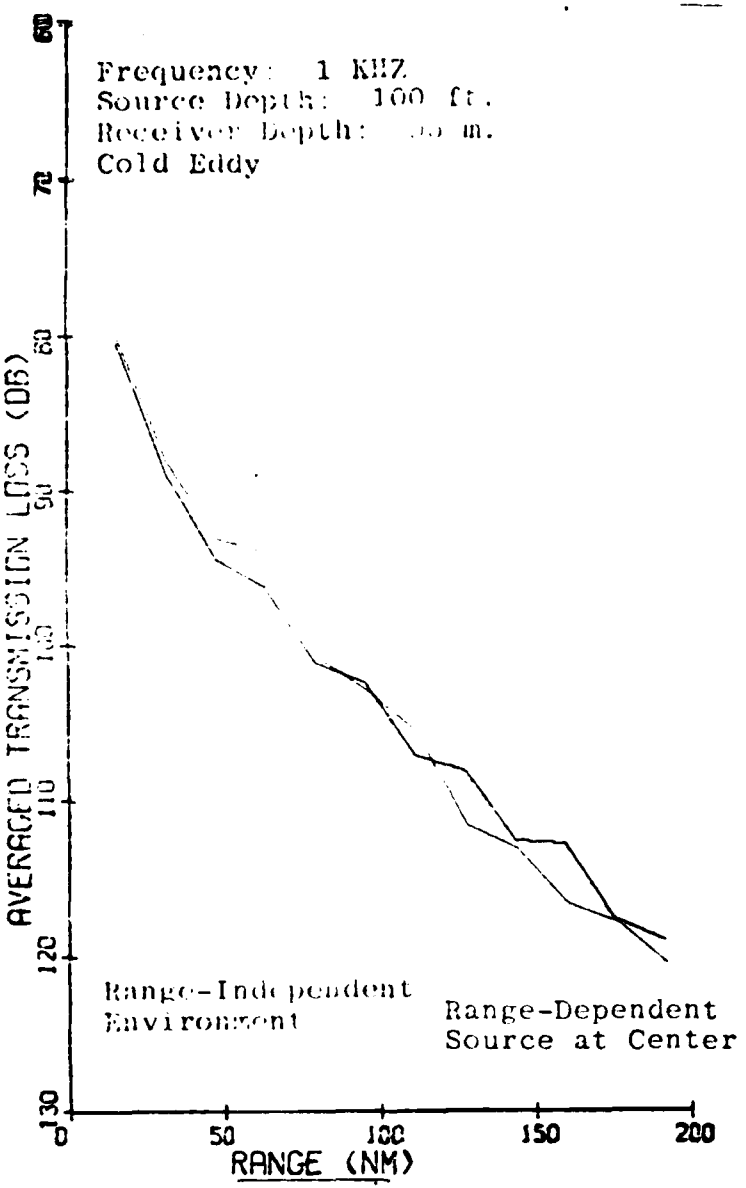
Frequency: 1 KHZ
Source Depth: 100 ft.
Receiver Depth: m.
Cold Eddy
AVERAGED TRANSMISSION LOSS (DB)
60
70
80
90
100
110
120
130
0
50
100
150
200
RANGE (NM)
Range-Independent Environment
Range-Dependent Source at Center

Figure 33

7.7 Frequency Effects

The effect of variations in source frequency on transmission loss is apparent from Figure 34, which shows transmission loss in the range-dependent environment for 20, 300, and 1000 Hz. The constant offset in transmission loss between the 20 and 300 Hz cases is primarily attributable to surface image interference. At low frequencies, for a shallow source and/or receiver, several paths combine destructively to yield higher levels of transmission loss than would be seen for a deeper source and receiver.

The effect of volume attenuation on the 1000 Hz case is demonstrated by the dramatically higher levels of transmission loss for that case. Recalling that volume attenuation at 1 kHz, over 200 nm, is approximately 25 dB, it is evident that were it not for volume attenuation, the 300 and 1000 Hz transmission loss curves would be quite similar. Thus, the largest differences attributable to frequency dependence are seen between 20 and 300 Hz. Above 300 Hz, there is relatively little additional impact on transmission loss resulting from the eddy.

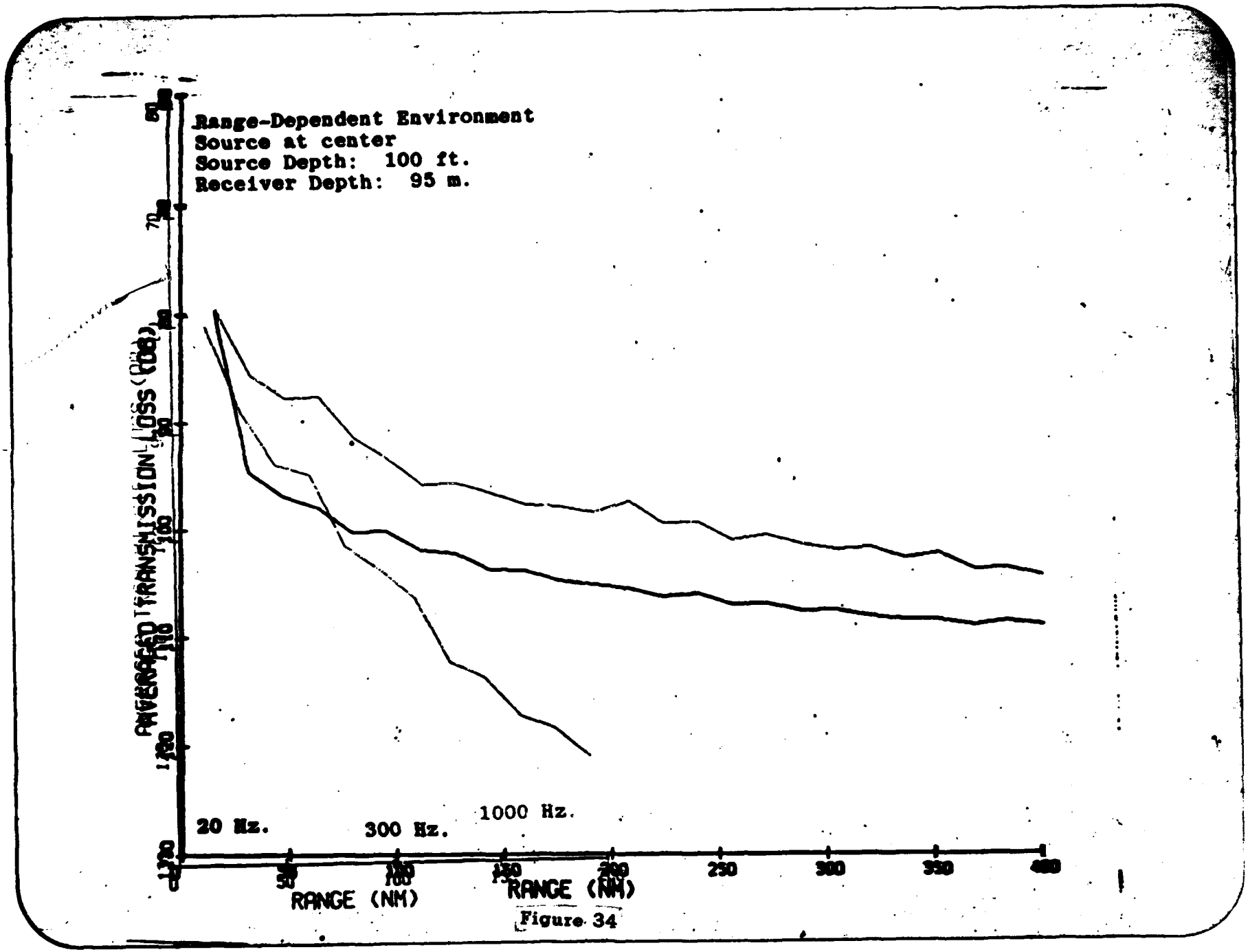
Range-Dependent Environment
Source at center
Source Depth: 100 ft.
Receiver Depth: 95 m.
AVERAGED TRANSMISSION LOSS (dB)
20 Hz.
300 Hz.
1000 Hz.
RANGE (NM)
RANGE (NM)

Figure 34

Section 8
COMPARATIVE ACOUSTIC STATISTICS

To quantify more precisely the differences between the range-independent and range-dependent environments which were seen in the previous transmission loss estimates, we have constructed a measure of statistical difference for comparative purposes. This measure is actually a relative intensity difference, which is found by determining the difference in intensity between any two environments relative to the intensity in a reference environment. The relative intensity difference may be computed on a point-by-point basis from the intensities of the acoustic field within a fixed range-depth window. Figure 35 shows a comparison of the range-dependent environment with the source at the eddy center relative to the range-independent environment at 20 Hz. The range window for this comparison is 35 - 55 km. The depth window is from the surface to 150 m. The histogram shows the relative frequency of occurrence within this window of the statistic (I1 - I2)/I2, where I1 is the intensity in the range-dependent environment and I2 is the reference intensity that of the range-independent environment. The histogram reveals that the majority of the observations are at the positive end of the scale, indicating that the range-dependent environment with the source at the eddy center, I1, has a higher intensity over this range-depth interval than does the range-independent environment, I2. This is reflected in the mean intensities, expressed in dB units, for each environment. The mean intensity for the range-dependent environment is 91.3 dB, whereas the mean intensity for the range-independent track in the same window is 94.8 dB, 3.5 dB less.

Figure 35

RELATIVE INTENSITY DIFFERENCES FOR
COLD EDDY (20HZ)--CENTER (I1) VS RANGE-1 (I2)

DEPTH-- 0.00 TO 500.00 FT
RANGE-- 20.00 TO 30.00 NMI
N= 133

MEAN(I1) =	74.419 X 10^{-11} =	91.283	DB
SDEV(I1) =	77.537 X 10^{-11} =	91.105	DB
MEAN(I2) =	33.084 X 10^{-11} =	94.804	DB
SDEV(I2) =	60.698 X 10^{-11} =	92.168	DB

MEAN $\left(\frac{I1-I2}{I2}\right)$ = 21.923

SDEV $\left(\frac{I1-I2}{I2}\right)$ = 32.238

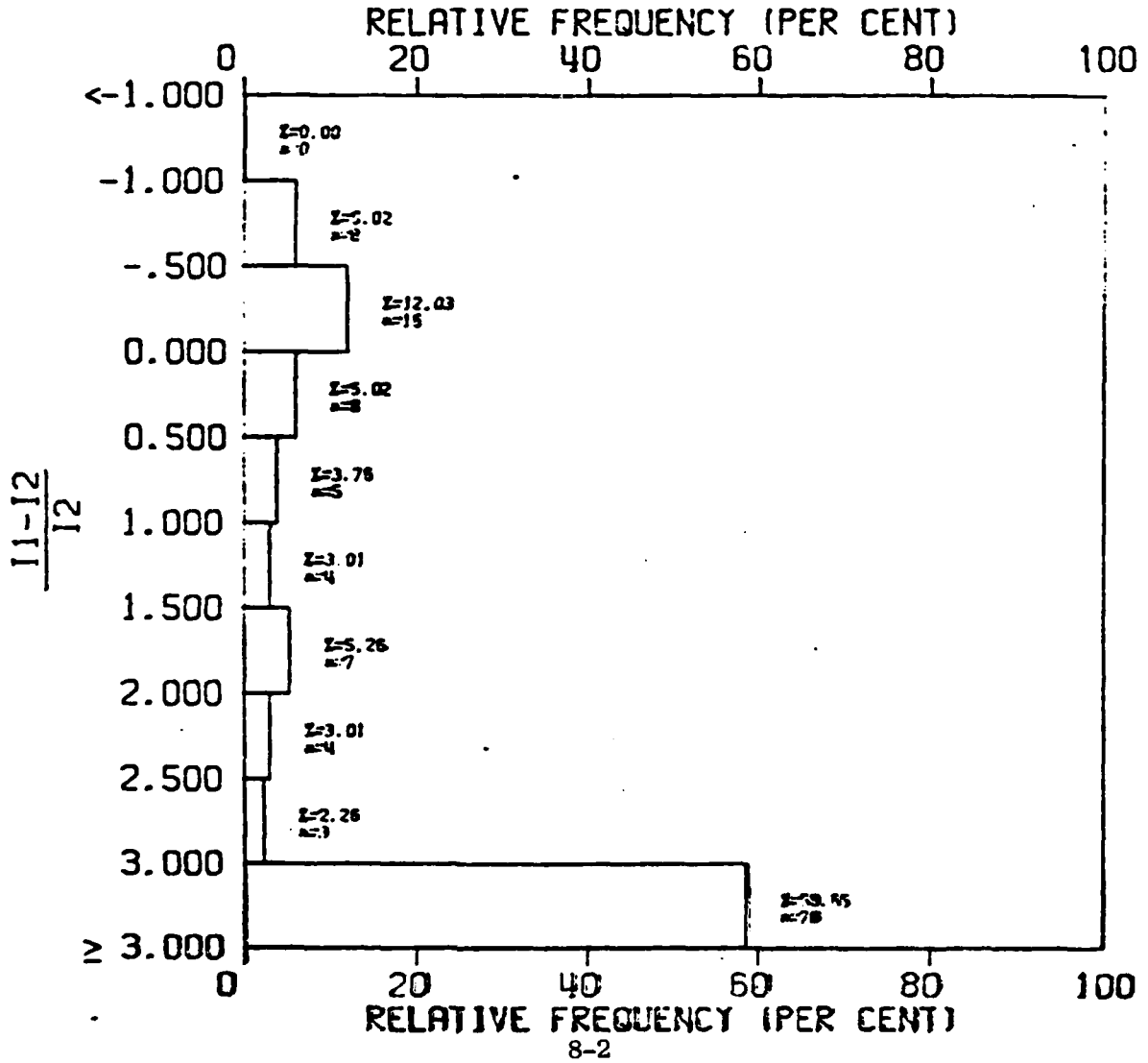

The nature of this relationship changes with horizontal range, as is seen in Figure 36, which shows a similar comparison for the range window between 55 and 75 km. In this instance, the distribution is positively skewed, indicating that the range-independent environment has more energy in it, for this range-depth window, than does the range-dependent environment. This is also evident in the mean intensities for these two environments, which show that the loss associated with the range-dependent environment is higher in this instance than the loss associated with the range-independent environment. In a similar manner, Figures 37 and 38 examine the distribution of energy in this fixed depth window for the next two 20 km range windows.

Figure 39 shows the relative intensity difference at 20 Hz for a warm eddy (I1) versus a range-independent environment (I2). The distribution in this instance is positively skewed, indicating that the range-dependent environment with the source at the eddy center shows higher levels of loss than does the range independent environment. This is consistent with the transmission loss curves examined earlier. Further, as both I1 and I2 are intensities greater than or equal to 0, the smallest value of the relative intensity difference $(I1 - I2)/I2$ is -1. It is evident from the histogram and from the mean value of this statistic that most of the points approach this lower limit of -1.

Figure 40 shows relative intensity differences for the next 20 km section of track, 55 - 75 km. In this instance, the distribution is actually bimodal, although the

Figure 36

RELATIVE INTENSITY DIFFERENCES FOR
COLD EDDY (20HZ)--CENTER (I1) VS RANGE-1 (I2)

DEPTH-- 0.00 TO 500.00 FT
RANGE-- 30.00 TO 40.00 NMI
N= 175

MEAN(I1) =	9.124 X 10^{-11} =	100.398	DB
SDEV(I1) =	16.400 X 10^{-11} =	97.851	DB
MEAN(I2) =	22.124 X 10^{-11} =	96.551	DB
SDEV(I2) =	45.080 X 10^{-11} =	93.460	DB

MEAN $\left(\frac{I1-I2}{I2}\right)$ = -.303

SDEV $\left(\frac{I1-I2}{I2}\right)$ = 0.373

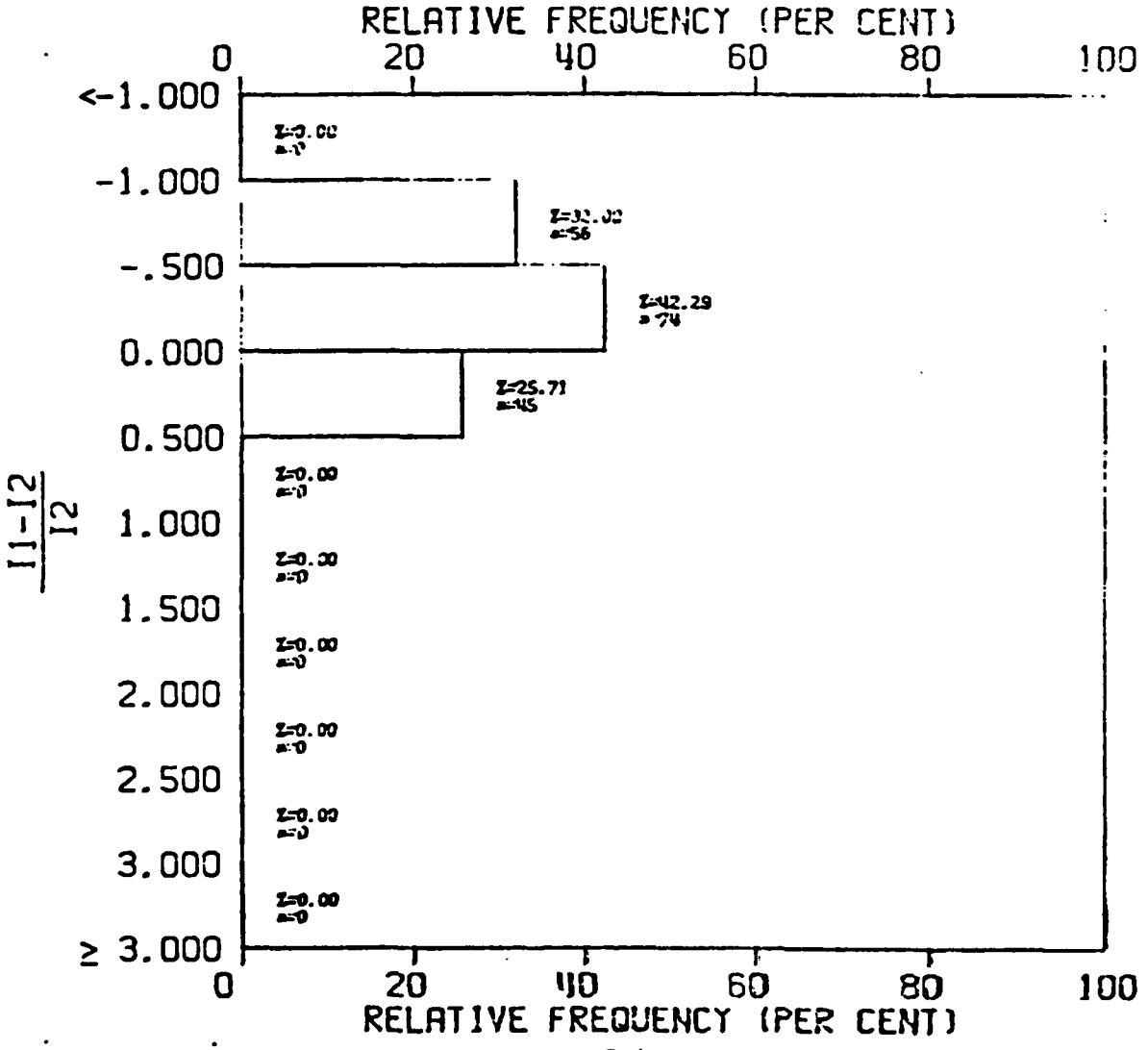

Figure 37

RELATIVE INTENSITY DIFFERENCES FOR
COLD EDDY (20HZ)--CENTER (I1) VS RANGE-1 (I2)

DEPTH-- 0.00 TO 500.00 FT
RANGE-- 40.00 TO 50.00 NMI
N= 119

MEAN(I1) =	3.483×10^{-11}	=	104.580	DB
SDEV(I1) =	6.245×10^{-11}	=	102.044	DB
MEAN(I2) =	0.025×10^{-11}	=	126.040	DB
SDEV(I2) =	0.040×10^{-11}	=	124.030	DB

MEAN $\left(\frac{I1-I2}{I2}\right)$ = 623.144

SDEV $\left(\frac{I1-I2}{I2}\right)$ = 874.317

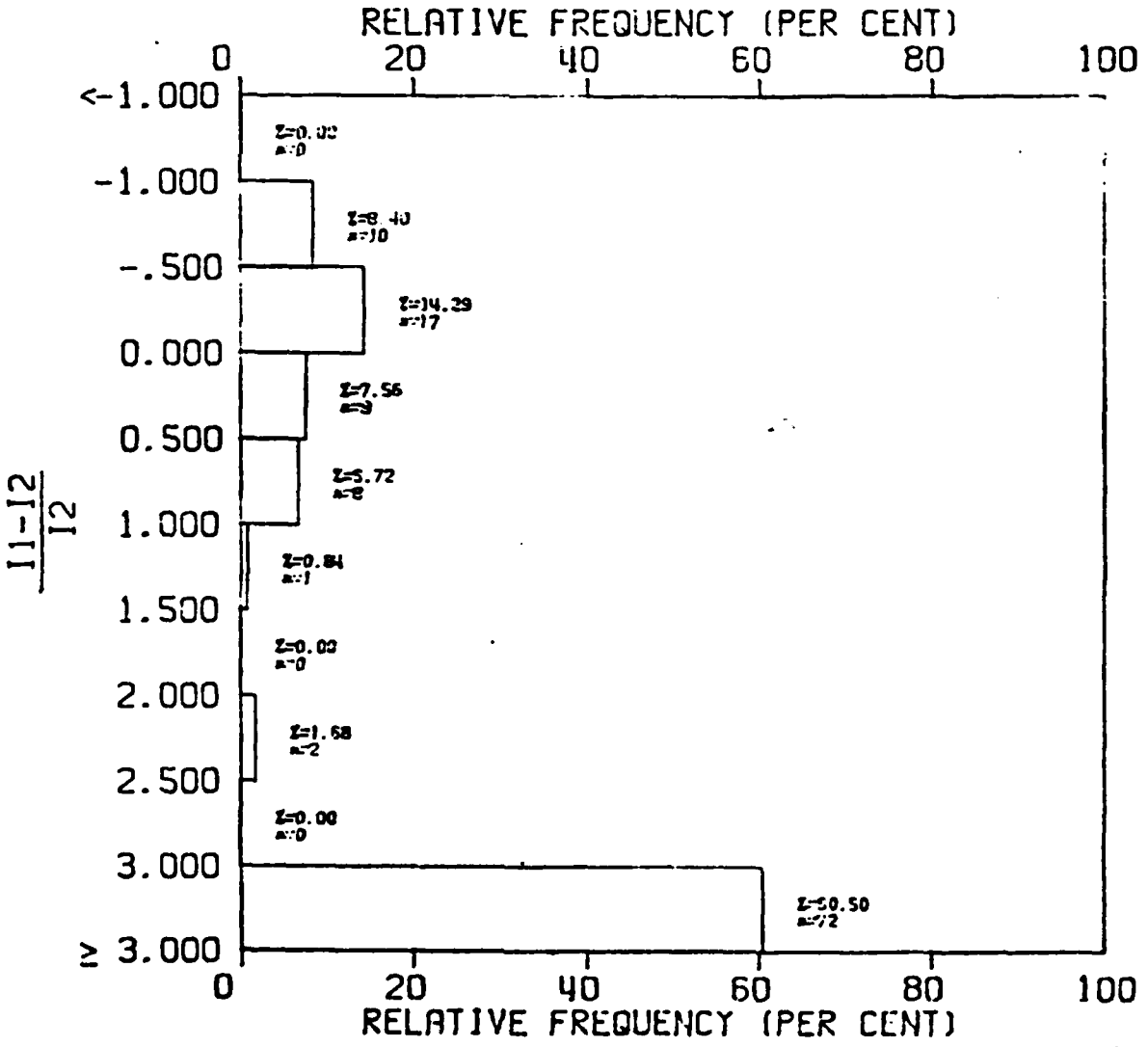

Figure 38

RELATIVE INTENSITY DIFFERENCES FOR
COLD EDDY (20HZ)--CENTER (I1) VS RANGE-I (I2)

DEPTH-- 0.00 TO 500.00 FT
RANGE-- 50.00 TO 60.00 NMI
N= 189

MEAN(I1) =	28.717 X 10^{-11} =	95.419	DB
SDEV(I1) =	20.614 X 10^{-11} =	96.858	DB
MEAN(I2) =	16.983 X 10^{-11} =	97.700	DB
SDEV(I2) =	25.693 X 10^{-11} =	95.902	DB

MEAN $\left(\frac{I1-I2}{I2}\right)$ = 107.717

SDEV $\left(\frac{I1-I2}{I2}\right)$ = 174.845

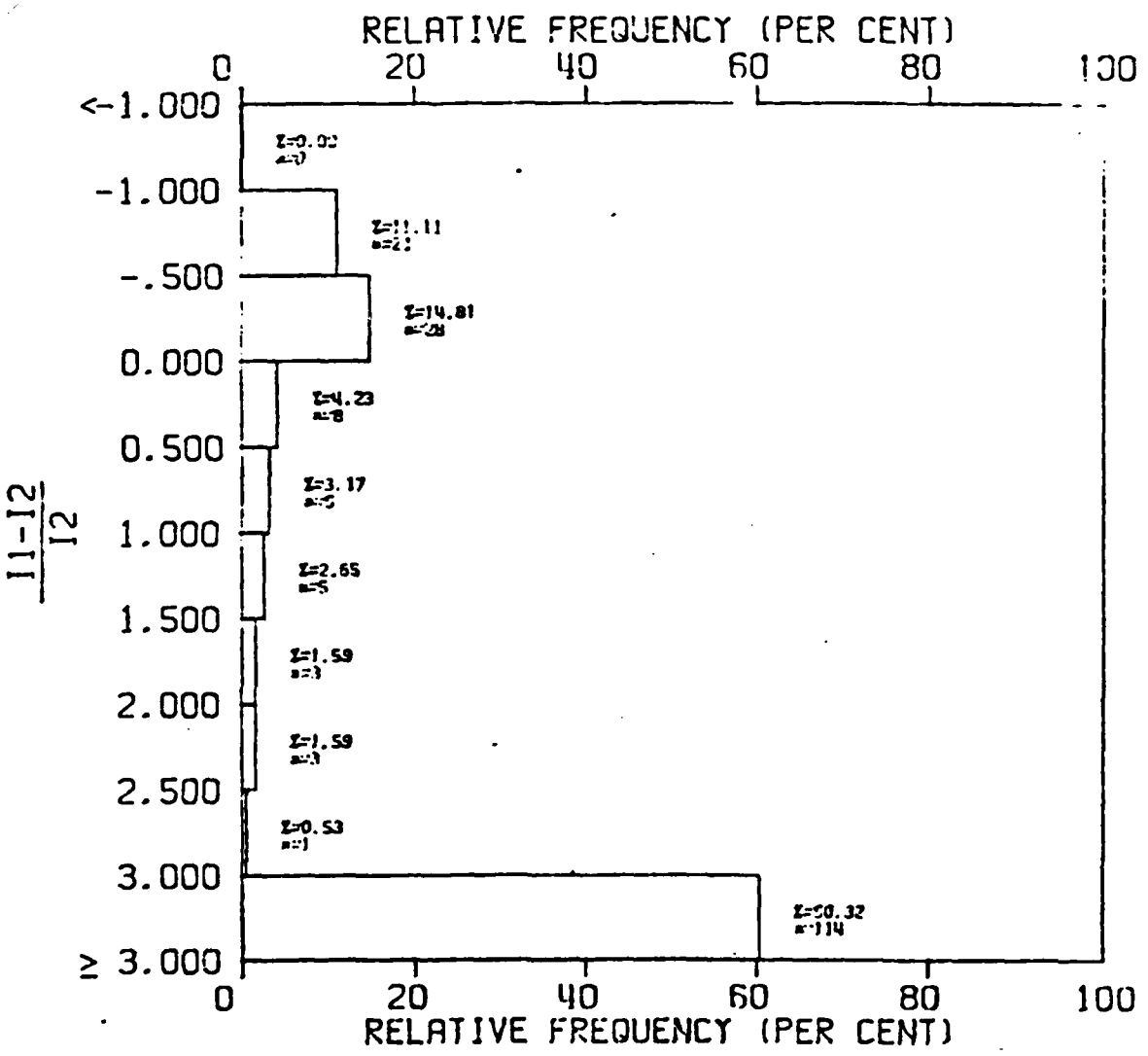

Figure 39

RELATIVE INTENSITY DIFFERENCES FOR
WARM EDDY (20 HZ)--RS=CENTER (I1) AND RANGE-1 (I2)

DEPTH-- 0.00 TO 500.00 FT
RANGE-- 20.00 TO 30.00 NMI
N= 133

MEAN(I1) =	0.523 X 10^{-11}	=	112.813	DB
SDEV(I1) =	0.852 X 10^{-11}	=	110.693	DB
MEAN(I2) =	31.691 X 10^{-11}	=	94.391	DB
SDEV(I2) =	45.386 X 10^{-11}	=	93.336	DB

MEAN $\left(\frac{I1-I2}{I2}\right)$ = -.782

SDEV $\left(\frac{I1-I2}{I2}\right)$ = 0.342

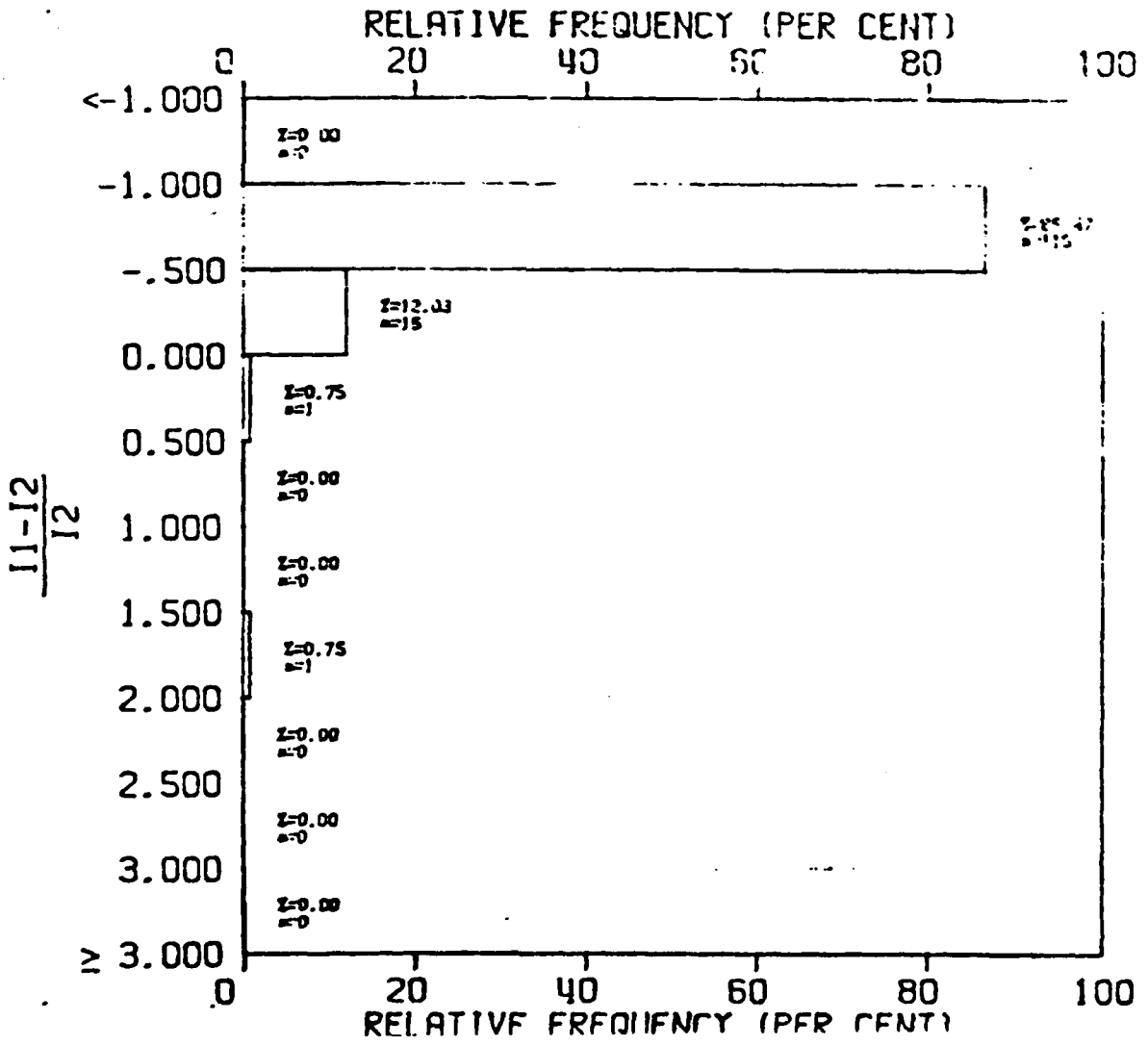

Figure 40

RELATIVE INTENSITY DIFFERENCES FOR
WARM EDDY (20 HZ)--RS=CENTER (I1) AND RANGE-1 (I2)

DEPTH-- 0.00 TO 500.00 FT
RANGE-- 30.00 TO 40.00 NMI
N= 175

MEAN(I1) =	10.382 X 10^{-11}	=	99.837	DB
SDEV(I1) =	10.078 X 10^{-11}	=	99.965	DB
MEAN(I2) =	12.002 X 10^{-11}	=	99.207	DB
SDEV(I2) =	21.032 X 10^{-11}	=	96.771	DB

MEAN $\left(\frac{I1-I2}{I2}\right)$ = 3.604

SDEV $\left(\frac{I1-I2}{I2}\right)$ = 4.138

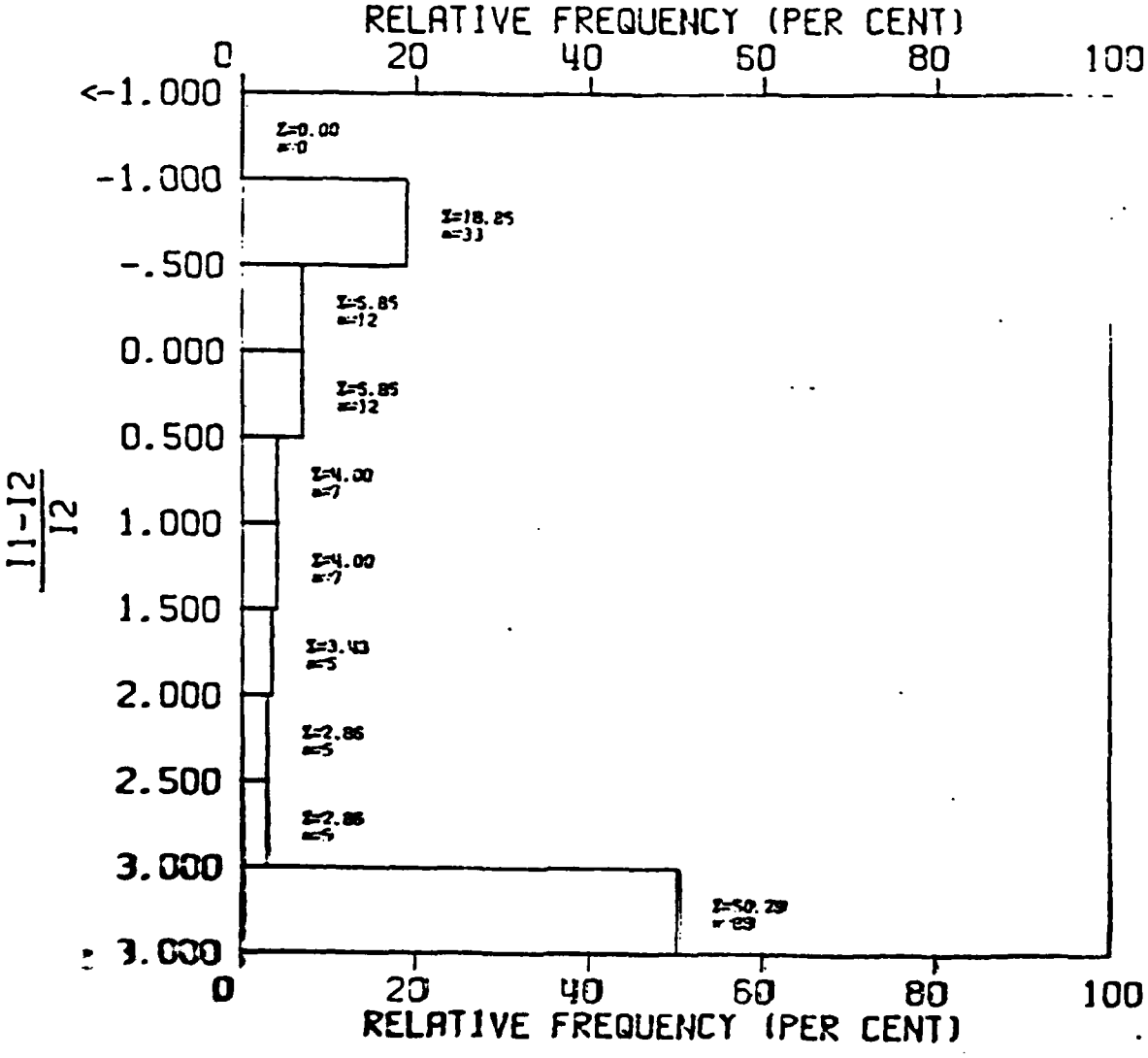

majority of observations indicate that the range-dependent environment has more energy in this range-depth window than does the range-independent environment. Examination of the mean intensity values in dB units for the two environments, however, shows that the mean intensity in this window is actually higher for the range-independent environment than it is for the range-dependent environment. This illustrates the potentially misleading conclusions that may be drawn from a simple comparison of mean intensity over an operational window of interest. Rather, the use of the histograms contributes significantly different information, which may be important from a tactical perspective. Similarly, Figures 41 and 42 depict the relative intensity differences for the next 40 km of the track.

Relative intensity differences within a cold eddy at 300 Hz may be seen in Figure 43. The depth window remains the same as that for the 20 Hz cases, from 0 to 150 m. The range window is considerably smaller in this instance, here a 2 km window from 55 to 57 km along the track. The histogram indicates that within this range-depth window, the range-independent environment contains more energy than does the range-dependent environment. This is also reflected in the mean intensities for the individual windows and in the mean value of the statistic $(I1 - I2)/I2$.

This relationship changes somewhat in the next range window considered, between 74 and 76 km (Figure 44). While the mean intensity for each environment as well as the mean value of the relative intensity difference indicates that the range-independent environment has more

Figure 41

RELATIVE INTENSITY DIFFERENCES FOR
WARM EDDY (20 HZ)--RS=CENTER (I1) AND RANGE-1 (I2)

DEPTH-- 0.00 TO 500.00 FT
RANGE-- 40.00 TO 50.00 NMI
N= 84

MEAN(I1) =	0.169 X 10^{-11} =	117.733	DB
SDEV(I1) =	0.287 X 10^{-11} =	115.426	DB
MEAN(I2) =	0.063 X 10^{-11} =	122.022	DB
SDEV(I2) =	0.136 X 10^{-11} =	118.677	DB

MEAN $\left(\frac{I1-I2}{I2}\right)$ = 3.471

SDEV $\left(\frac{I1-I2}{I2}\right)$ = 3.465

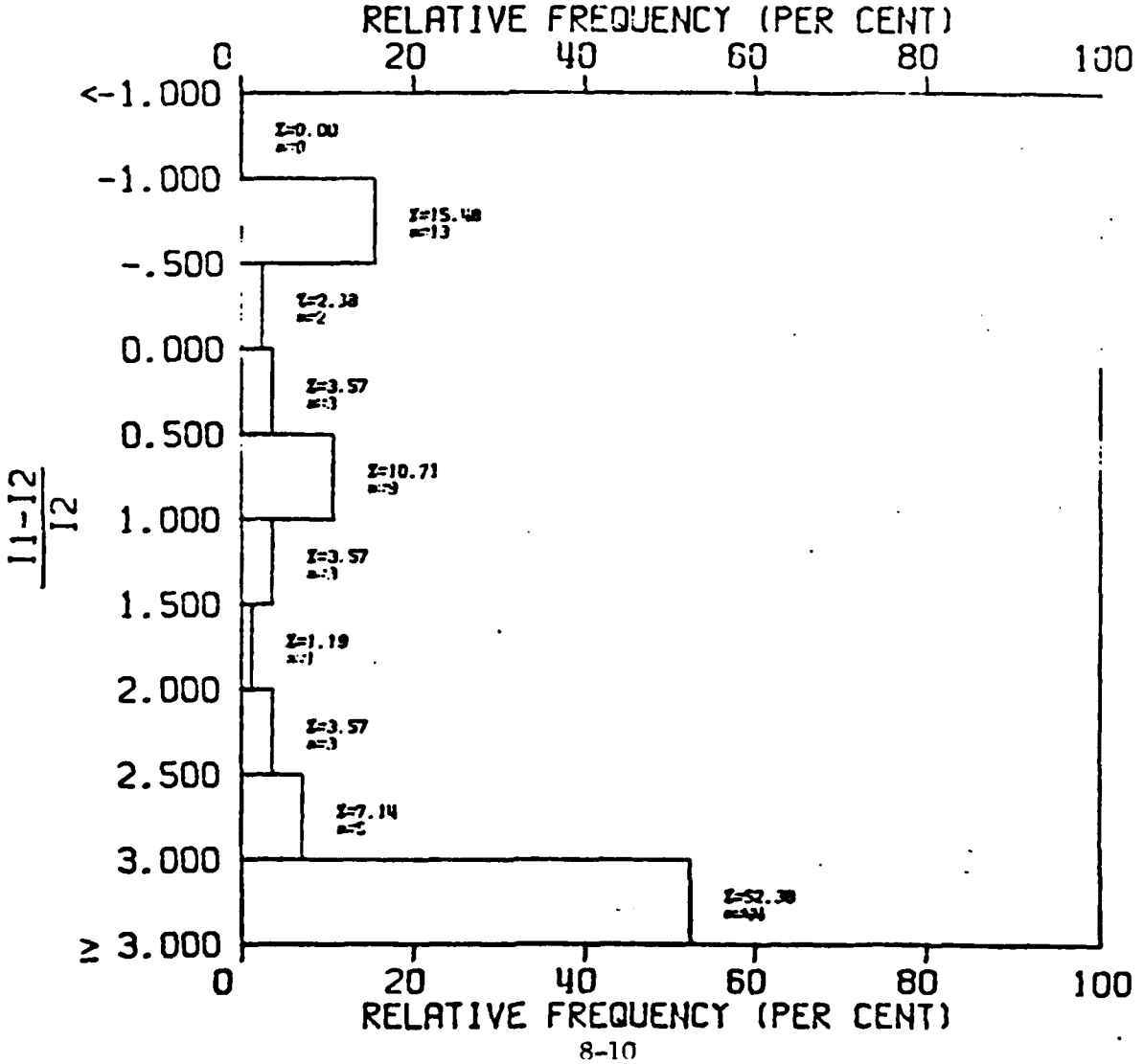

Figure 42

RELATIVE INTENSITY DIFFERENCES FOR
WARM EDDY (20 HZ)--RS=CENTER (I1) AND RANGE-I (I2)

DEPTH-- 0.00 TO 500.00 FT
RANGE-- 50.00 TO 60.00 NMI
N= 154

MEAN(I1) =	0.047 X 10^{-11}	=	123.310	DB
SDEV(I1) =	0.085 X 10^{-11}	=	120.712	DB
MEAN(I2) =	13.667 X 10^{-11}	=	98.643	DB
SDEV(I2) =	14.932 X 10^{-11}	=	98.259	DB

MEAN $\left(\frac{I1-I2}{I2}\right)$ = -.990

SDEV $\left(\frac{I1-I2}{I2}\right)$ = 0.034

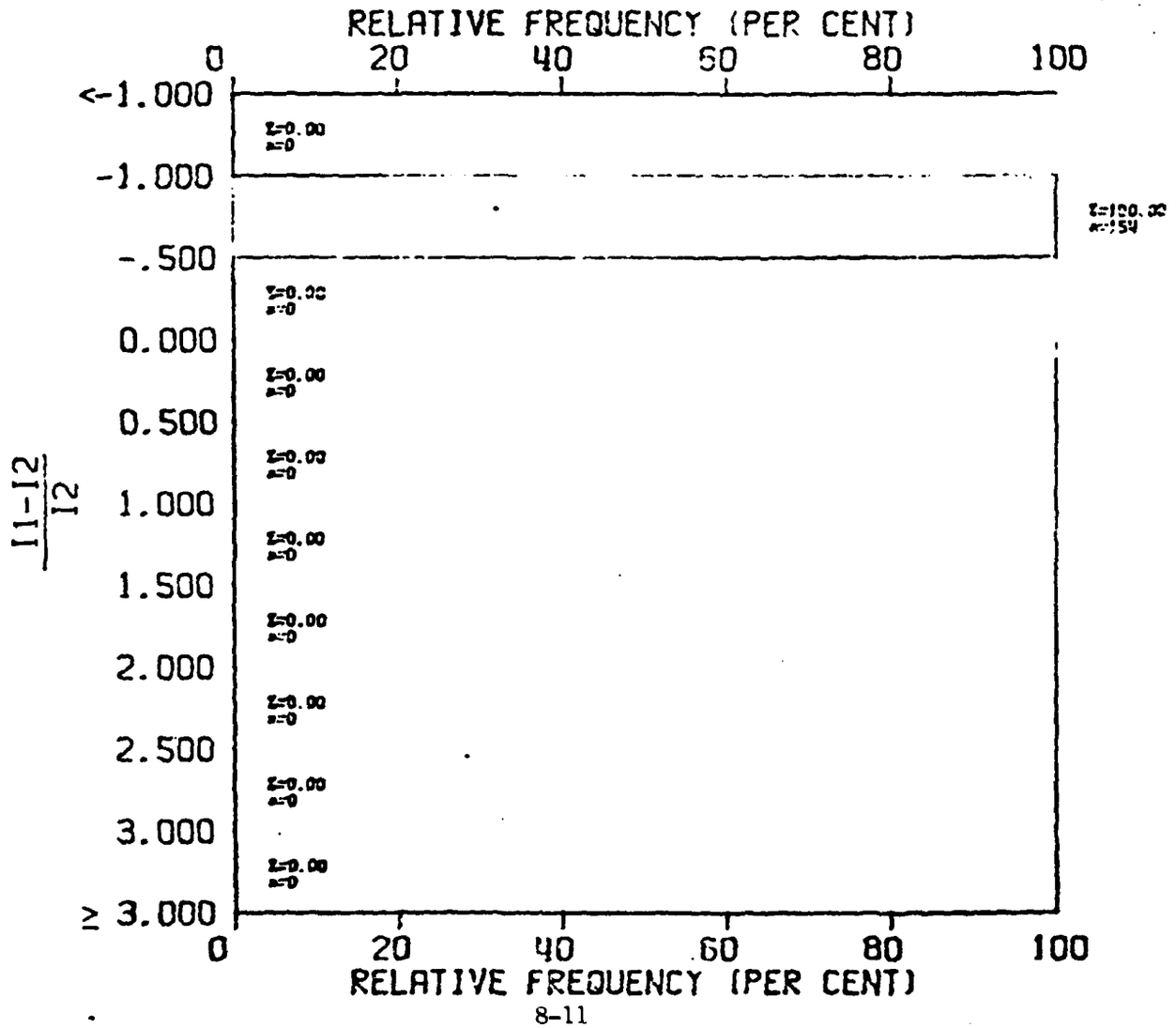

Figure 43

RELATIVE INTENSITY DIFFERENCES FOR
COLD EDDY (300 HZ)--RS=CENTER (11) VS RANGE-1 (12)

DEPTH-- 0.00 TO 500.00 FT
RANGE-- 30.00 TO 31.00 NMI
N= 435

MEAN(11) =	8.916	X 10^{-11} =	100.498	DB
SDEV(11) =	7.172	X 10^{-11} =	101.444	DB
MEAN(12) =	1690.883	X 10^{-11} =	77.719	DB
SDEV(12) =	1430.991	X 10^{-11} =	78.444	DB

MEAN $\left(\frac{11-12}{12}\right)$ = -.979

SDEV $\left(\frac{11-12}{12}\right)$ = 0.087

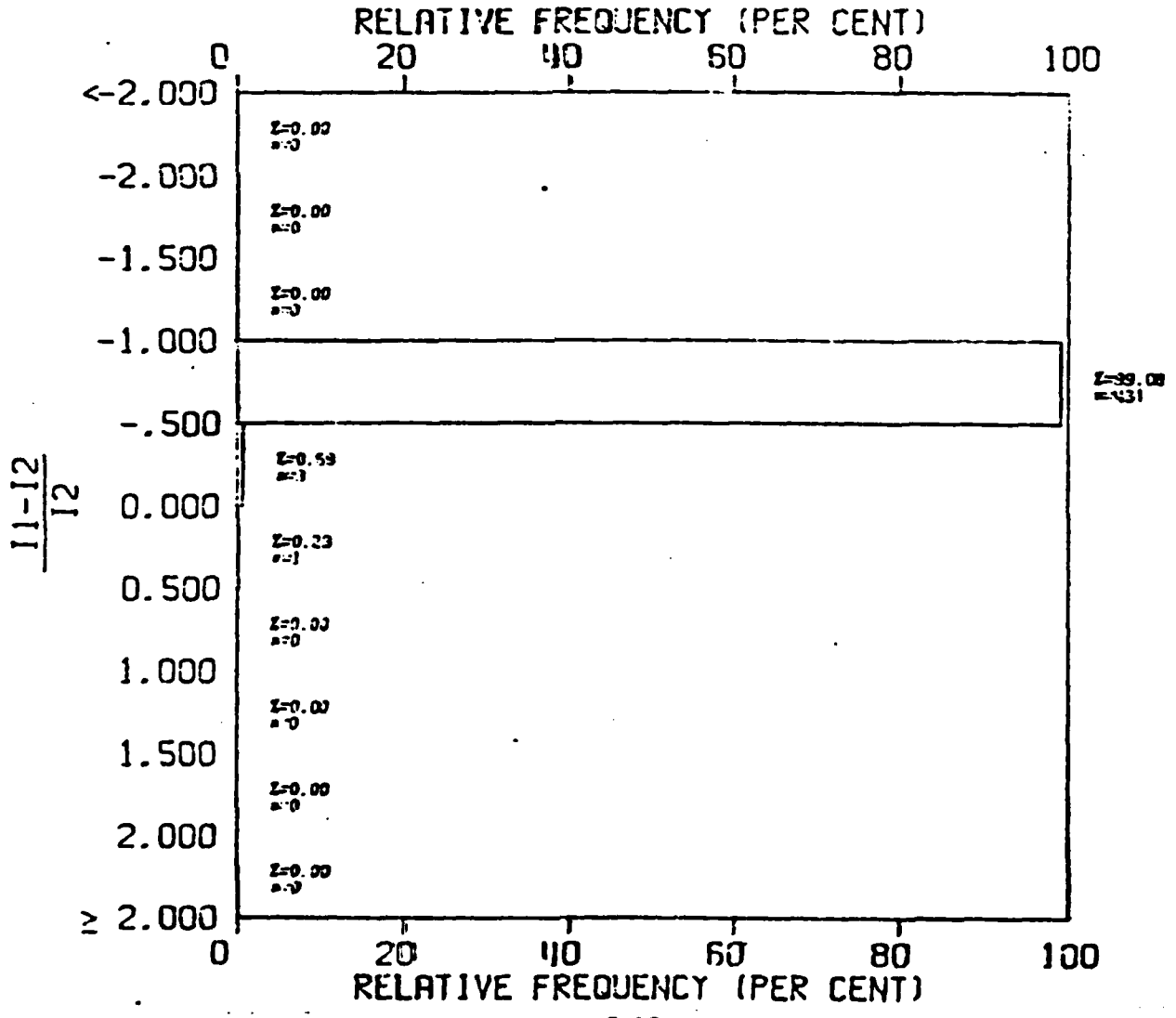

Figure 44

RELATIVE INTENSITY DIFFERENCES FOR
COLD EDDY (300 HZ)--RS=CENTER (I1) VS RANGE-1 (I2)

DEPTH-- 0.00 TO 500.00 FT
RANGE-- 40.00 TO 41.00 NMI
N= 145

MEAN(I1) =	0.021 X 10^{-11} =	126.711	DB
SDEV(I1) =	0.014 X 10^{-11} =	128.523	DB
MEAN(I2) =	0.063 X 10^{-11} =	121.394	DB
SDEV(I2) =	0.042 X 10^{-11} =	123.812	DB

MEAN $\left(\frac{I1-I2}{I2}\right)$ = -.351

SDEV $\left(\frac{I1-I2}{I2}\right)$ = 1.010

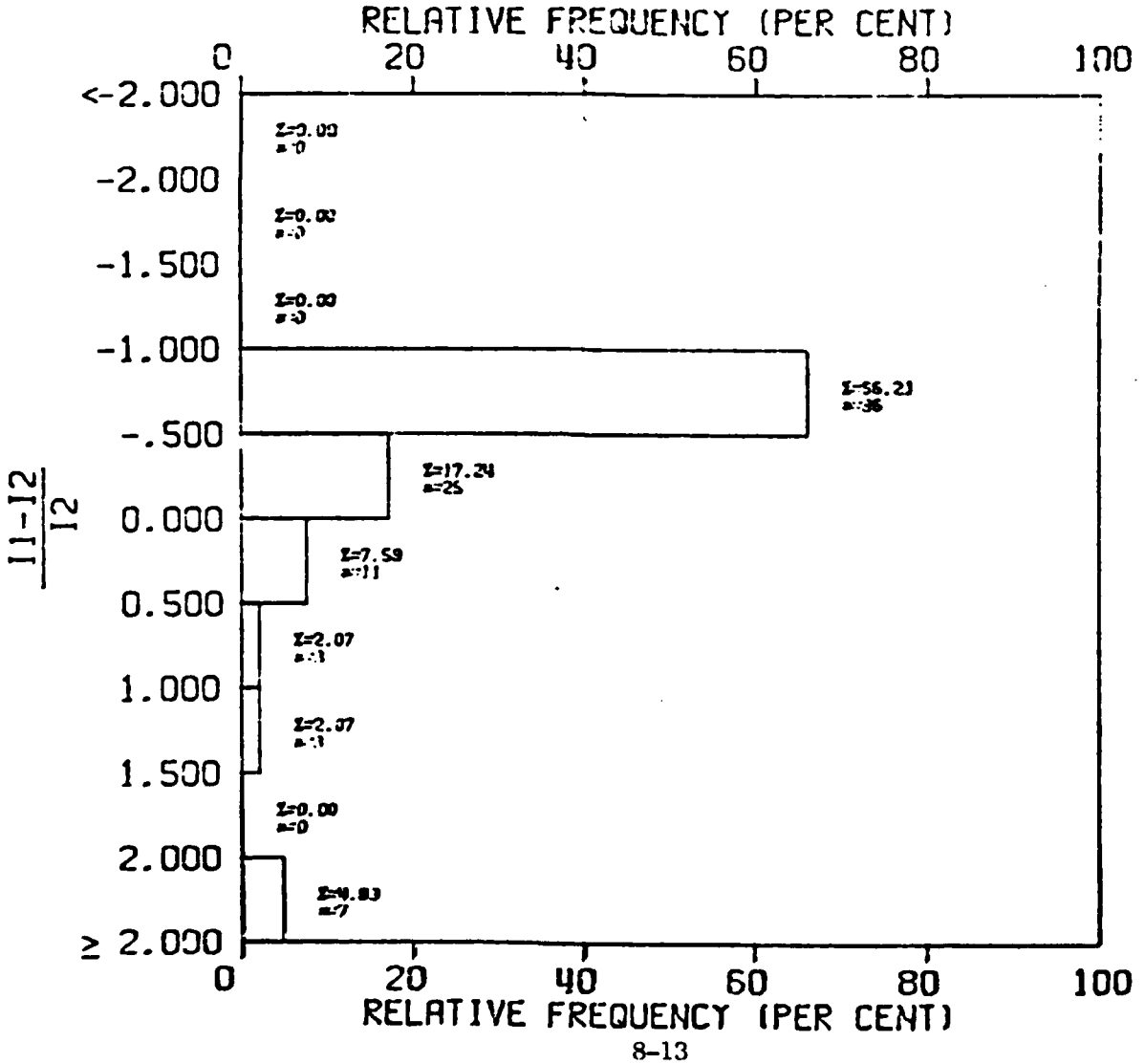

energy in it than does the range dependent environment, the nature of this relationship has shifted somewhat, as is seen in the histogram.

Relative intensity differences for a warm eddy at 300 Hz may be seen in Figure 45. The histogram indicates that a significant number of observations within this range-depth window show that the range-independent environment has more energy associated with it than does the range-dependent environment. The mean relative intensity difference within this range depth window, however, indicates that the range dependent environment has more energy associated with it than does the range independent environment. This is another example of the misleading conclusions that may be drawn from the use of a single summary statistic. Figure 46 shows, for the range window 74 to 76 km, a reversal of this relationship. In this instance, the range-dependent environment shows significantly higher intensity than the range independent environment.

Figure 45

RELATIVE INTENSITY DIFFERENCES FOR
WARM EDDY (300 HZ)--RS=CENTER (I1) VS RANGE-1 (I2)

DEPTH-- 0.00 TO 500.00 FT
RANGE-- 30.00 TO 31.00 NMI
N= 493

MEAN(I1)	=	368.023	X 10^{-11}	=	84.341 DB
SDEV(I1)	=	177.399	X 10^{-11}	=	87.510 DB
MEAN(I2)	=	1128.393	X 10^{-11}	=	79.475 DB
SDEV(I2)	=	1254.160	X 10^{-11}	=	79.016 DB

MEAN $\left(\frac{I1-I2}{I2}\right)$ = 1.045

SDEV $\left(\frac{I1-I2}{I2}\right)$ = 5.477

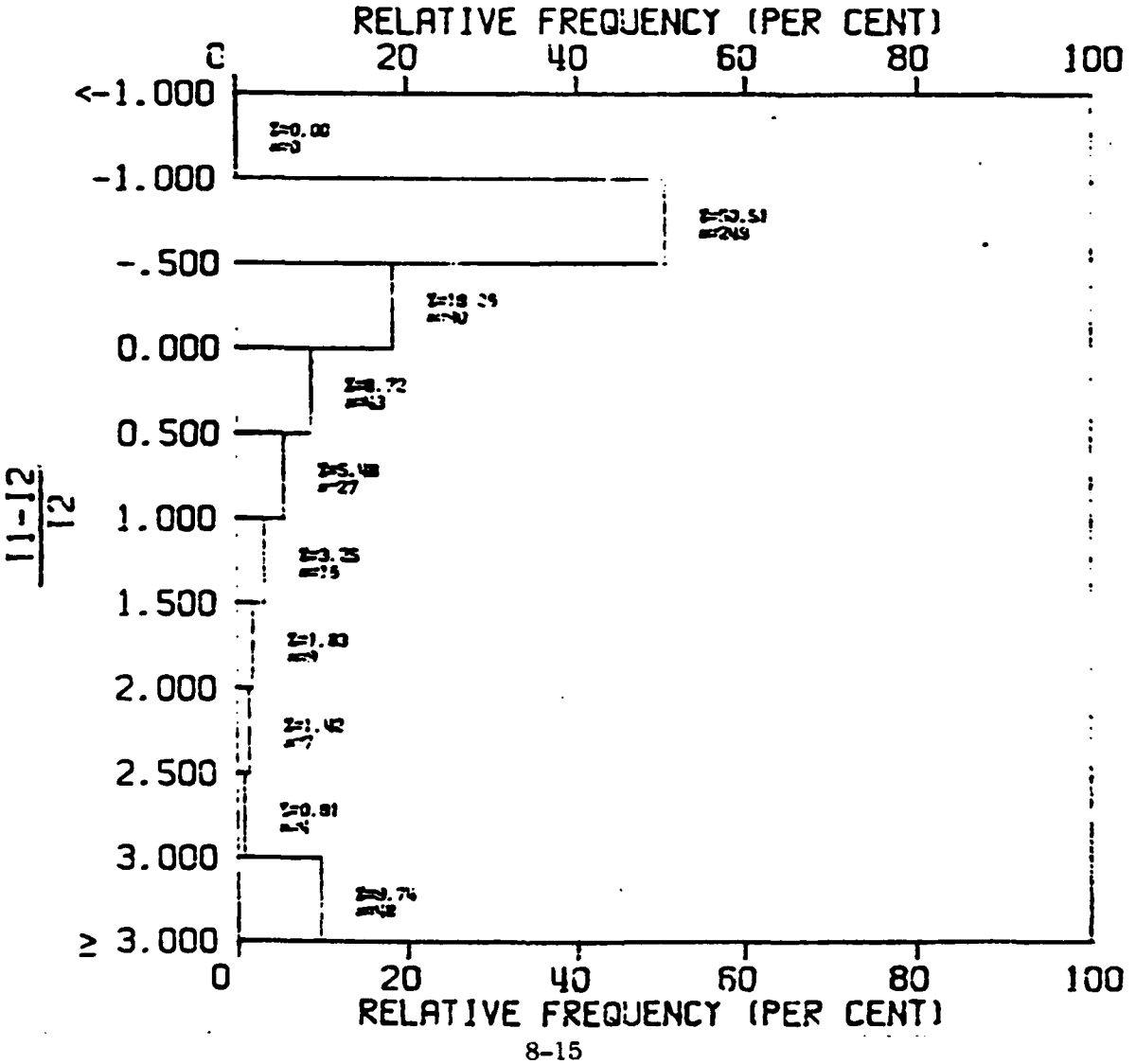

Figure 46

RELATIVE INTENSITY DIFFERENCES FOR
WARM EDDY (300 HZ)--RS=CENTER (I1) VS RANGE-I (I2)

DEPTH-- 0.00 TO 500.00 FT
RANGE-- 40.00 TO 41.00 NMI
N= 290

MEAN(I1) =	25.859 X 10^{-11} =	95.709	DB
SDEV(I1) =	28.401 X 10^{-11} =	95.467	DB
MEAN(I2) =	0.252 X 10^{-11} =	115.982	DB
SDEV(I2) =	0.179 X 10^{-11} =	117.477	DB

MEAN $\left(\frac{I1-I2}{I2}\right)$ = 239.047

SDEV $\left(\frac{I1-I2}{I2}\right)$ = 355.164

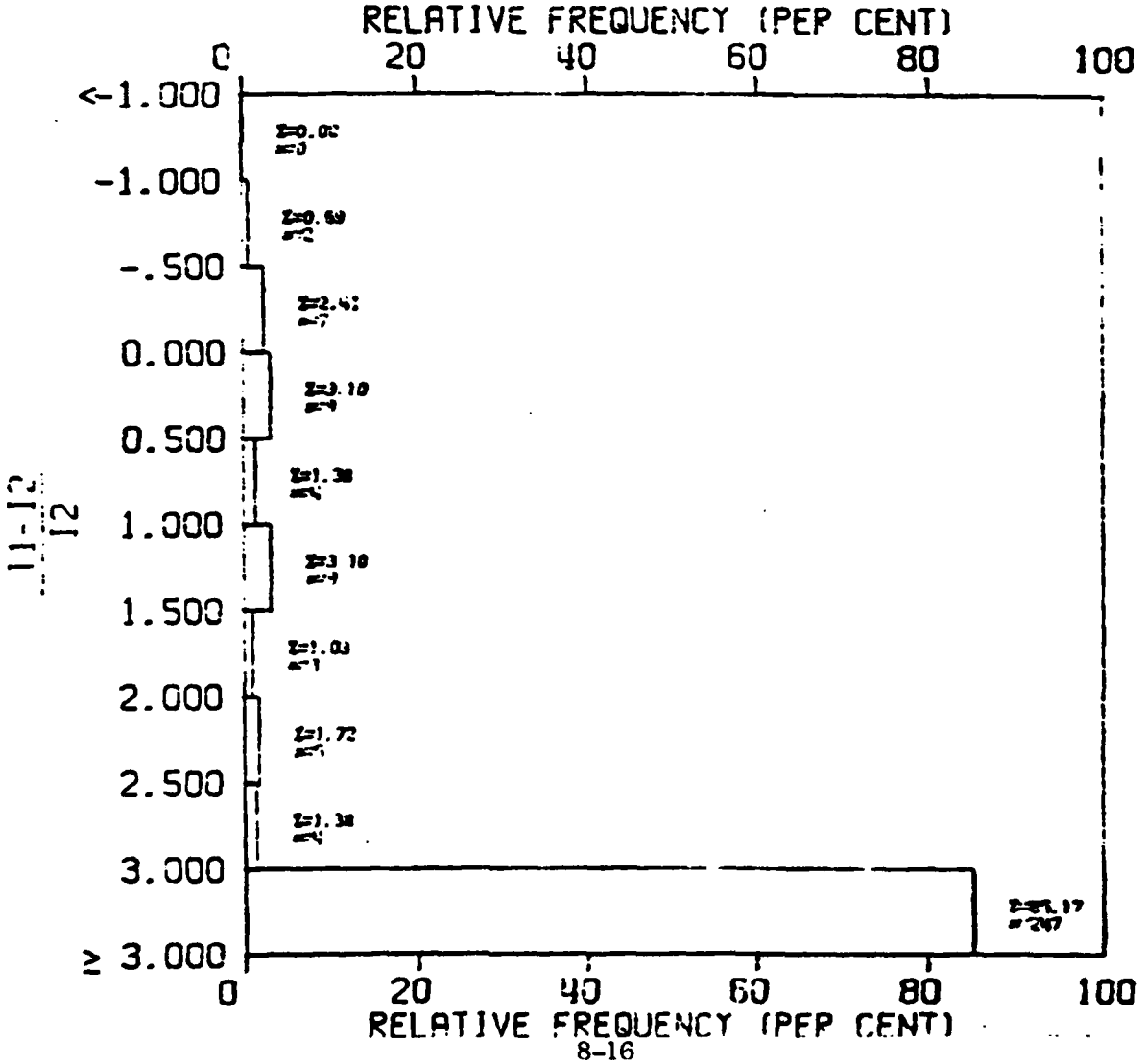

Section 9
SUMMARY

In summary, the eddy model developed by Henrick has been examined in detail. This model examines the perturbations to density, temperature, and sound velocity structures which result from the presence of an eddy. Statistically, the modeled density, temperature, and sound velocity profiles agree fairly well with the background conditions. The largest deviations from the observed conditions occur in the upper 600 m. This is due primarily to the lack of surface expression in the model, as well as to its inability to model irregular profiles. This poses a particular problem from an acoustic perspective as, for ASW depths of interest, significant differences between the observed and the modeled conditions will result. A model upgrade is in order, to permit the modeling of irregular profiles and eddy surface expressions. Cubic spline techniques have been suggested as one means for modeling the irregular profiles.

From the acoustic analysis, it has been demonstrated that little difference exists between a range-dependent environment with the source at 0 km and one in which the source is located at 30 km. Shifting the source by half a convergence zone, therefore, exerts relatively little influence on transmission loss. The most significant differences occurred between the range-dependent environment with the source at the eddy center and the range-independent environment. At 20 Hz, within a cold eddy, the range-dependent environment may show as much as 10 db less loss

than the range-independent environment. In the warm eddy this relationship is reversed, with the range-dependent environment showing more loss than the range-independent environment. At 300 Hz, within the cold eddy, the same general trends as those seen at 20 Hz are observed, with the exception of 95 m, where the range-independent environment shows less loss than the range-dependent environment. For the warm eddy, the same trends are observed at 300 Hz that were observed at 20 Hz. In general, there is less overall difference between the two environments at 300 Hz than at 20 Hz. At 1000 Hz, in a cold eddy, the range-dependent environment shows less loss. The major difference in transmission loss between 300 Hz and 1000 Hz is attributable to volume attenuation.

The differences observed in the transmission loss estimates were examined in more detail with the use of comparative statistics such as a relative intensity difference. These measures of statistical difference depict the changing distribution of energy as a function of range and depth along a given track, and may be used to pinpoint more precisely areas where the presence of an eddy may have a significant impact on tactical systems.

Section 10
CONCLUSIONS

From the work described here, three principal conclusions can be drawn:

- With respect to ASW applications, eddies have an appreciable influence on the distribution of energy in range and depth only when the target is near the eddy center. Furthermore, the influence appears greater at low frequencies (20 Hz) than at high frequencies (300 Hz) and may amount to 10 dB, on average, for some geometries.

- The Henrick eddy model is not sufficiently flexible in its present form to fit measured Pacific data with enough accuracy to be used for acoustic studies. However, some possible improvements appear to be straightforward.

- Some progress has been made here toward developing an objective, useful measure of the acoustic influence of mesoscale features.

ACKNOWLEDGEMENTS

The authors wish to acknowledge R. F. Henrick and W. L. Siegmann for helpful discussions about their eddy model. We also wish to acknowledge D. C. Towery for his help in developing the computer code for this work.

References

Bialek, E. L. (ed) (1966). Handbook of Oceanographic Tables, U.S. Naval Oceanographic Office, SP-68.

Brock, H. K. (1978). The AESD Parabolic Equation Model, internal report, NORDA TN 12, Naval Ocean Research and Development Activity, NSTL Station, MS.

Eckart, C. (1958). Properties of water, Part II. The Equation of State of Water and Sea Water at Low Temperatures and Pressures, Am. J. Sci.. 256, p. 225 - 240.

Fairbridge, R. W. (ed) (1966). Encyclopedia of Oceanography, Johy Wiley and Sons, Inc.

Henrick, R. F., Siegmann, W. L., and M. J. Jacobson (1977). General Analysis of Ocean Eddy Effects for Sound Transmission Applications, J. Acoust. Soc. Am., 62(4), p. 860 - 870.

Henrick, R. F., Jacobson, M. J., Siegmann, W. L., and J. G. Clark (1979). Use of Analytical Modeling and Limited Data for Prediction of Mesoscale Eddy Properties, J. Phys. Ocean., 9(1), p. 65 - 78.

Levenberg, K. (1944). A Method for the Solution of Certain Non-Linear Problems in Least Squares, Quart. Appl. Math., 2, p. 164 - 168.

Mamayev, O. I. (1975). Temperature - Salinity Analysis of World Ocean Waters, Elsevier Scientific Publishing Co.

Marquardt, D. W. (1963). An Algorithm for Least-Squares Estimation of Nonlinear Parameters, SIAM J. Appl. Math., 11, p. 431 - 441.

Neumann, G. and W. J. Pierson, Jr. (1966). Principles of Physical Oceanography, Prentice-Hall, Inc.

Tappert, F. D. and Hardin, R. H. (1973). A Synopsis of the AESD Workshop on Acoustic Modeling by Non-Ray Techniques, 22-25 May 1973, Washington, D.C., internal report, AESD TN 73-05, ONR, Arlington, VA.

Tappert, F. D. (1974). Parabolic Equation Method in Underwater Acoustics, J. Acoust. Soc. Am., 35. S34(A).

Thorp, W. H. (1965). Deep Ocean Sound Attenuation in the Sub and Low Kilocycle per Second Region, J. Acoust. Soc. Am., 38, p. 648.

Watson, J. G., Siegmann, W. L., and M. J. Jacobson (1976). Deep-Ocean Dynamics for Environmental Acoustics Models, J. Acoust. Soc. Am., 60(2), p. 355 - 364.

Wilson, W. S., and J. P. Dugan (1978). Mesoscale Thermal Variability in the Vicinity of the Kuroshio Extension, J. Phys. Ocean., 8(3), p. 537 - 540.

APPENDIX A

TRACK ISOTHERMAL AND ISOVELOCITY CONTOURS

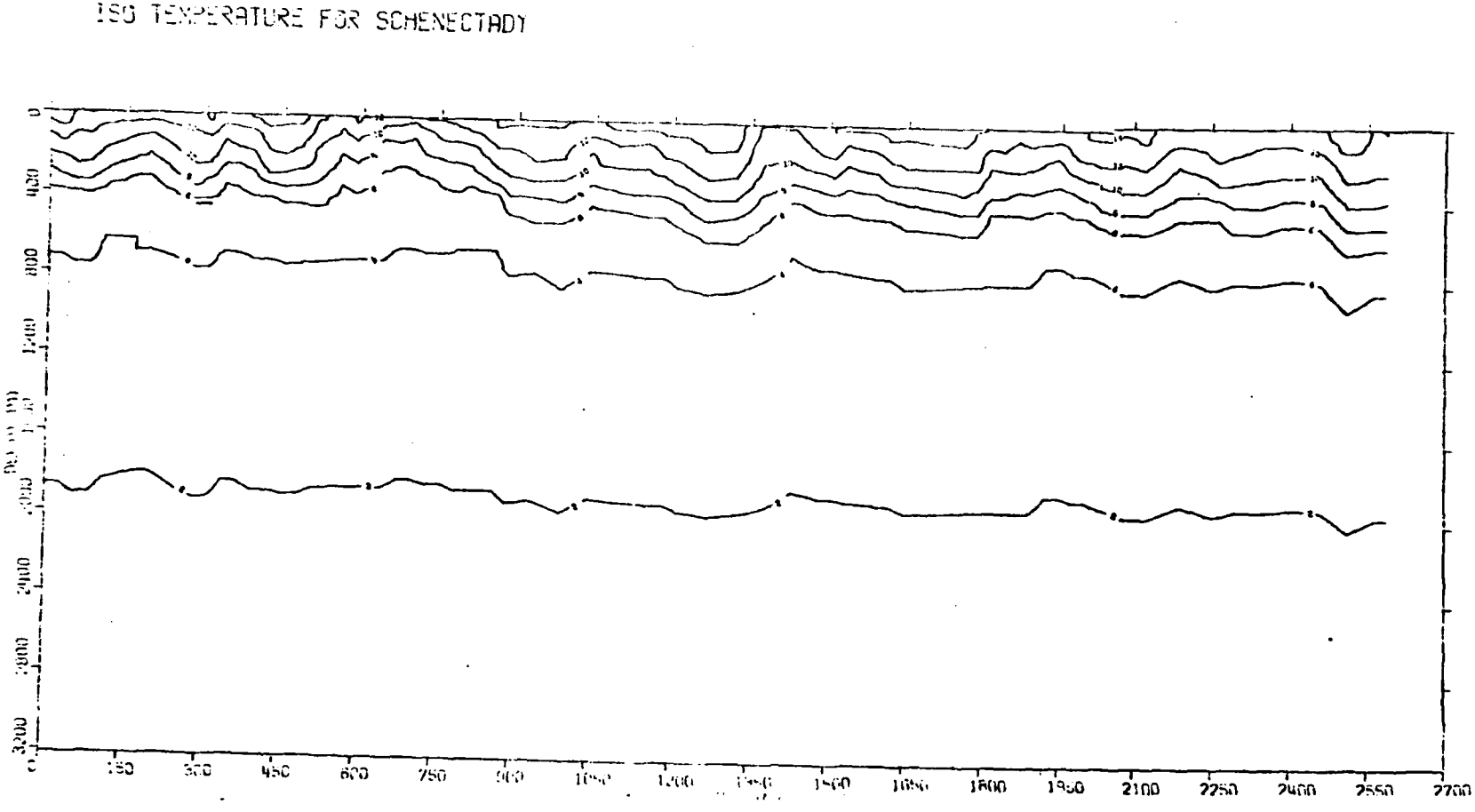

Figure A-1 Isothermal contours for Schenectady Track

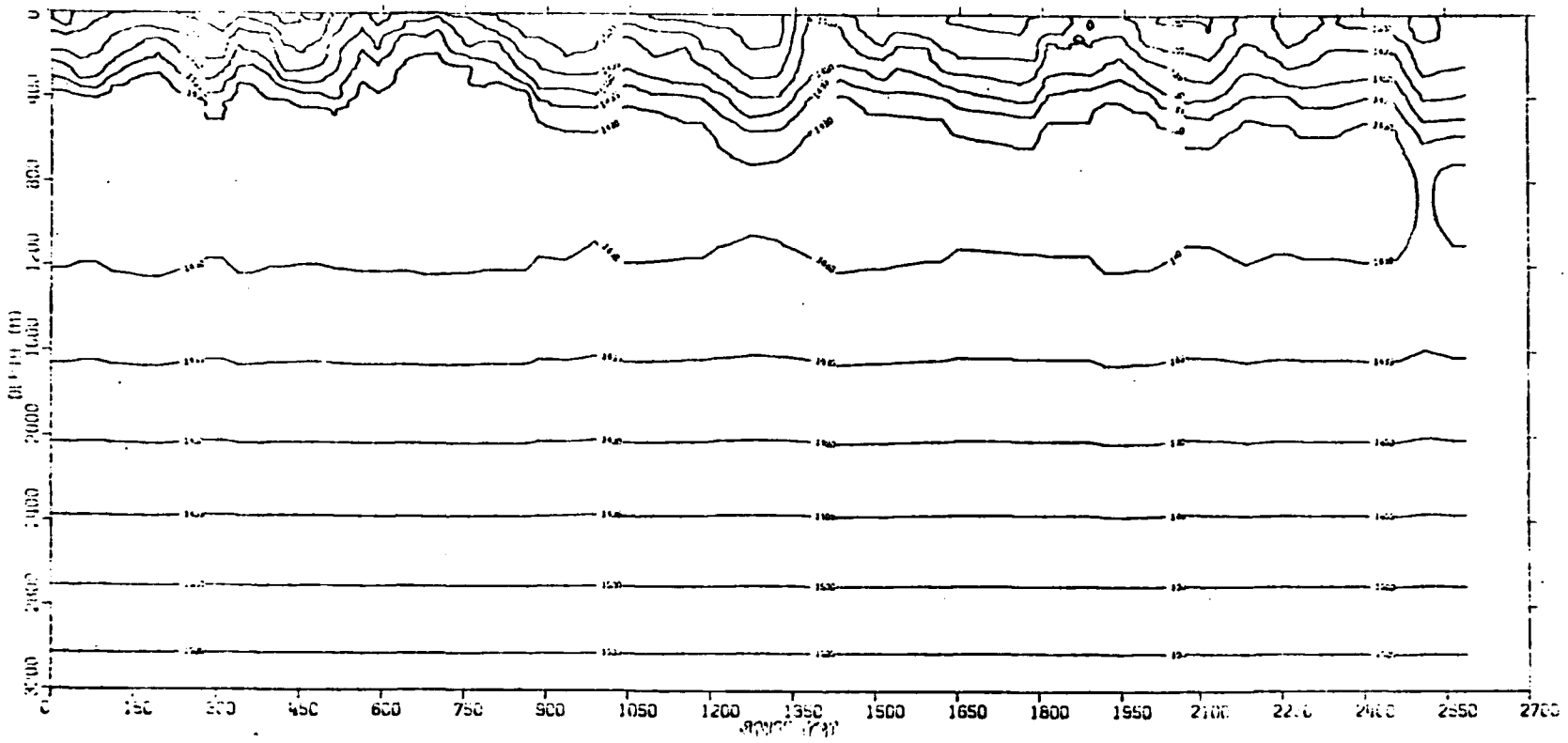

Figure A-2 Isovelocity contours for Schenectady Track

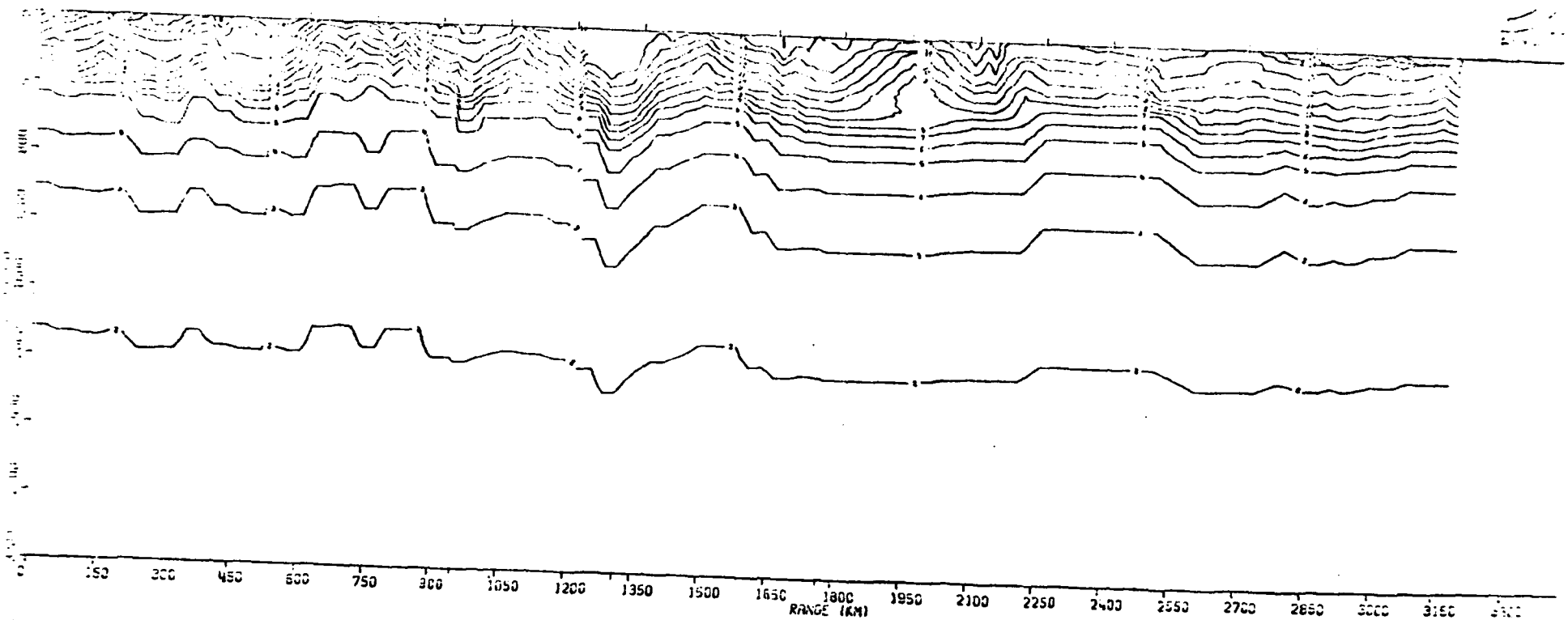

Figure A-3 Isothermal contours for St Louis Track

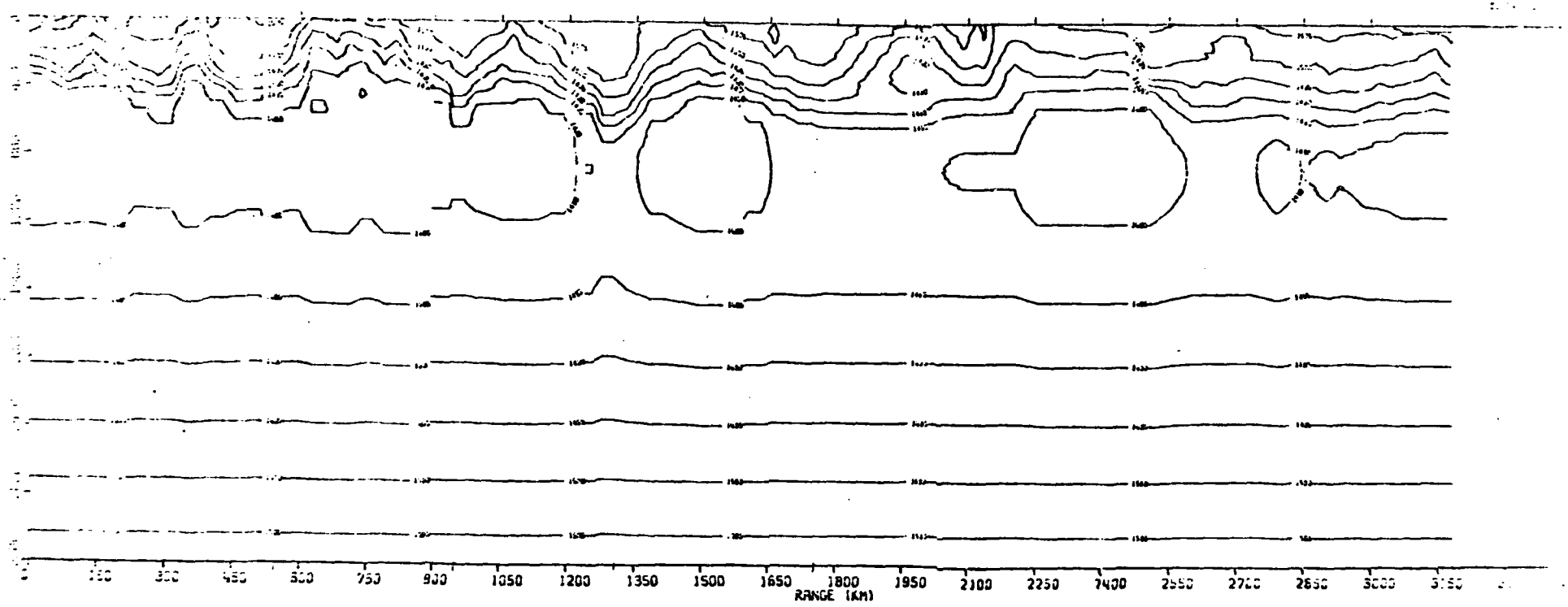

Figure A-4 Isovelocity contours for St Louis Track

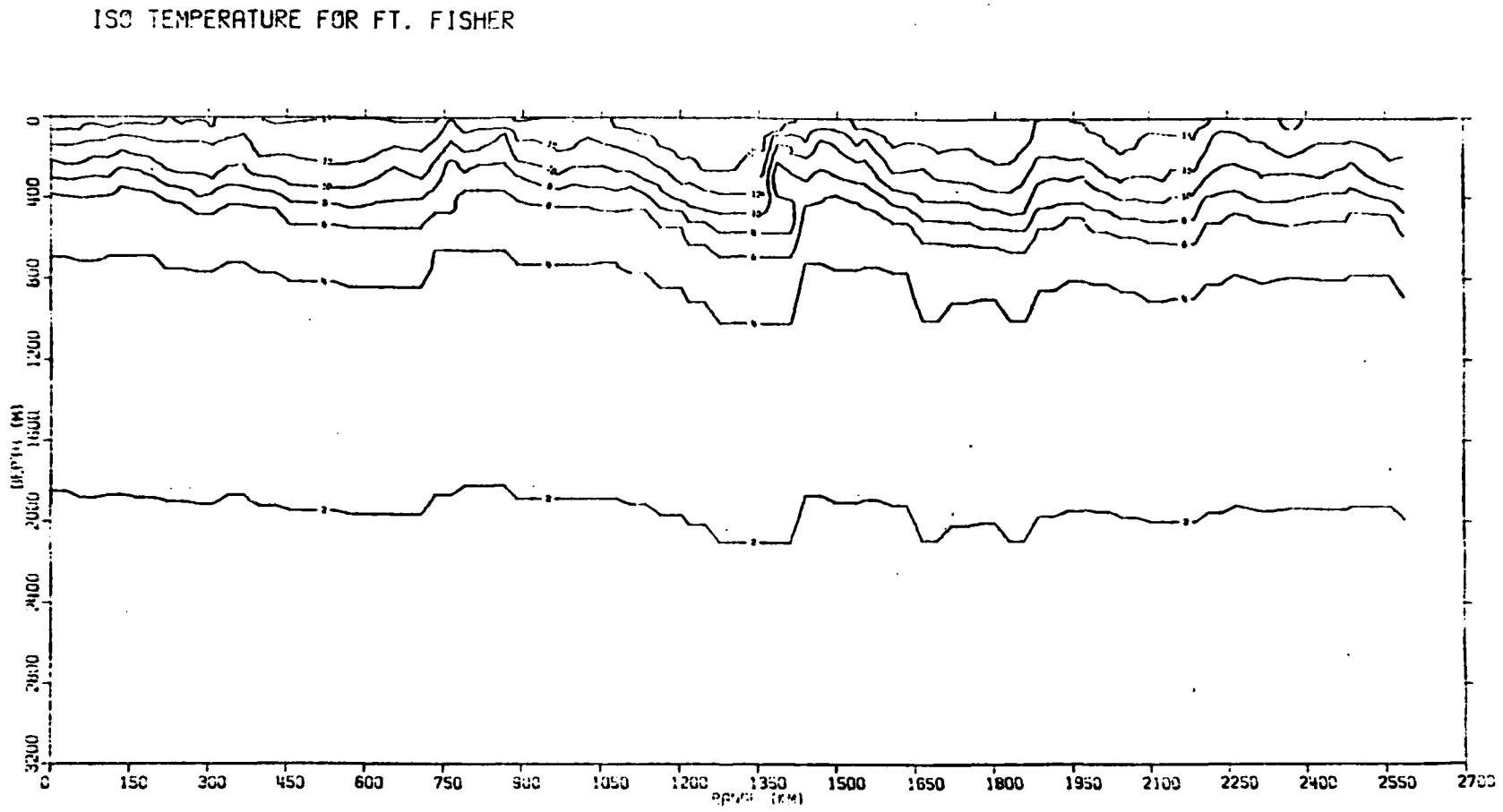

Figure A-5 Isothermal contours for Ft. Fisher Track

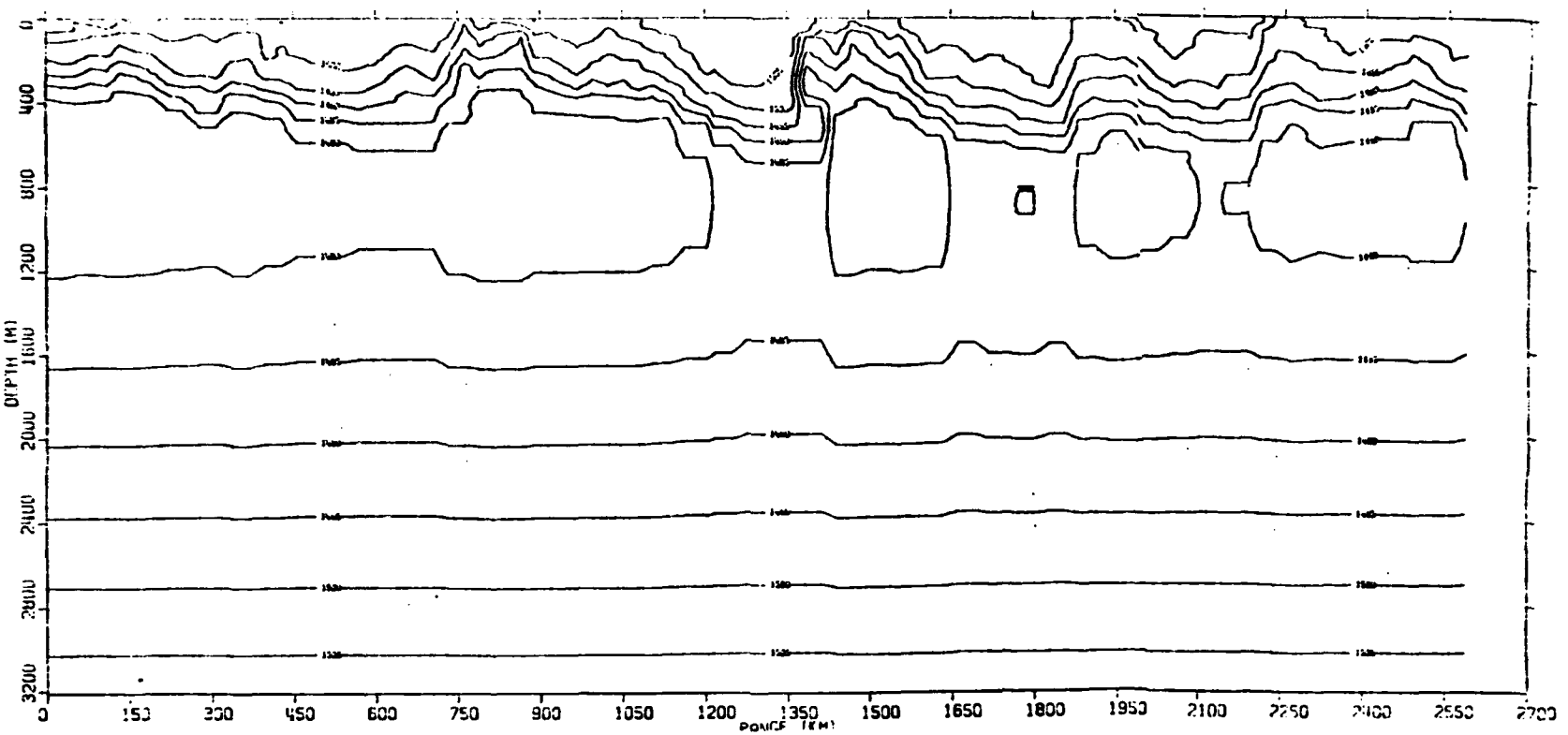

Figure A-6 Isovelocity contours for Ft. Fisher Track

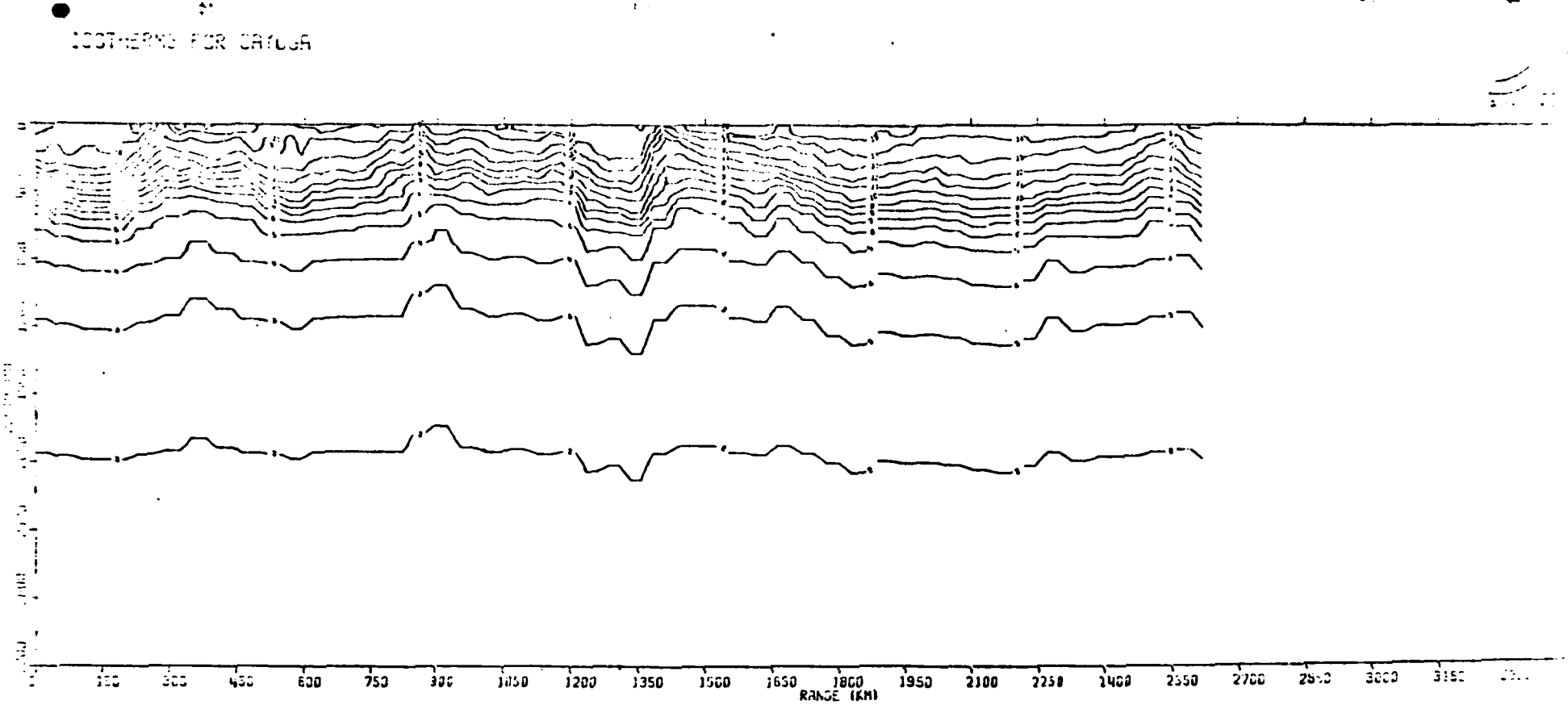

Figure A-7 Isothermal contours for Cayuga Track

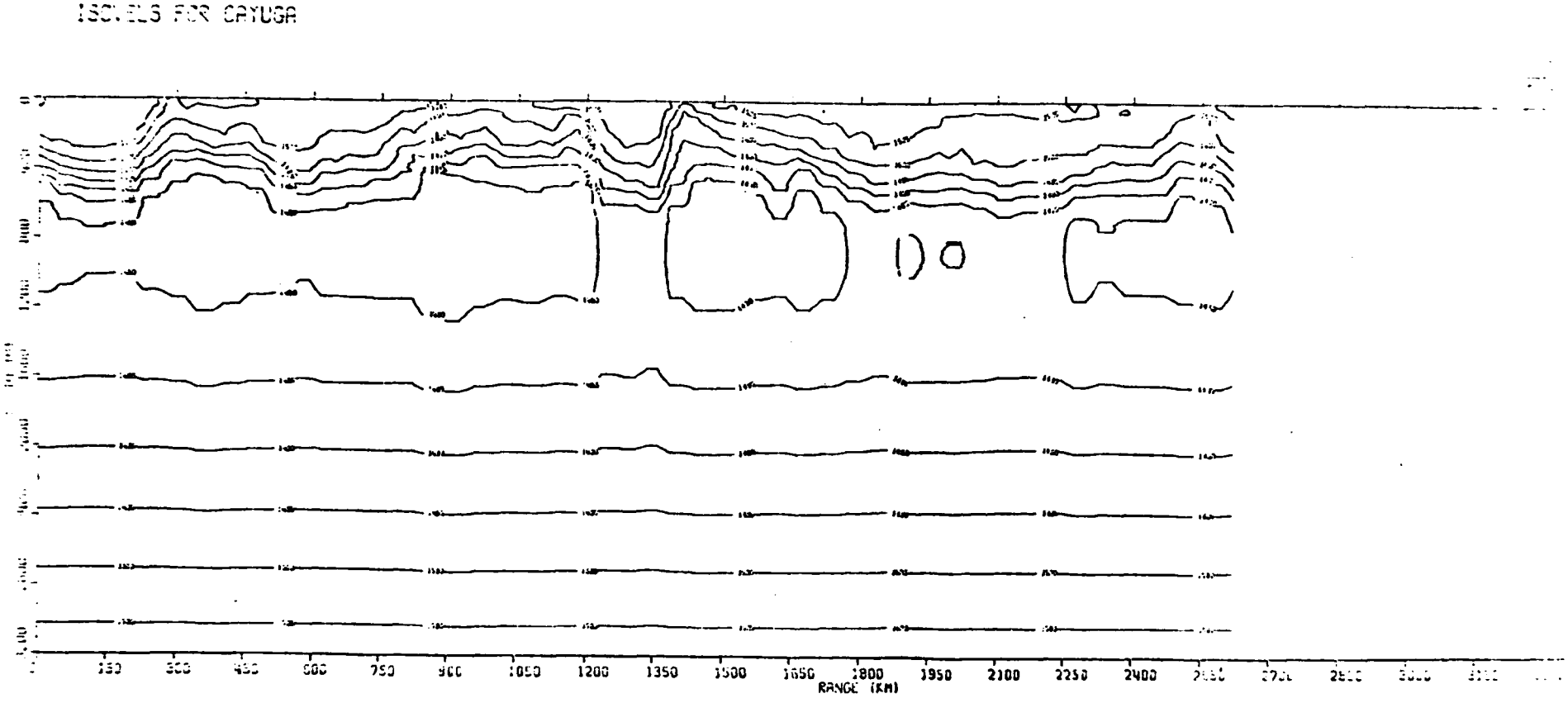

Figure A-8 Isovelocity contours for Cayuga Track

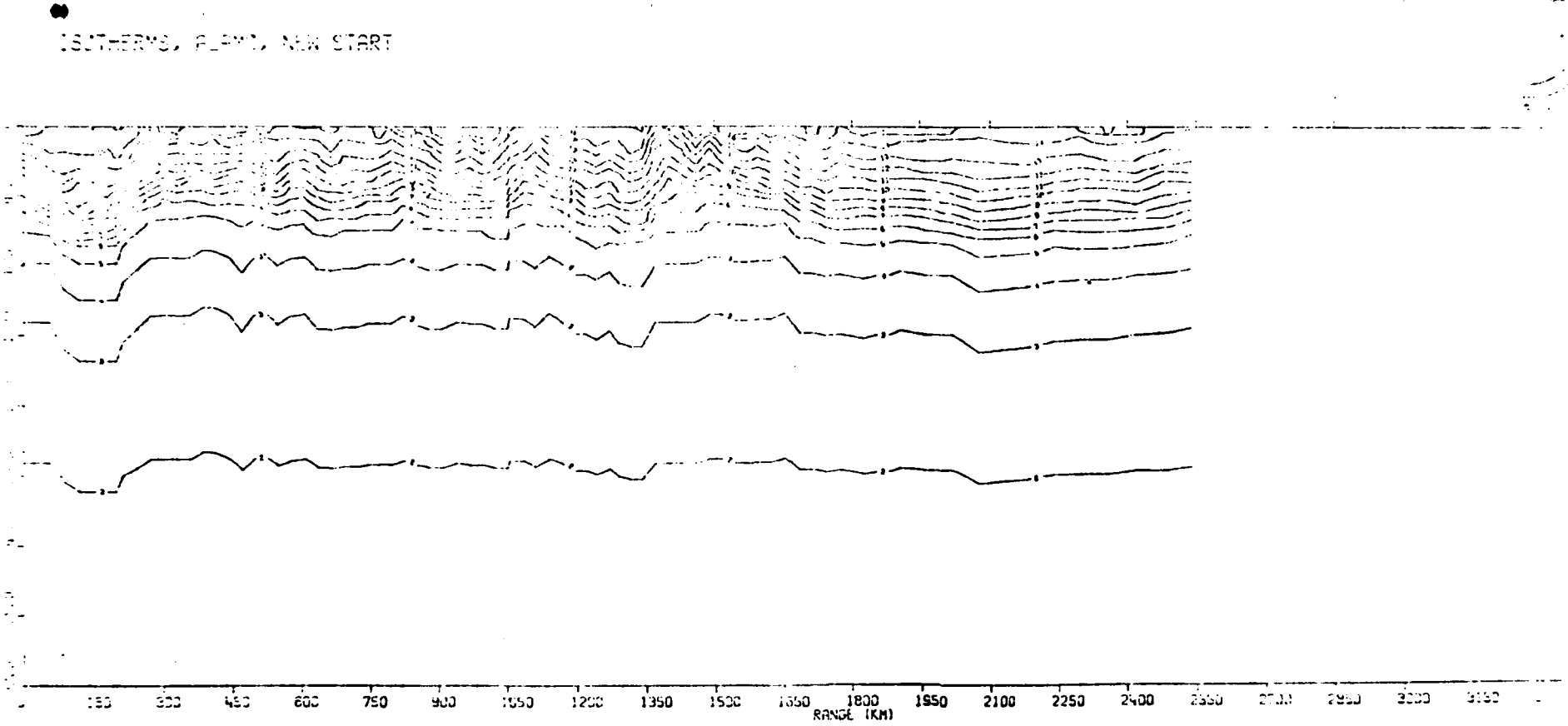

Figure A-9 Isothermal contours for Alamo Track

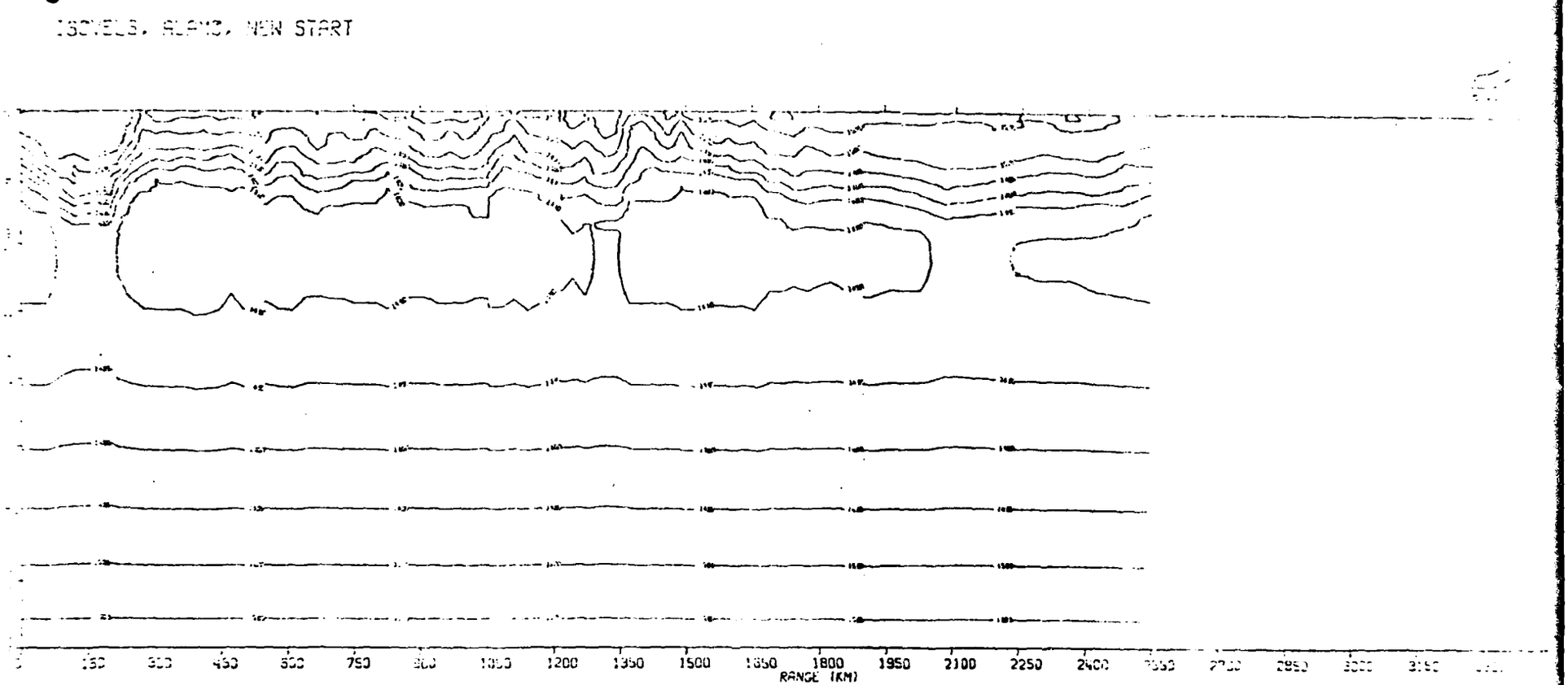

Figure A-10 Isovelocity contours for Alamo Track

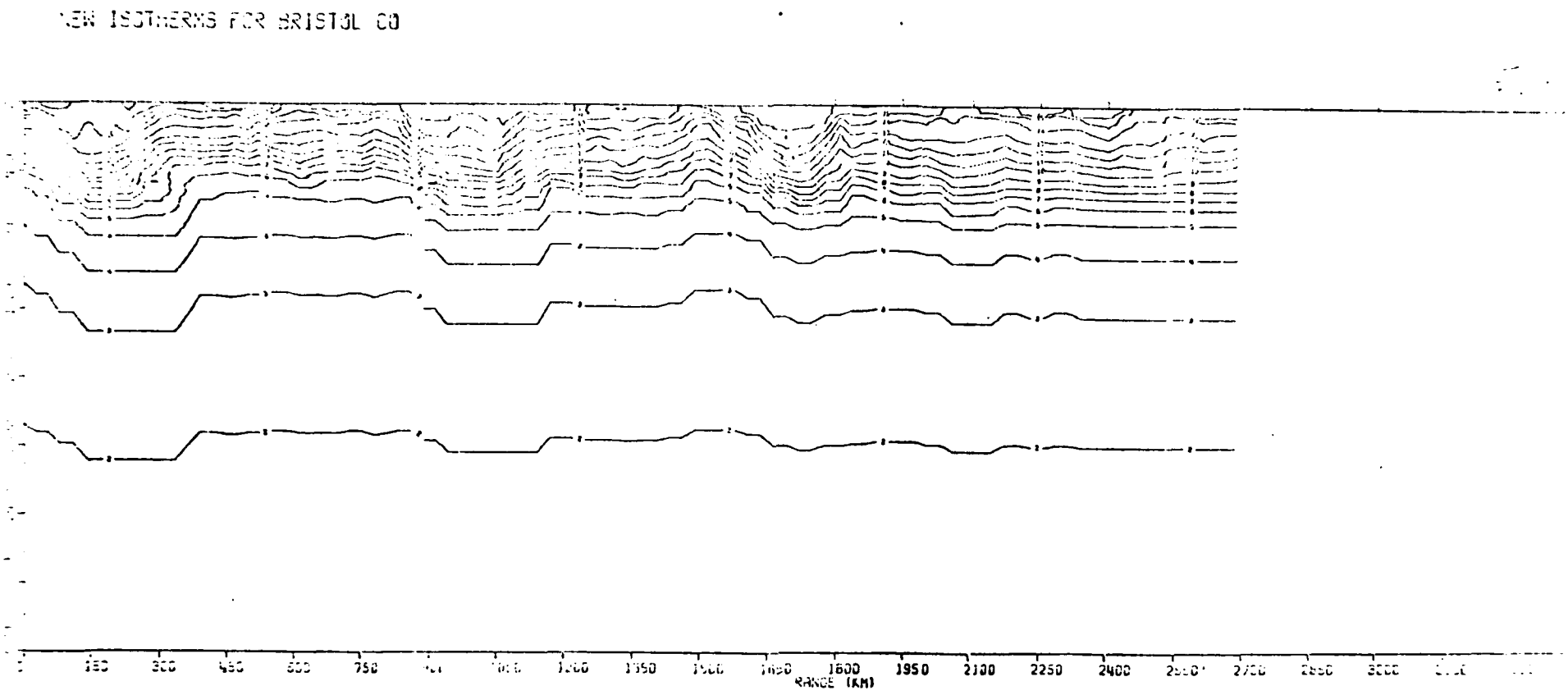

Figure A-11 Isothermal contours for Bristol Co Track

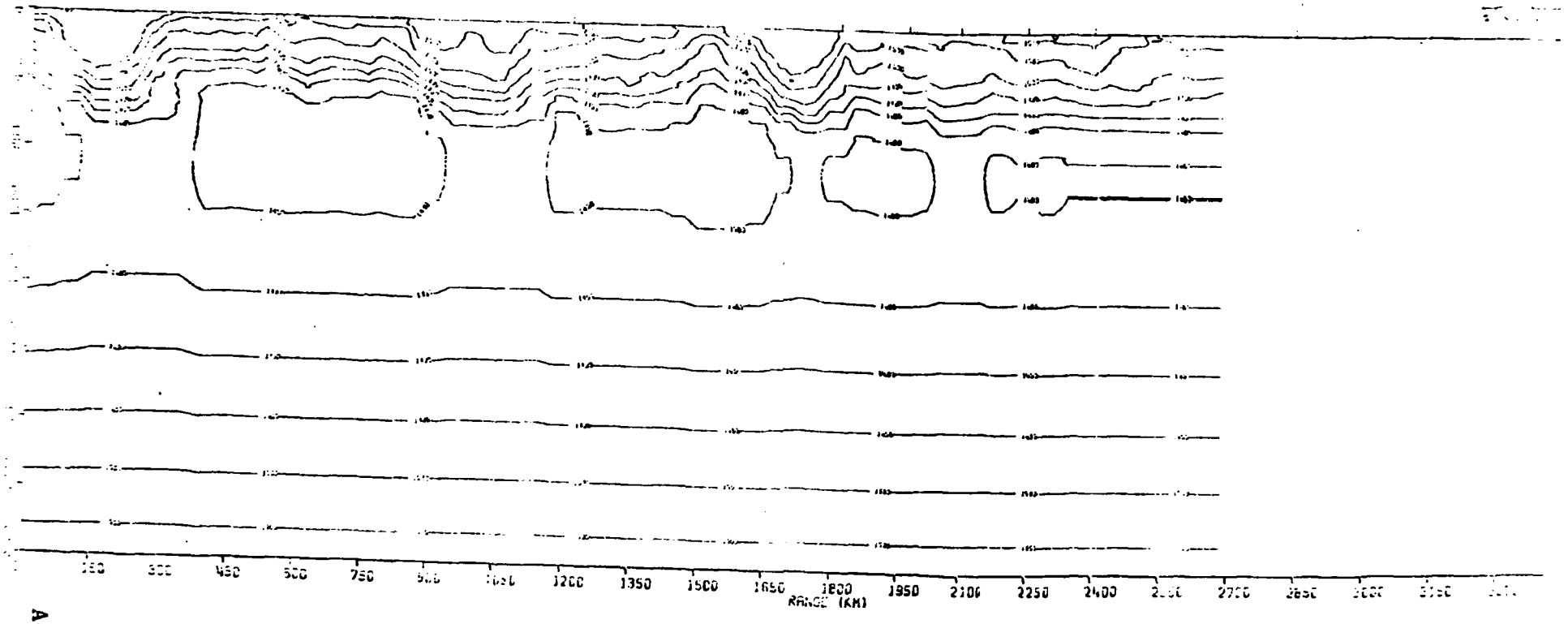

Figure A-12 Isovelocity contours for Bristol Co Track

APPENDIX B

DISTRIBUTION LIST

Distribution List for

"Acoustic Implications of Mesoscale Oceanographic Phenomena"

Name	Number of Copies
Under Secretary of Defense for Research & Engineering Washington, D.C. 20301	
Dr. E. J. McKinney	1
Chief of Naval Operations Department of the Navy Washington, D.C. 20350	
OP-951	1
OP-953	1
OP-961	1
OP-987 (Dr. Bosman)	1
Chief of Naval Material Department of the Navy Washington, D.C. 20360	
Mr. G. R. Spalding, Code 08T24	1
Mr. Flum, PM-4	1
Naval Sea Systems Command Department of the Navy Washington, D.C. 20360	
Code 06H1	1
Code 06H2	1
Office of Naval Research Department of the Navy Arlington, Virginia 22217	
Code 431	2
Code 222	1
Code 481	1
Code 486	1
Naval Ocean Research and Development Activity NSTL Station, Mississippi 39522	
Mr. M. G. Lewis, Code 500	1
Dr. A. Anderson, Code 320	1
Naval Research Laboratory Washington, D.C. 20375	
Code 2620	2
Code 8109	1
Naval Ocean Systems Center San Diego, California 92152	
Code 16	1
Code 71	1

Name	Number of Copies
Naval Underwater Systems Center New London Laboratory New London, Connecticut 06329 Mr. Mellburg	2
David W. Taylor Naval Ship Research and Development Center Code 1806 Bethesda, Maryland 20084	1
Naval Air Development Center Warminster, Pennsylvania 18974 Mr. J. Howard	1
Naval Surface Weapons Center Silver Spring, Maryland 20910 Code U-20 Code U-40	1 1
Naval Intelligence Support Center 4301 Suitland Road Washington, D.C. 20390	1
Commander, Second Fleet Code N4 Norfolk, Virginia 23511	1
Commander, Third Fleet N7 Division FPO San Francisco, California 96610	2
Commander - Submarine Development Squadron 12 Box 70, Naval Submarine Base New London, Connecticut 06342	1
Naval War College Technical Library Newport, Rhode Island 02840	1
The Numerical Weather Facility Naval Postgraduate School Monterey, California 93940	2
Defense Documentation Center Cameron Station Alexandria, Virginia 22314	12
Center for Naval Analyses Technical Library 1401 Wilson Boulevard Arlington, Virginia 22209	1

Name	Number of Copies
Johns Hopkins University Applied Physics Laboratory Laurel, Marylnad 20810 Dr. R. Henrick	1
Rensselaer Polytechnic Institute Troy, New York 12181 Dr. W. Siegmann	1
University of Texas Applied Research Laboratory P.O. Box 8029 Austin, Texas 78712 Dr. K. Hawker	1